UNIVERSITAT POLITÈCNICA DE VALÈNCIA

CAMPUS DE GANDIA

Positioning System and Acoustic Studies for the KM3NeT deep-sea Neutrino Telescope

---

Doctoral Thesis

Dídac Diego i Tortosa

Supervisors:

Prof. Miguel Ardid Ramírez
Dr. Juan A. Martínez Mora

September, 2022

Per totes i cadascuna de les persones
que estan, que han estat i estaran.

"En la meva feina he triat ser una aliada de la raó, no de la passió."

Leila Khaled.

Contents

Abstract

Neutrinos are subatomic particles that travel through the Universe with tiny or no change in their trajectory. This means that, if they are detected traveling along their way, the position of their origin can be studied. Despite being the most abundant particle in space so far discovered, as it has no electrical charge and it only interacts, it has a very low probability of interaction, which is necessary to prove its presence. Given the possibilities of evidencing the presence of a neutrino, it is necessary to have huge volumes controlled by sensors capable of detecting them. In the case of interaction in a fluid such as water or ice with sufficient energy, a muon (or other charged particles), which travels faster than the speed of light, may be generated producing radiation called Cherenkov light. This is the light that underwater neutrino telescopes aim to detect, so they have installed optical sensors in the form of a three-dimensional array.

KM3NeT is a neutrino detector belonging to the new generation of underwater telescopes designed to hold one cubic kilometer. It is currently under construction in the depths of the Mediterranean Sea. It consists of two detector nodes: ARCA, which is located 100 km off the coast of Portopalo di Capo Passero at a depth of 3400 m, and ORCA, 40 km off the coast of Toulon, submerged at a depth of 2400 m. The Detection Units (DUs) used are composed of a base that anchors them to the sea floor, 18 Digital Optical Modules (DOMs) attached along a pair of cables linking the base to a top buoy. Thus, it has a fixed DU on the seabed, standing in a vertical position (given the buoyancy of its elements), but susceptible to the sea currents. In order to be able to reconstruct the trajectory of a detected muon, it is necessary to

know the position and orientation of each DOM. Therefore, KM3NeT has an Acoustic Positioning System (APS) and an Attitude and Heading Reference System (AHRS).

On the one hand, the APS has acoustic receivers installed in each DOM (piezoceramic sensors) and at the base of each DU (hydrophones). On the other hand, there are Acoustic Beacons (ABs) at known positions that emit specific signals, which are used for the Acoustic Data Filter to register their detection at each receiver. By recording three or more emissions belonging to different ABs, the position of each piezoceramic sensor can be estimated. On the other hand, the AHRS indicates the value of yaw, pitch, and roll, suggesting the orientation of the DOM. With a combination of APS and AHRS (or independently), and making use of a Mechanical Model, the shape of the DU can be reconstructed. In this way, the situation of each DOM is known with higher accuracy. As far as the ABs are concerned, each one has been characterized in the laboratory thanks to a process that has been standardized, both in terms of measurements and subsequent analysis. In addition, a possible location for the installation of ABs is presented, ensuring good reception in all DOMs.

Finally, it is intended to use the APS receivers in KM3NeT for the possible acoustic detection of neutrinos. There are theories that explain that when the interaction of an Ultra-High-Energy neutrino is produced, a peculiar thermoacoustic signal as a Bipolar Pulse (BP), with a narrow angle directivity is propagated. Thus, a complete calibration of the detector has been designed to determine whether the APS is ready for the possible capture of this type of signal. Moreover, an algorithm capable of selecting possible BP candidates is designed, developed, and tested. So far, 2.9 days of data have been analyzed using three hydrophones in ORCA and promising results have been obtained to pursue this line of research, proposing an alert system (trigger) to register the candidate events.

As indicated in the title, the present thesis addresses two main parts: th first one about the positioning system and the second one about signal analysis for acoustic neutrino detection. Both were developed for the KM3NeT neutrino detector. The document is composed of five chapters, the first one introducing the context for understanding the work, and two chapters pertaining to each part (which come with its own Summary, Conclusions, and a final section on Future Steps).

Resum

Els neutrins són unes partícules subatòmiques que viatgen per l'Univers sense alterar la seva trajectòria. Això significa que, de ser detectats recorrent el seu camí, es pot estudiar la posició del seu origen. Malgrat ser la partícula més abundant de l'espai fins ara descoberta, com no posseeix càrrega elèctrica i sols interacciona dèbilment, presenta molt baixa probabilitat d'interacció, necessària per a evidenciar la seva presència. Llavors, per evidenciar la presència d'un neutrí, es necessita tenir enormes volums controlats per sensors capaços de detectar-los. En el cas d'interactuar en un fluid com l'aigua o el gel, es pot proporcionar un muó (o altres partícules carregades) que viatja a major velocitat que la llum, produint una radiació anomenada llum de Cherenkov. És aquesta llum la que els detectors de neutrins submarins pretenen detectar, per això instal·len sensors òptics en forma de matriu tridimensional.

KM3NeT és un detector de neutrins que pertany a la nova generació d'aquest tipus de telescopis submarins i que està dissenyat per a albergar un quilòmetre cúbic. Actualment, es troba en fase de construcció, en les profunditats de la Mar Mediterrània. Es compon de dos nodes detectors: ARCA que es situa a 100 km de la costa de Portopalo di Capo Passero a 3400 m de profunditat, i ORCA a 40 km de la costa de Toulon submergit a 2400 m. Les Unitats de Detecció (DU) utilitzades es componen d'una base que les ancora al fons marí, 18 Mòduls Òptics Digitals (DOM) subjectes al llarg d'un parell de cables que uneixen la base amb una boia. Així, es té una DU fixa en el fons de la mar, alçada en posició vertical (donada la flotabilitat dels seus elements), però susceptible als corrents marins. Així que, per a ser capaços de reconstruir la trajectòria d'un muó detectat, és necessari tenir clara la posició i orientació

de cada DOM. Per això, KM3NeT compta amb un Sistema de Posicionament Acústic (APS) i un Sistema de Referència d'Actitud i Rumb (AHRS).

D'una banda, l'APS té receptors acústics instal·lats en cada DOM (sensors piezoelèctrics) i en la base de cada DU (hidròfons). A part, instal·la Balises Acústiques (AB) en posicions conegudes que emeten senyals particulars, que s'utilitzen perquè el Filtre de Dades Acústic registra la seva detecció en cada receptor. Amb el registre de tres o més emissions pertanyents a diferents AB, es pot estimar la posició de cada sensor piezoelèctric. D'altra banda, el AHRS indica el valor de l'ullet, cabotejo i balanceig, facilitant l'orientació del DOM. Amb una combinació de APS i AHRS (o de manera independent), i fent ús d'un Model Mecànic es pot reconstruir la forma de la DU. Així es coneix la situació de cada DOM amb una major exactitud. Pel que fa als ABs, cadascun es caracteritza en el laboratori gràcies a un procés que s'ha estandarditzat, tant en realització de mesures com en la seva posterior anàlisi. A més, es presenta una possible ubicació per a instal·lar-los, assegurant una bona recepció en tots els DOM.

Finalment, es pretén aprofitar els receptors del APS en KM3NeT per a la possible detecció acústica de neutrins. Existeixen teories que expliquen que en la interacció d'un neutrí ultraenergètic es propaga un peculiar senyal termo-acústica en forma de Pols Bipolar (BP), de directivitat estreta per a les freqüències que té. Així que s'ha dissenyat un calibratge complet del detector capaç de determinar si el APS està preparat per a la possible captura d'aquesta mena de senyals. Per això, es dissenya, desenvolupa i prova un algoritme capaç de seleccionar possibles candidats de BP. Aquest algoritme usa la tècnica de l'espectrograma per analitzar l'energia, la freqüència i la durada de cada pols. Ara com ara s'han analitzat 2.9 dies de dades usant tres hidròfons en ORCA i s'han obtingut resultats prometedors per a seguir aquesta línia de recerca, proposant un sistema d'alerta per a registrar events d'interès.

Com s'indica en el títol, la present tesi aborda dues parts nuclears: una primera sobre el sistema de posicionament i una segona sobre l'anàlisi en el senyal per a la detecció acústica de neutrins. Ambdues, desenvolupades per al detector de neutrins KM3NeT. El document es compon de cinc capítols, un primer que introdueix el context per a comprendre el treball realitzat, i dos capítols pertanyents a cada part (els quals venen amb el seu propi Resum, les seves Conclusions i una secció final de Passos Futurs).

Resumen

Los neutrinos son partículas subatómicas que viajan por el Universo sin apenas alterar su trayectoria. Esto quiere decir que, de ser detectados recorriendo su camino, se puede saber de donde provienen. Sin embargo, a pesar de ser la partícula más abundante del espacio descubierta hasta ahora, al no poseer carga eléctrica, presenta una baja probabilidad de interacción, necesaria para evidenciar su presencia. Con todo lo anterior, dadas las posibilidades de evidenciar la presencia de un neutrino, se necesita tener enormes volúmenes controlados por sensores capaces de detectarlos. En el caso de que los neutrinos interactúen en un fluido como el agua o el hielo, se pueden proporcionar partículas cargadas como el muon, que viajan a mayor velocidad que la luz, produciendo una radiación llamada luz de Cherenkov. Es esta luz la que los detectores de neutrinos submarinos pretenden detectar, por ello se instalan sensores ópticos en forma de matriz tridimensional.

KM3NeT es un detector de neutrinos perteneciente a la nueva generación de este tipo de telescopios submarinos y diseñado para albergar un kilómetro cúbico. Actualmente, se encuentra en fase de construcción en las profundidades del Mar Mediterráneo. Se compone de dos nodos detectores: ARCA que se sitúa a 100 km de la costa de Portopalo di Capo Passero a 3400 m de profundidad, y ORCA a 40 km de la costa de Toulon sumergido a 2400 m. Las Unidades de Detección (DU) usadas se componen de una base que las ancla al lecho marino, 18 Módulos Ópticos Digitales (DOM) sujetos a lo largo de un par de cables que unen la base con una boya. Así, se tiene una DU fija en el fondo del mar, erguida en posición vertical (dada la flotabilidad de sus elementos), pero susceptible a las corrientes marinas. Así que, para ser capaces de reconstruir la trayectoria de

un muon detectado, es necesario tener clara la posición y orientación de cada DOM. Por ello, KM3NeT cuenta con un Sistema de Posicionamiento Acústico (APS) y un Sistema de Referencia de Actitud y Rumbo (AHRS).

Por un lado, el APS tiene receptores acústicos instalados en cada DOM (sensores piezoeléctricos) y en la base de cada DU (hidrófonos). Además, instala Balizas Acústicas (AB) en posiciones conocidas que emiten señales particulares, que se usan para que el Filtro de Datos Acústico registre su detección en cada receptor. Con el registro de tres o más emisiones pertenecientes a diferentes AB, se puede estimar la posición de cada sensor piezoeléctrico. Por otro lado, el AHRS indica el valor de la guiñada, cabeceo y balanceo, facilitando la orientación del DOM. Con una combinación de APS y AHRS (o de forma independiente), y haciendo uso de un Modelo Mecánico se puede reconstruir la forma de la DU. Así, se conoce la situación de cada DOM con una mayor exactitud. Los AB se caracterizan en laboratorio gracias a un proceso que se ha estandarizado, tanto en realización de medidas como en su posterior análisis. Además, se presenta una posible ubicación para instalarlos, asegurando una buena recepción en todos los DOM.

Por último, se pretende aprovechar los receptores del APS en KM3NeT para la posible detección acústica de neutrinos. Existen teorías de que al producirse la interacción de un neutrino ultra-energético se propaga una peculiar señal termo-acústica en forma de Pulso Bipolar (BP), de directividad estrecha para las frecuencias que abarca. Es por esto que se ha diseñado una calibración completa del detector capaz de determinar si el APS está preparado para la posible captura de este tipo de señales. Por ello, se diseña, desarrolla y prueba un algoritmo capaz de seleccionar posibles candidatos de BP. Este algoritmo usa la técnica del espectrograma para analizar la energía, la frecuencia y la duración de cada pulso. Por ahora se han analizado 2.9 días de datos usando tres hidrófonos en ORCA y se han obtenido resultados prometedores para seguir esta línea de investigación, proponiéndose un sistema de alerta para registrar estos eventos de interés.

Como se indica en el título, la presente tesis aborda dos partes nucleares: una primera acerca del sistema de posicionamiento y una segunda sobre análisis en la señal para la detección acústica de neutrinos. Ambas desarrolladas para el detector de neutrinos KM3NeT. El documento se compone de cinco capítulos, un primero que introduce el contexto para comprender el trabajo realizado, y dos capítulos pertenecientes a cada parte (los cuales vienen con su propio Resumen, sus Conclusiones y una sección final de Pasos Futuros).

Acronyms

AB Acoustic Beacon.

ACDC Alternating Current to Direct Current.

ADC Analog-to-Digital Converter.

ADCP Acoustic Doppler Current Profiler.

ADF Acoustic Data Filter.

AHRS Attitude and Heading Reference System.

AMANDA Antarctic Muon And Neutrino Detector Array.

ANTARES Astronomy with a Neutrino Telescope and Abyss environmental RESearch.

APS Acoustic Positioning System.

ARCA Astroparticle Research with Cosmics in the Abyss.

BAIKAL-GVD Baikal Gigaton Volume Detector.

BDUNT Baikal Deep Underwater Neutrino Telescope.

BP Bipolar Pulse.

CB Calibration Base.

CET Central European Time.

CLB Central Logic Board.

CPU Central Processing Unit.

CVC Capacitor Voltage Charge.

DAC Digital-to-Analog Converter.

DAQ Data Acquisition.

DAR Digital Acoustic Receiver.

DB Data Base.

DIR Directivity.

distER Emitter-Receiver distance.

DOM Digital Optical Module.

DP Digital Penetration.

DU Detection Unit.

DW Data Writer.

EMSO European Multidisciplinary Seafloor Observatory.

ENU East, North, Up.

FFR Free Flooded Ring.

FFT Fast Fourier Transform.

GNN Global Neutrino Network.

GPS Global Positioning System.

IGIC Institut d'Investigació per a la Gestió Integrada de Zones Costaneres.

JB Junction Box.

KM3NeT Cubic Kilometre Neutrino Telescope.

LBL Long Baseline.

LOM Launcher of Optical Modules.

MII Instrumented Interface Module.

MM Mechanical Model.

MSM Mediterráneo Señales Marítimas, S.L..

NEMO NEutrino Mediterranean Observatory.

NESTOR Neutrino Extended Submarine Telescope with Oceanographic Research.

ORCA Oscillation Research with Cosmics in the Abyss.

P-ONE Pacific Ocean Neutrino Experiment.

PCB Printed Circuit Board.

PMT Photomultiplier Tube.

PSD Power Spectral Density.

Pvar Power Variation.

PWM Pulse-Width Modulation.

PXI PCI eXtensions for Instrumentation.

QF Quality Factor.

RMS Root Mean Square.

ROV Remotely Operated Vehicle.

RVR Received Voltage Response.

SEB Sound Emission Board.

SNR Signal-to-Noise Ratio.

SPL Sound Pressure Level.

SVP Sound Velocity Profle.

ToA Time of Arrival.

ToE Time of Emission.

ToF Time of Flight.

TriDAS Trigger and Data Acquisition System.

TVR Transmitted Voltage Response.

UHE Ultra High Energy.

UPV Universitat Politècnica de València.

Capítulo 1

Preámbulo de la Tesis. KM3NeT: telescopio de neutrinos en las profundidades del Mar Mediterráneo

KM3NeT es un detector de neutrinos submarino diseñado para llegar a ser el más grande del mundo. Por el momento, se divide en dos nodos: ARCA a 3400 m de profundidad y ORCA a 2400 m de profundidad. La Unidad de Detección usada en KM3NeT consiste en una base anclada al lecho marino que sujeta dos cables en paralelo con 18 Módulos Ópticos Digitales y una boya al final. Estas bases se reparten por cada nodo para crear un array en 3D de sensores ópticos que monitorean un gran volumen de agua. Cuando un neutrino interacciona en el agua y se produce la denominada luz de Cherenkov, los módulos ópticos la detectan. Al conocer la posición de estos detectores, es posible ubicar el evento en el espacio. Sin embargo, las corrientes marinas mantienen los sensores ópticos de las Unidades de Detección moviéndose, así que se precisa de un Sistema de Posicionamiento capaz de monitorizar su estado a cada momento. Por ello, KM3NeT cuenta con un Sistema de Posicionamiento Acústico que instala emisores fijos y receptores por todo el detector. Además, hay teorías que demuestran la posible detección acústica de neutrinos en el agua, pudiendo ampliar el uso de los receptores para estos fines.

Este primer capítulo contextualiza el trabajo realizado durante la tesis. La *Sección 1.1* detalla el proyecto KM3NeT, donde se explica la detección de neutrinos (*Subsección 1.1.1*), la tecnología que lo permite y su localización en KM3NeT (*Subsección 1.1.2*), y se expone brevemente la historia de este tipo de detectores (*Subsección 1.1.3*). Seguidamente, la *Sección 1.2* introduce el sistema de posicionamiento usado en KM3NeT, el cual es abordado en la *Parte 1* de la tesis por dos capítulos (*Capítulo 2* y *Capítulo 3*). Y, por último, la *Sección 1.3* describe en qué se basa la posible detección acústica de neutrinos, que se comenta en la *Parte 2* de la tesis (*Capítulo 4* y *Capítulo 5*).

La presente tesis ha sido desarrollada durante el despliegue y puesta en marcha de las primeras unidades de detección del telescopio de neutrinos submarinos Cubic Kilometre Neutrino Telescope (KM3NeT).

1.1 Proyecto KM3NeT

En el Mar Mediterráneo se está construyendo KM3NeT, el que pretende ser el telescopio de neutrinos submarino más grande del mundo [1]. KM3NeT pertenece a la próxima generación de detectores de neutrinos bajo el agua. Estos detectores usan sensores ópticos para estudiar la luz de Cherenkov producida por las partículas generadas tras la interacción de un neutrino en dicho fluido. Para ello, se instalan fotomultiplicadores (PMT) repartidos en un gran volumen del fondo marino, alejándose de la luz natural y de otras fuentes de ruido.

1.1.1 La detección de un neutrino

Los neutrinos ("pequeños neutrones") son partículas subatómicas pertenecientes al grupo de los Leptones, dentro del grupo de los Fermiones, según la teoría del modelo estándar de la física. De los seis leptones descubiertos, tres tienen carga negativa: electrón, muon y tauon, de las cuales sus familias asociadas de neutrinos corresponden al neutrino electrónico ν_e, neutrino muónico ν_μ y neutrino tauónico ν_τ (ordenados de menor a mayor masa). Sus masas han sido predichas, pero nunca medidas experimentalmente. Los neutrinos son esenciales para entender la radioactividad, es más, un agujero negro, el Sol, la atmósfera, el interior de la Tierra, las centrales nucleares, las bombas atómicas, entre otros, son fuentes que generan neutrinos, por lo que es la partícula más abundante del Universo descubierta hasta ahora.

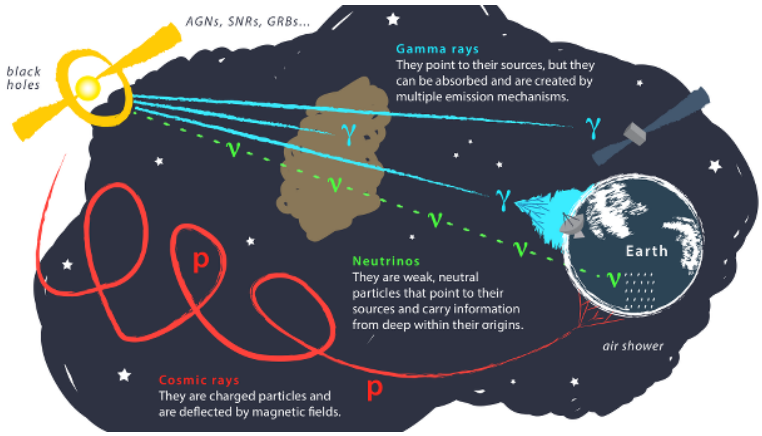

Figura 1.1: Esquema de astropartículas viajando a través del espacio y su posible detección en La Tierra. [*Créditos: Juan Antonio Aguilar & Jamie Yang, IceCube/WIPAC*].

El neutrino viaja grandes distancias de años luz sin alterar su trayectoria (ver *Figura 1.1*), ya que interactúa muy débilmente con la materia: al no tener carga eléctrica presentan una muy baja probabilidad de interacción. Por ello, estudiar sus flujos revela procesos físicos de su fuente de origen. Los neutrinos de energía extremadamente alta son producidos fuera de este sistema solar, lo que hace de su investigación un estudio muy preciado. A pesar de su gran abundancia (el modelo de Bahcall estima un flujo de 5 millones de neutrinos/cm^{2}s únicamente de neutrinos solares) no es fácil constatar su presencia, mucho menos clasificarlos o estudiarlos. Para conseguir detectarlos se necesita una interacción que evidencie su presencia y esto no es común (se estima que únicamente un neutrino solar interactua en la Tierra de cada diez teras que la atraviesan). Dada la rareza de sus interacciones, se deben albergar grandes volúmenes con sensores capaces de detectarlas. Las primeras estimaciones sobre el mínimo volumen necesario hablan de un kilómetro cúbico. Se predice que los neutrinos con energías alrededor de un PeV interactuarán cruzando la Tierra a un ritmo de un evento por año por km^2, mientras que los de 10^{11} GeV sólo interactuarán con una tasa de un evento por siglo por km^2.*

Una de las interacciones del neutrino cargada con un núcleo, por ejemplo de agua, proporciona un muon (caso del neutrino muónico). Si el neutrino tiene suficientemente energía, el muon generado viajará a una velocidad cercana a la de la luz, o sea mayor que la de los fotones (ver *Figura 1.2*), produciendo la radiación de Cherenkov. Esta radiación es una especie de luz azulada que se

*https://masterclass.icecube.wisc.edu/en/learn/detecting-neutrinos [Consulta: 2021-12-12]

produce cuando en un medio transparente la partícula cargada viaja a través de él más rápidamente de lo que lo harían los fotones de luz (es un efecto análogo al de romper la barrera del sonido en el aire).

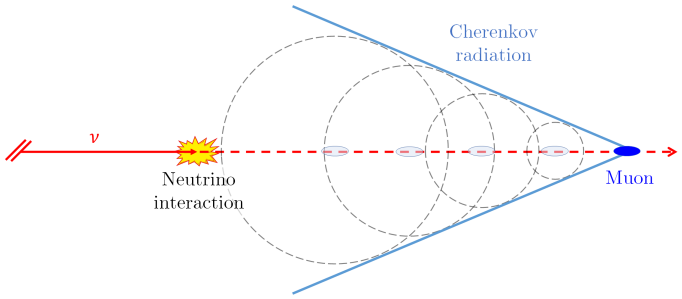

Figura 1.2: Interacción de un neutrino muónico que produce radiación Cherenkov.

Es este fenómeno el que intentan capturar los telescopios de neutrinos acuáticos (o en el hielo), por ello se instalan detectores de luz repartidos en grandes volúmenes.

1.1.2 El detector

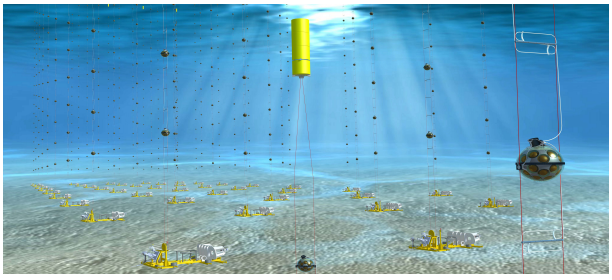

Figura 1.3: Diseño artístico desde el interior de KM3NeT. La ilustración no está a escala: la luz del sol no llega a las profundidades donde se despliega KM3NeT. [*Créditos: Edward Berbee, Nikhef*].

KM3NeT usa unidades de detección repartidas por el lecho marino para construir un array 3D de sensores (ver *Figura 1.3*). La *Figura 1.4.a* muestra una Unidad de Detección (DU), la cual está formada por tres elementos principales: la base, la boya superior y el par de cables en paralelo que las une con 18 esferas de cristal. La base actúa principalmente como ancla evitando el libre desplazamiento de la línia, la boya la mantiene en posición vertical y los DOM

contienen, cada uno, 31 PMT cubriendo toda la superficie de la esfera y tres sensores de calibración [2].

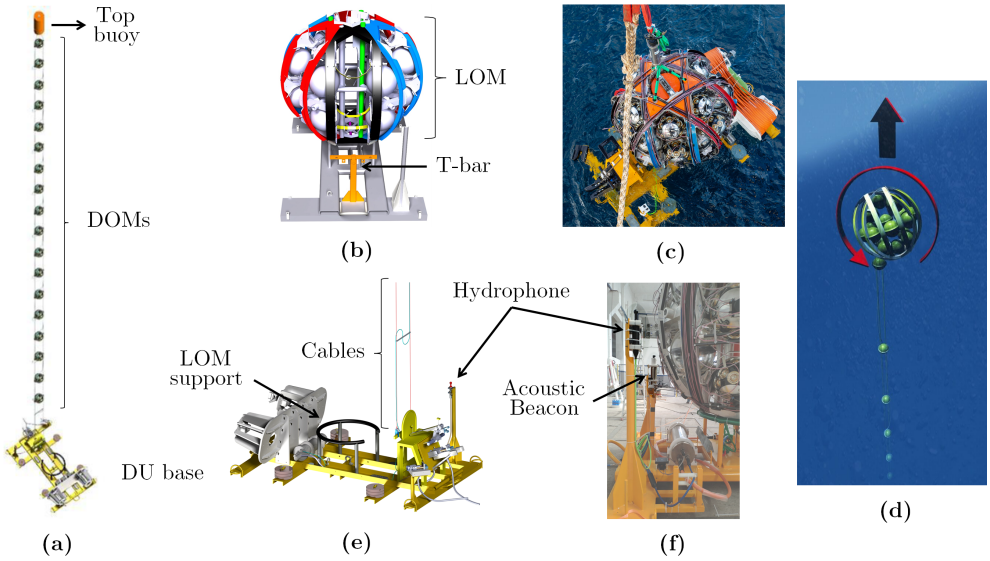

Figura 1.4: (a) Esquema de una DU desplegada. **(b)** DU con esquema de un LOM listo para instalar [3]. **(c)** DU a punto de ser arrojado al mar durante el despliegue. **(d)** Despliegue del LOM después de ser activado por el ROV [*Credits: Marijn van der Meer, Quest*]. **(e)** Esquema de una base de DU para ORCA donde se indica el soporte para hidrófono. **(f)** Imagen de base de DU con Hidrófono y Baliza Acústica montada (AB).

Unidad de Detección

La tecnología de despliegue para una DU viene aportada por la experiencia adquirida de experimentos anteriores y las primeras DU instaladas en KM3NeT. La base está diseñada para transportar toda la línea con los DOM enrollada en una esfera flotable, llamada Lanzadora de Módulos Ópticos (LOM), lista para su instalación (ver *Figura 1.4.b*). Desde el barco, se arroja la DU con el LOM sobre el punto deseado (ver *Figura 1.4.c*). Ésta queda bajo el mar inmóvil, esperando que el Vehículo Operado a Distancia (ROV) se acerque a comprobar su disposición y a liberar el LOM. Cuando el LOM es liberado, sale disparado hacia la superficie mientras va desenrollándose y desprendiéndose de los DOM (ver *Figura 1.4.d*). Posteriormente, el LOM se recupera para ser usado en futuros despliegues de nuevas unidades. Por su parte, el ROV enlaza la nueva DU a la infraestructura ya desplegada, quedando

conectada al detector y operativa. La *Figura 1.4.e* muestra el esquema de una base ya operativa, en ella se observa como los cables desenrollados quedan en paralelo. Además, una base de DU sirve como sujeción para otros sensores como Balizas Acústicas (AB) e hidrófonos (ver *Figura 1.4.f*).

Módulo Óptico Digital

Un Módulo Óptico Digital (DOM) de KM3NeT es una esfera de cristal de radio 21.6 cm (8.5") con 31 PMT cubriendo su superficie para detectar la radiación de Chrenkov. Con dos soportes laterales se sujeta a las línias de la DU y se minimiza su rotación (ver *Figura 1.5.a*). Un DOM también está equipado con un sensor piezocerámico en la parte inferior (ver *Figura 1.5.b*), un LED llamado "nanobeacon" en la parte superior y una placa electrónica con brújula e inclinómetro en el interior. Todo los componentes se operan desde una Placa Lógica Central (CLB) que controla cada sensor y dirige los datos (ver *Figura 1.5.c*). La CLB debe ser capaz de administrar los datos recolectados con una precisión de 1 ns para la sincronización del resto de sensores en el detector [4].

(a)

(b)

(c)

Figura 1.5: (a) DOM unido a los cables de una DU. **(b)** Vista inferior de un DOM. **(c)** Exposición de todos los componentes que forman un DOM.

Localización

KM3NeT tiene dos nodos detectores llamados Astroparticle Research with Cosmics in the Abyss (ARCA) y Oscillation Research with Cosmics in the Abyss (ORCA). Ambos usan la misma tecnología, aunque con fines diferentes: ARCA ha sido diseñada con el fin de estudiar neutrinos cósmicos de muy alta energía, mientras que ORCA estudia las propiedaes de neutrinos creados por los rayos cósmicos en la atmósfera terresstre. ARCA se sitúa a 100 km de la costa de *Portopalo di Capo Passero* a 3400 m de profundidad, y ORCA a 40 km de la costa de *Toulon* sumergido a 2400 m (ver *Figura 1.6.a*).

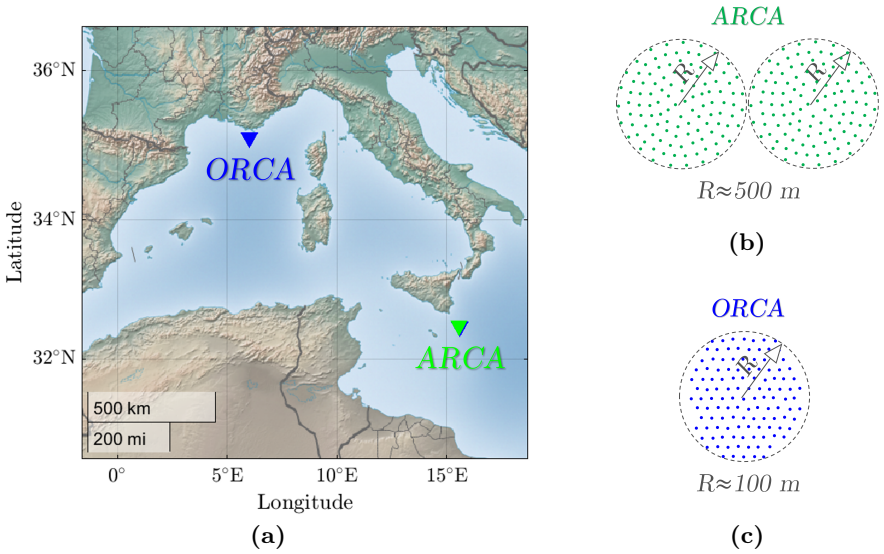

Figura 1.6: **(a)** Localización KM3NeT. **(b)** Nodo detector ARCA. **(c)** Nodo detector ORCA.

ARCA pretende instrumentalizar al menos 1 km^3 repartiendo un total de 220 DU en dos bloques (ver *Figura 1.6.b*). Las DU de ARCA tienen una altura aproximada de 700 m, la distancia entre ellas es de unos 90 metros y la distancia vertical entre DOM es de 36 m. El primer DOM se sitúa a 65 m de altura y la boya se distancia a 5 m del último DOM. Este diseño tiene como fin la detección de neutrinos cósmicos de muy alta energía (en el rango de TeV–PeV) [5]. La primera DU en ARCA fue instalada en diciembre de 2015 y actualmente cuenta con 19 DU desplegadas y operativas.

ORCA ocuparía un volumen de 0.018 km^3 en un espacio apropiado por 120 DU en un único bloque (ver *Figura 1.6.c*). Las DU de ORCA tienen una altura aproximada de 190 m, la distancia entre ellas es de unos 20 metros, mientras que la distancia entre DOM de una misma base es de unos 9.5 m. El primer DOM se sitúa a 25 m de altura y la boya se distancia 5 m del último DOM. ORCA está diseñado para la detección de neutrinos atmosféricos en el rango de 3–100 GeV [6]. La primera DU en ORCA fue instalada en febrero de 2019 y hasta ahora cuenta con 11 DU operativas.

Con KM3NeT completado se estima tener una cobertura amplia del cielo, permitiendo cierta superposición en el plano del centro galáctico. El centro galáctico en sí es visible principlalmente desde el hemisferio norte [7].

Este tipo de detectores que registran grandes cantidades de datos están programados para analizar casi en tiempo real la información recolectada y desechar todo aquello que no supere cierto nivel umbral de interés. En KM3NeT el Trigger and Data Acquisition System (TriDAS) se usa para ejecutar algoritmos de activación y los Data Writers (DWs) para escribir datos en la Base de Datos (DB), así las señales sin procesar registradas por cada sensor se analizan prácticamente en tiempo real y no se requiere un almacenamiento masivo para ellas. Cuando el umbral es superado por varios sensores a la vez, se activa el TriDAS y se guarda la información de este evento. Cuando se habla de superar el umbral, no únicamente se refiere a un sólo parámetro, si no que se pueden evaluar diversos (cada uno formará un "cut" diferente). Así que es muy importante optimizar cada "cut" y tener calibrados todos los sensores. Los detectores de KM3NeT están conectados a unas granjas computacionales en la costa para el rápido procesado de estos datos. La preparación y recolección de datos de ARCA y ORCA se organiza en periodos llamados RUNs, almacenando en sus respectivos ficheros los datos de interés convenientemente organizados para facilitar el análisis posterior.

1.1.3 Otros telescopios submarinos

El mayor inconveniente de los telescopios submarinos de neutrinos es la dificultad de su instalación, seguimiento y puesta a punto. No obstante, las aguas profundas permiten la interacción de neutrinos para detectar la radiación de Cherenkov de forma protegida de los rayos cósmicos (reducción considerable de los eventos). Además, el fondo marino tiene mucho espacio libre donde se pueden construir enormes infraestructuras de este tipo. Por todas estas razones, actualmente existe gran interés en el proceso de desarrollar y explotar este tipo de infraestructuras. La comunidad científica está entusiasmada con

estos telescopios, no sólo para detectar neutrinos, sino también como una forma de contribuir al desarrollo de las tecnologías secundarias involucradas y la importancia de ser capaz de estudiar el cosmos. Desde finales del siglo pasado, se han llevado a cabo diversos experimentos que han demostrado la viabilidad de este tipo de telescopio en el estudio de neutrinos: Baikal Deep Underwater Neutrino Telescope (BDUNT) en el lago Baikal [8, 9], Antarctic Muon And Neutrino Detector Array (AMANDA) en el Polo Sur [10] o NEutrino Mediterranean Observatory (NEMO) y Neutrino Extended Submarine Telescope with Oceanographic Research (NESTOR) en el Mar Mediterráneo [11, 12]. En base a los resultados prometedores de todos ellos, el próximo paso fue desarollar la construcción de telescopios más grandes de este tipo en dichas ubicaciones: Baikal Gigaton Volume Detector (BAIKAL-GVD) [13], IceCube [14] y Astronomy with a Neutrino Telescope and Abyss environmental RESearch (ANTARES) [15].

KM3NeT ya pertenece a la nueva generación de este tipo de detectores. ANTARES ha sido desconectado (12 de Febrero de 2022) después de más de 15 años operando, dado que se había completado su vida útil y ARCA y ORCA empezaban a superar sus capacidades. BAIKAL-GVD pretende ampliarse hasta el kilómetro cúbico e IceCube ha aprobado su próximo plan de crecimiento y llegar a cubrir hasta 10 km^3. Además existe un experimento reciente llamado Pacific Ocean Neutrino Experiment (P-ONE) para la construcción de un nuevo detector en el Océano Pacífico Norte [16] (ver *Figura 1.7*).

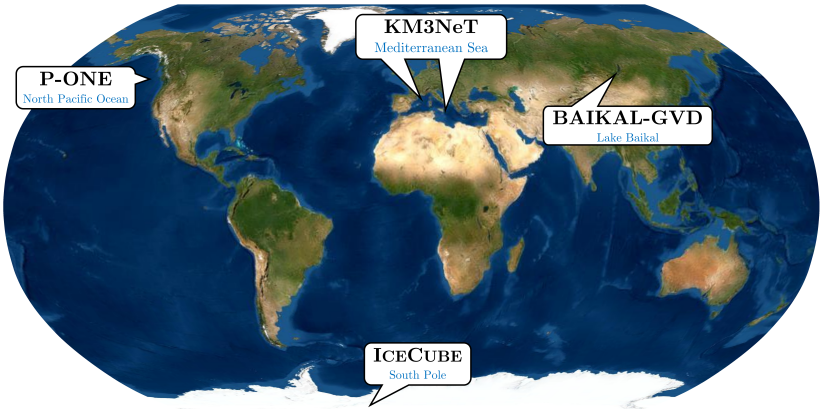

Figura 1.7: Detectores submarinos de neutrinos en funcionamiento y desarrollo en el mundo.

Todos estos telescopios (KM3NeT, BAIKAL-GVD e IceCube) conforman la Global Neutrino Network (GNN), la cual tiene como objetivo una colaboración más estrecha y una estrategia coherente entre los proyectos de telescopios de neutrinos.*

1.2 Sistema de Posicionamiento

Como se ha comentado anteriormente, una DU en KM3NeT consiste en un par de cables sujetos al fondo del mar en posición vertical por la flotabilidad de una boya superior y la propia de cada DOM. Así pues, la DU queda expuesta al efecto de las corrientes marinas que alteran la forma de la línea y los DOM permanecerán inclinados respecto a su posición. Si se desconoce la posición y orientación de los DOM a la hora de detectar una partícula, será imposible ubicar el evento en el espacio y mucho menos reconstruir su trayectoria para estimar la localización de su origen. Por ello, KM3NeT cuenta con un sistema de posicionamiento, con el objetivo de controlar la situación de los DOM en cada momento. KM3NeT usa un Sistema Acústico de Posicionamiento (APS) para localizar el sensor piezoeléctrico que hay en cada DOM. Además, cada DOM cuenta con una brújula y un inclinómetro, formando un Sistema de Referencia de Actitud y Rumbo (AHRS) el cual indica el valor de la guiñada, cabeceo y balanceo, facilitándo la orientación del DOM. Como se verá en la Parte I de esta tesis, una combinación de ambos es lo que se usa para monitorizar la posición de cada PMT.

1.2.1 Las propiedades del entorno

Antes de instalar KM3NeT se llevaron a cabo muchas medidas que validaron el entorno para ARCA y ORCA. Son entornos tranquilos donde raramente se registran picos de corriente superiores a 7 cm/s, aún así estas corrientes mantienen las DU en constante movimiento y alejadas de su posición natural que correspondería a la línea (totalmente en vertical).

ARCA está instalada en la zona donde en su día estuvo European Multidisciplinary Seafloor Observatory (EMSO) Western Ionian Sea, un Módulo de Interfaz Instrumentada (MII) con diferentes sensores que monitoreaba (entre otros) el estado de la corriente marina. La *Figura 1.8* muestra las velocidades de corriente tomadas por este Perfilador Acústico de Corrientes Doppler (ADCP). Se observa que el 93 % del tiempo en ARCA, las corrientes son inferiores a 6 cm/s, siendo el 24 % menores a 3 cm/s.

*https://www.globalneutrinonetwork.org/ [Consulta: 2022-07-13]

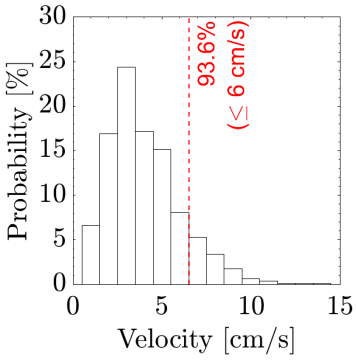

Figura 1.8: Velocidades de la corriente marina en la ubicación de ARCA. Datos extraídos en el periodo de 2001–2004 y 2007–2009 [17].

Actualmente, ORCA comparte ubicación con EMSO Ligure Ouest [18]. La *Figura 1.9* muestra los datos de corriente tomados durante un año por este ADCP. Esto demuestra como el 90 % del tiempo en ORCA las corrientes son inferiores a 7 cm/s, siendo el 19 % menores a 3 cm/s.

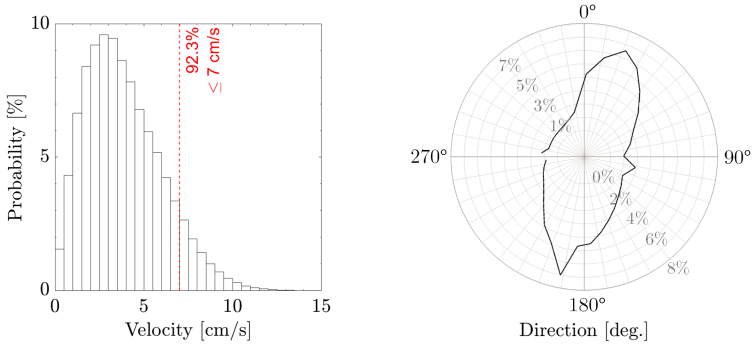

(a) (b)

Figura 1.9: Propiedades de la corriente marina en ORCA durante un año (del 15 de noviembre de 2020 al 15 de noviembre de 2021) proporcionados por EMSO Ligure Ouest. **(a)** Velocidad de la corriente marina. **(b)** Dirección de la corriente marina respecto al Norte (0 grados).

1.2.2 El Sistema de Posicionamiento Acústico (APS)

El APS de KM3NeT consta de tres partes principales: los emisores, los receptores y el Filtro de Datos Acústicos (ADF). Los emisores son AB que se instalan en una posición fija y conocida. Los receptores son los piezocerámicos instalados en cada DOM (siempre en movimiento) y los hidrófonos en cada base de DU (fijos). El ADF se encarga de procesar los datos que registra cada receptor y guarda aquellos parámetros de interés. El *Capítulo 2* describirá el APS capaz de posicionar el sensor piezocerámico existente en cada DOM.

El ADF es la parte de TriDAS que realiza el análisis de los datos acústicos sin procesar, por ahora su trabajo principal es determinar y guardar en la DB el Tiempo de Llegada (ToA) y su amplitud en forma de Factor de Calidad (QF) de las señales emitidas por cada AB. Además, también se usa para programar el registro entre un intervalo específico de tiempo y grabar las señales sin procesar directamente de los receptores. El sistema de generación de reloj KM3NeT funciona con un reloj de señal interno de 25 MHz [19], por lo que controla la marca de tiempo de las señales acústicas grabadas. Los receptores graban con una frecuencia de muestreo f_s de 195.3125 kHz ($25MHz/2^{8_{bits}-1}$), por lo que pueden usarse para estudiar señales de frecuencia inferior a unos 100 kHz. En el *Capítulo 5* se analizan las señales directamente grabadas por los hidrófonos de KM3NeT.

1.2.3 El Sistema de Referencia de Actitud y Rumbo (AHRS)

El AHRS de KM3NeT usa la información de la brújula e inclinómetro instalados en cada DOM para conocer su guiñada, cabeceo y balanceo. Con su orientación se puede saber la posición exacta de cada PMT relativa al centro del DOM. El *Capítulo 3* explicará cómo conocer la orientación del DOM a partir de la información del AHRS. Además, desarolla una combinación de APS y AHRS para ajustar el perfil de la línea de la DU usando un Modelo Mecánico (MM).

1.3 Detección Acústica de Neutrinos

Cuando un neutrino de ultra alta energía interactua en el agua, produce una cascada de partículas de forma cuasi instantánea, provocando un pequeño calentamiento en esa región del fluído, ocasionando una pequeña señal acústica. Esta señal creada por el cambio de temperatura del agua instantáneamente, tiene unas características peculiares. En este apartado se comentará dicha señal y las posibilidades de ser detectada de forma experimental.

Los detectores de neutrinos acuáticos diseñados hasta ahora usan tecnología óptica para detectar la luz de Cherenkov. Tal y como se observa en la *Figura 1.10*, por razones físicas de la atenuación de la luz en el agua están limitados a la detección de neutrinos de hasta 100 PeV. Hay estudios que estiman la posibilidad de detectar neutrinos de más alta energía con otro tipo de tecnología (acústica, radio...) si se monitorizara un enorme volumen [20].

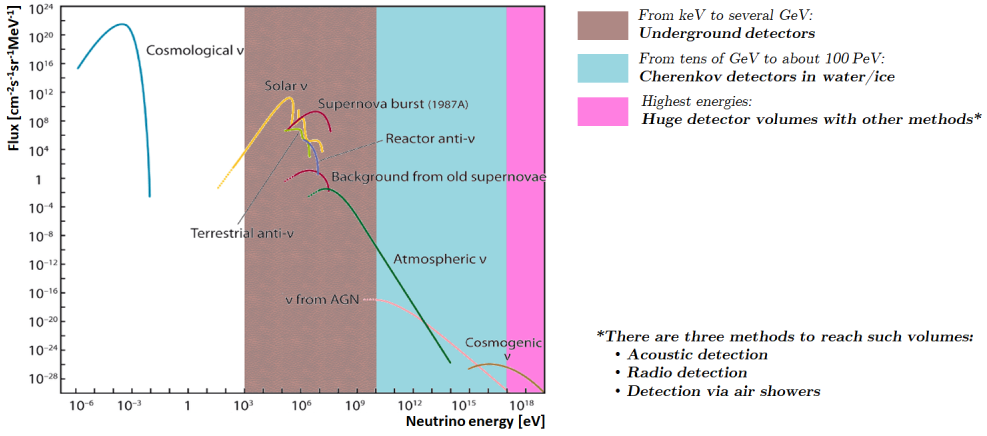

Figura 1.10: Flujos medidos y esperados de neutrinos naturales y de reactor. El rango de energía de keV a varios GeV es del dominio de los detectores subterráneos. La región de entre decenas de GeV y alrededor de 100 PeV, con flujos mucho más pequeños, está cubierta por detectores de luz de Cherenkov bajo el agua y en el hielo. Las energías más altas sólo son accesibles con detectores de enorme volúmen y distinta tecnología [20].

1.3.1 Pulso bipolar

La señal que deja la interacción de un neutrino en el agua es realmente peculiar ya que presenta una estrecha directividad teniendo en cuenta las frecuencias que la componen. Al sobrecalentar el agua en instantes de tiempo tan cortos, se produce un Pulso Bipolar (BP) termoacústico [21]. Este representa la compresión (pico positivo) y decompresión (pico negativo) del medio durante la cascada de partículas que se genera tras la interacción (ver *Figura 1.11.a*). La energía de la cascada se distribuye en una especie de cilindro de unos 10 cm de diámetro y entre 5 y 10 metros de longitud. Esta cascada va a tener componente electro-magnética y componente hadrónica, y producirá su expansión en forma de cilindro a su alrededor, lo que propagará el BP perpendicularmente a la cascada con un patrón muy directivo [22, 23].

El hecho de que los detectores hayan de poseer enormes dimensiones es favorable a la detección acústica, ya que las señales ultrasónicas en el agua tienen menor atenuación en comparación con la óptica. Aunque la dificultad de capturar una de estas señales no sólo reside en el amplio componente frecuencial que dificulta su identificación o su estrecha directividad, sino también en su corta duración (la distancia entre picos del BP se estima de alrededor de los 10 μs), la cual requiere un sistema con una frecuencia de muestreo capaz de capturar la forma del BP.

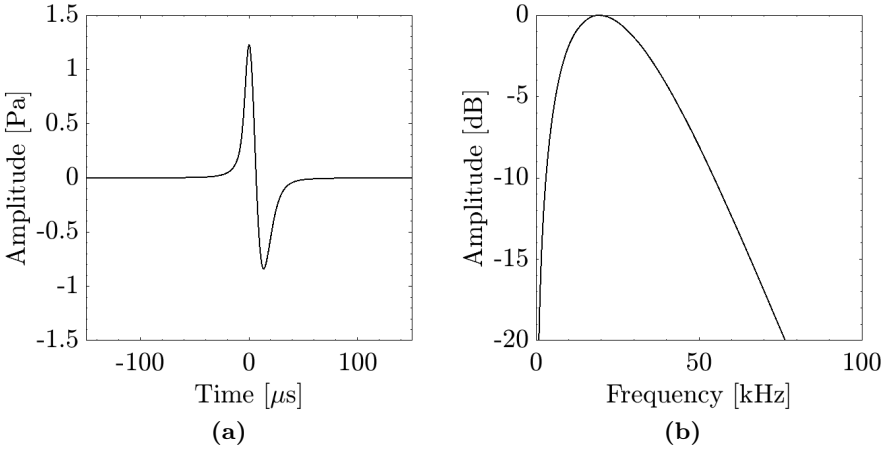

Figura 1.11: Señal acústica resultante de la simulación de una cascada hadrónica de partículas de $5{\cdot}10^{11}$ GeV (donde la partícula primaria cósmica es un protón) [22]. La señal se recibiría a 1 km de distancia y a una profundidad de 6 m a lo largo del eje de la cascada (lo que correspondería a 0^o del plano del haz acústico). **(a)** Señal en el dominio del tiempo. La distancia entre picos es de 14 μs **(b)** Señal en el dominio de la frecuencia. La caída de -6 dB se produce entre los 5.2 y 44.8 kHz.

Según la información de la *Figura 1.11.b* este BP podría ser registrado por los receptores acústicos del APS en KM3NeT, siendo la motivación principal de la Parte II de la tesis.

1.3.2 Calibración y detección

La calibración de un sistema acústico en recepción proporciona información sobre la capacidad de registrar ciertas señales. Si además esta se realiza "in situ", los datos proporcionados serán mucho más fiables, ya que tendrán en cuenta el ruido de fondo del ambiente donde esté operando. Las calibraciones necesitan que un sensor figure como referencia, es decir, uno que haya sido calibrado previamente (método calibración directa [24]).

Para estudiar si un sistema acústico como el APS de KM3NeT podría servir para la detección acústica del neutrino, debe ser calibrado *in situ*. El *Capítulo 4* presenta un array diseñado y desarrollado para dicho cometido, capaz de emitir señales desde el barco al detector. Además, este capítulo expone una calibración completa dividida en tres pasos (de menor a mayor dificultad): *Emisión Lineal*,

para conocer la respuesta en frecuencia. *Emisión Paramétrica Larga*, para estudiar su directividad. *Emisión Paramétrica de BP*, para saber si es capaz de capturar el tipo de señal producida por la interacción de un neutrino en el agua.

Acerca de la *Emisión Paramétrica*, es necesario comentar que es una técnica de la acústica no lineal que permite propagar bajas frecuencias de forma directiva [25, 26]. Se origina al emitir con intensidad dos tonos cercanos de alta frecuencia. Al propagarse estos tonos por un medio como el agua, aparecen no linealidades que provocan frecuencias fruto de su combinación. Una de ellas es la frecuencia diferencia (baja frecuencia) que adquire las características directivas de las altas frecuencias originarias, es decir que, a pesar de ser una señal de baja frecuencia se propaga con la directividad de los tonos emitidos. Es por ello que esta frecuencia diferencia se usa para conseguir señales muy directivas que en el campo de la acústica lineal no sería posible.

Para aprovechar el APS de KM3NeT y usarlo también para la detección acústica de otras señales que no fuese la de los AB (en este caso el BP por la posible interacción de un neutrino) se necesitaría reprogramar el ADF para este cometido y dejar constancia de un posible evento de interés y así estudiarlo con más detalle en un post procesado. De esta manera, en el *Capítulo 5* se propone un primer algoritmo de activación para la detección de BP.

Part I

KM3NeT Positioning System

Chapter 2

The Acoustic Positioning System of KM3NeT

The Acoustic Positioning System in KM3NeT consists of Acoustic Beacons, Digital Acoustic Receivers (hydrophones and piezoceramic sensors), and the Acoustic Data Filter that determines the Time of Arrivals for each recorded emission and registers them in the Data Base. All this is necessary to monitor the movement of the Digital Optical Modules. In addition, different analyses are presented to study the detection and estimation of the amplitude of a signal, as well as the attenuation and propagation. These analyses are used to characterize the Acoustic Beacons in a laboratory (power, directivity, and delay measurements) and to decide their posterior deployment in the detector. Finally, a basic process to check the sensitivity of an emitter-receiver system in situ is also proposed.

Section 2.1 presents each element of the APS in detail and explains how it works. *Section 2.2* presents the complete production and characterization of an AB in the laboratory. For this purpose, different signal analyses are described, some of which are used in *section 2.3* to study the propagation of a signal and to design the ideal position of an AB in the detector. In addition, in *section 2.4* a basic test to know the sensitivity of the emitter-receiver system once installed is proposed. And finally, in *section 2.5* the trilateration process to position the piezoceramic sensor in every DOM is presented.

Due to the currents on the seabed where KM3NeT is built, the lines of the Detection Units (DUs) are in constant movement. This phenomenon means that the Digital Optical Modules (DOMs) are not completely vertically aligned, and it is, therefore, necessary to monitor their position and orientation. This is of vital importance for the neutrino telescope since, by knowing the location of its detectors, the trajectory of the detected neutrino can be reconstructed. So, if the DOM positioning is known using the Acoustic Positioning System (APS) and the orientation is provided by the Attitude and Heading Reference System (AHRS), it is possible to know the position in space of each Photomultiplier Tube (PMT). As Global Positioning System (GPS) signals reach only a few meters into the water due to their rapid attenuation, the most accurate solution is to set up an APS.

An APS consists of a network of acoustic sensors spread over a known location that aims to detect the position of another acoustic sensor (of unknown position, e.g. in movement). Usually, the trilateration method is used to find out the unknown position [27, 28]. The known position sensors must be of the same type (receivers or emitters) and the sensor to be located should be analogous. This is because the trilateration method is based on the arrival times of the emitted signal. For trilateration to work, a minimum of three sensors of known location is required, and as the number of sensors increases, the more accurate detection will be, so a minimum of four sensors is commonly used for redundancy [29].

2.1 Acoustic system sensors and operation

The APS in KM3NeT contains piezoceramic sensors as receivers in each of the DOMs and distributes fixed Acoustic Beacons (ABs) as emitters on the seabed. It will work as follows: the ABs emit a known signal which is received by the piezoceramic sensor, and the system records the Time of Arrival (ToA). When at least three ToAs are registered from different ABs, the position of the receiver can be triangulated. The APS also includes a hydrophone installed in each APS base.

The acoustic receivers in KM3NeT are always passively "listening": they record the signal in a buffer, the Acoustic Data Filter (ADF) analyses it, and the parameters of interest are saved. Due to the large amount of memory these signals occupy, it is not possible to store raw data continuously, so it is important that the ADF only records the data of greatest interest.

The acoustic emitters in KM3NeT are programmed to manage their emission, either autonomously or via a trigger (*autonomous AB* or *triggered AB*). In the case of autonomous emission, the duty cycle is known, but not the Time of Emission (ToE).

2.1.1 Acoustic Beacons (ABs)

The AB is a broadband range acoustic emitter from 20 kHz to 60 kHz and the power of emission is managed by the Capacitor Voltage Charge (CVC). It is able to generate any signal such as sine (tone), sweep, MLS, or even preload a user-configured signal. Although the APS uses sweeps up to 5 kHz, given its propagation and easy detection. An AB weighs between 10 and 12 kg, depending on the encapsulation material (aluminium or titanium), and is about 57 cm long and 10 cm in diameter. It has three main parts: the Sound Emission Board (SEB), the Free Flooded Ring (FFR) transducer, and its cylindrical vessel (see *Figure 2.1*). Their current purpose is to work on the APS of KM3NeT as Long Baseline (LBL), and they are installed vertically in fixed positions of the seabed.

Figure 2.1: AB in aluminium 3D scheme.

Figure 2.2 shows the digital signal loaded into the SEB of the AB3 for their emission.

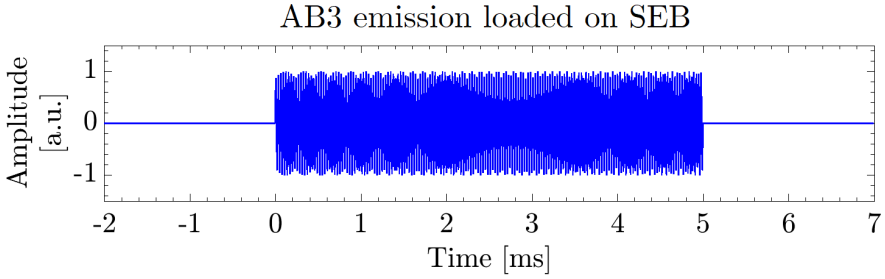

Figure 2.2: A sweep of 5 ms from 34 to 36 kHz loaded on the SEB for AB3.

2.1.2 Digital Acoustic Receivers (DARs)

There are two types of Digital Acoustic Receivers (DARs) in KM3NeT, hydrophones (external) and piezoceramic sensors (internal). On the one hand, the hydrophones (see *Figure 2.3.a*) are mounted in the DU bases and remain fixed, while the piezoceramic sensors (see *Figure 2.3.b*) are glued to the glass sphere of each DOM from the inside.

(a) **(b)**

Figure 2.3: **(a)** External DAR: Hydrophone DG0330. **(b)** Internal DAR: Pz27 piezoceramic sensor encapsuled.

External DARs: Hydrophones

The main purpose of the hydrophones in KM3NeT is to position the DU base and/or the triggered ABs. Also to give variety to the type of sensors for acoustic monitoring studies at sea. They have a wide (and flat) frequency response and higher sensitivity than piezoceramic sensors. As they remain fixed and data processed from a PC farm onshore, they provide an excellent opportunity for bioacoustics, ship noise monitoring, environmental noise control, acoustic neutrinos detection, etc. At the moment, they are essential for the APS, since the only ABs installed are *autonomous*: if the distance between them is known and the ToA is recorded on the hydrophone, the ToE can be known (which is critical for the trilateration of moving acoustic receivers).

Figure 2.4 shows the AB3 emission recorded by a hydrophone in ORCA.

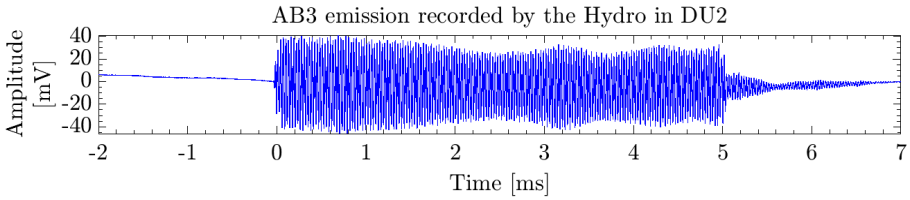

Figure 2.4: A captured sweep of 5 ms from 34 to 36 kHz emitted by the AB3 and received by the hydrophone in DU2.

The hydrophone is a DG0330/DG1330 designed and manufactured by CO.L.MAR company for the KM3NeT project. There are two different hydrophone versions, without and with an analog high-pass filter signal stage of 700 Hz, to reject the low frequency ambient sea-noise. It is omnidirectional, works in the 5–90 kHz range with 24 bits of resolution, and it has two channels (the first channel has +26 dB gain and the other one has +46 dB gain). Two channels are to avoid signal saturation in case there is AB installed near it. The Received Voltage Response (RVR) is around -176 dB (re 1 V/μPa at 1 m) in the first channel and -156 dB (re 1 V/μPa at 1 m) in the other channel at 5 kHz [30].

Internal DARs: Piezoceramic sensors

The cost of the piezoceramic sensor is low and its size is small, which is convenient for having one in each DOM. The ceramic material is a Pz27, manufactured by Ferroperm. It is in an aluminium capsule with the pre-amplifier board, the Analog-to-Digital Converter (ADC) AD7764BRUZ-TSSOP28, produced by Analogue Devices and glued to the glass of the DOM facing downwards. The RVR is -160 $\pm$ 6 dB (re 1 V/μPa at 1 m) in the 10-70 kHz range [31]. Continuous waveforms, such as tones, are well understood, but the response to transients shows complex waveforms. There are a number of resonance frequencies and the amplitude depends on the position of the source with respect to the DOM [32].

Figure 2.5 shows the AB3 emission captured by a piezoceramic sensor in ORCA.

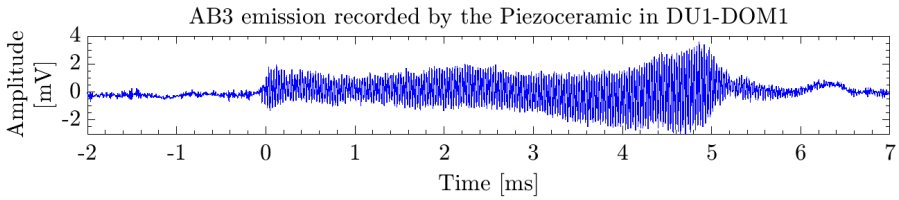

Figure 2.5: A captured sweep of 5 ms from 34 to 36 kHz emitted by the AB3 and received by the piezoceramic in DU1-DOM1.

2.1.3 The Acoustic Data Filter (ADF)

Regarding ToA registration, the ADF analyzes the recorded signals every 5 seconds (in a buffer). It performs a correlation for each expected signal of the installed ABs (linear sweeps from 2 to 5 kHz of broadband) and records its maximum peak amplitude, the Quality Factor (QF), together with its ToA in the KM3NeT Data Base (DB). *Figure 2.6.a* displays the spectrogram of the AB3 emission displayed in *Figure 2.2*. It can be clearly seen how the sweep initializes at one frequency and it is increasing during the 5 ms of the signal. In the spectrograms of the received signal (experimental data), the AB3 sweep is also distinguishable: in *Figure 2.6.b* it is recorded by a hydrophone, and in *Figure 2.6.c* by a piezoceramic sensor. In both cases, there would be no confusion when distinguishing them from other emissions (AB1 and AB2), despite less piezoceramic sensor quality

The ADF identification of the emitted AB signal in the record is also clearly distinguishable by the higher QF. *Figure 2.7* shows the ToA and the QF value recorded by the piezoceramic sensor on last DOM for a DU of ORCA during 25 minutes. The pulse train of the AB emissions (every 10 minutes) is clearly distinguishable. Everything below the dotted line (the dotted line represents the 70% of the maximum valid QF) is invalid data: high QFs are seen between signals that do not correspond (AB3 in AB2 emissions or AB1 and AB2 in AB3 emissions), although always the highest peak clearly identifies the emitter, and there are even peaks in the case of hydrophones corresponding to the signal reflected on the floor (much lower than the direct signal). Currently, it is being discussed whether to force a dynamic threshold level for each receiver and reduce the low quality or noise signals considerably.

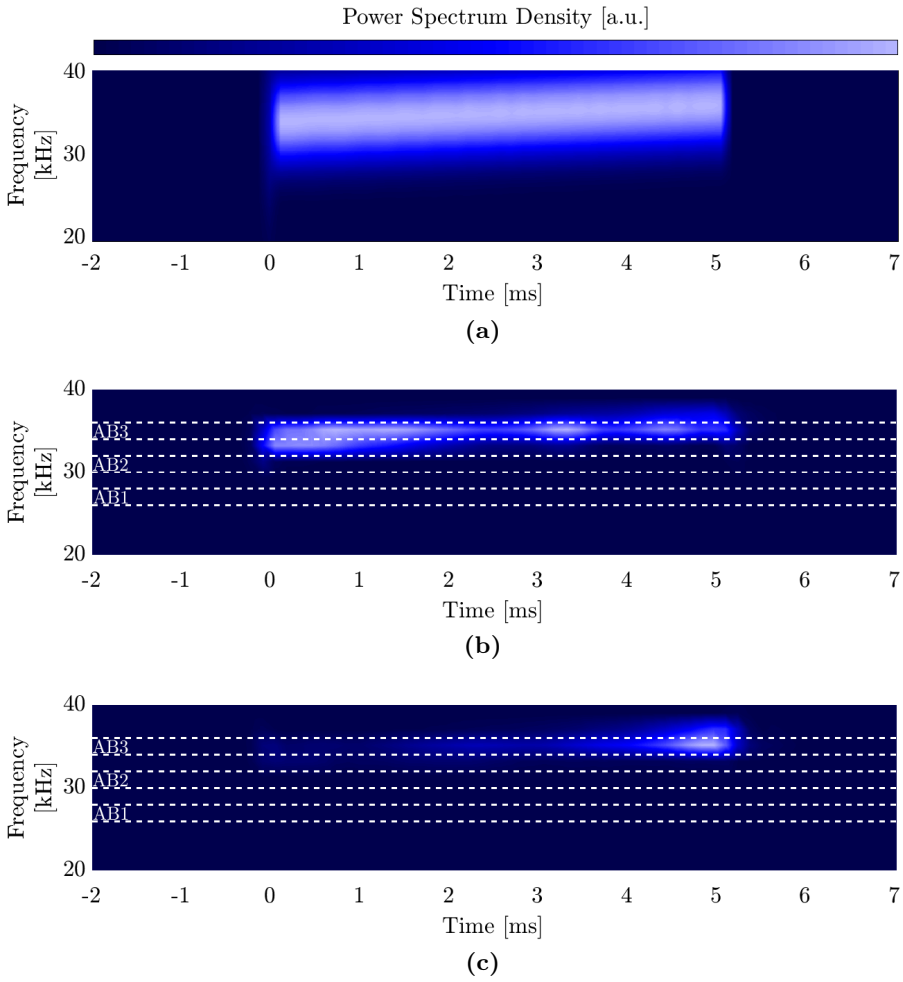

Figure 2.6: **(a)** Spectrogram of the signal displayed in *Figure 2.2* (emitted by the AB3). **(b)** Spectrogram of the signal displayed in *Figure 2.4* (recorded by a hydrophone). **(c)** Spectrogram of the signal displayed in *Figure 2.5* (recorded by a piezoceramic).

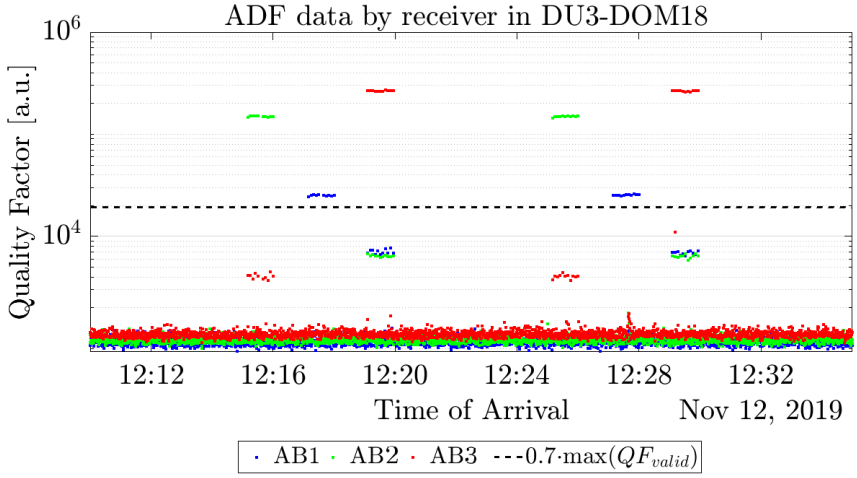

Figure 2.7: ADF data on DU3-DOM18 of ORCA. The data shows the ToAs registered on the DB. The dashed line marks the difference between the ToA of an AB emission and disposable ToA.

On the other hand, *Figure 2.8* shows how the ToA of the same AB3 emission is recorded. It is plotted on a logarithmic scale to show how the same signal arrives one by one at each DOM. As it will be seen at the end of this chapter, the work of capturing the ToAs is crucial for positioning each piezoceramic sensor.

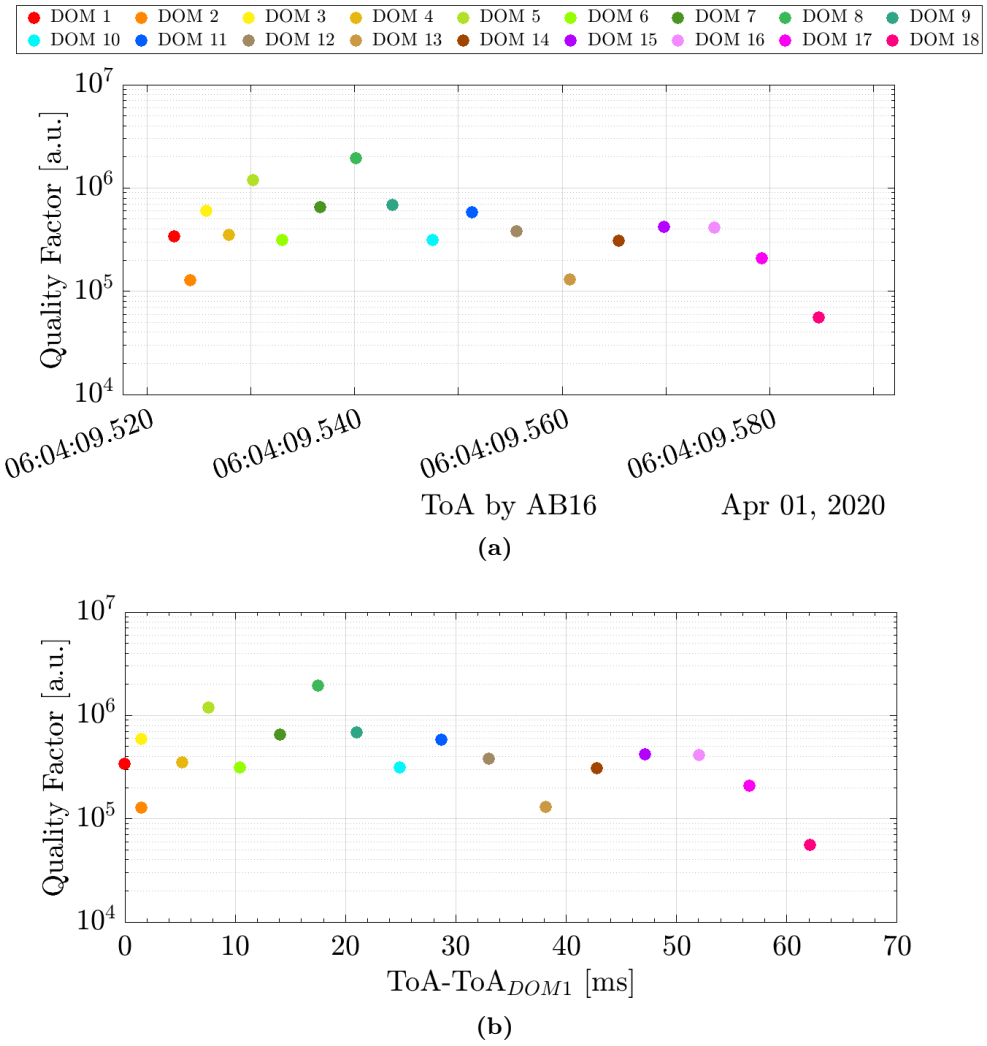

Figure 2.8: **(a)** Registration of an AB3 emission received by all piezoceramic sensors in ORCA-DU11. **(b)** ToAs relative to the one registered in the first DOM.

2.2 AB production and characterization in laboratory

The design and production of the ABs has been done in a collaboration between the *Astroparticle Physics* research group of Universitat Politècnica de València (UPV) and the Mediterráneo Señales Marítimas, S.L. (MSM) company. The electronic board design arises from a PhD thesis [33], but the transducer moulding, connectors, and mechanics are responsability of the company. Each newly produced AB is calibrated and characterized in the UPV laboratories before it goes into operation. In addition, they usually undergo a pressure test in Hiperbaric, S.A. to check that they can withstand 4000 m.a.s.l.

The SEB generates the wave to emit, controls its power, and it can manage the recording for received signals [34]. The signal modulation is done using the Pulse-Width Modulation (PWM) technique which permits the emission of arbitrary intense short signals. The PWM sampling frequency is 400 kHz [35]. The SEB is connected to a commercial transducer FFR SX30 manufactured by Sensor Technology Ltd, and moulded by McArtney company.

2.2.1 Ultrasound transducer

The transducer FFR SX30 used for the AB is a cylindrical ring (see *Figure 2.9.a*) of 2.54 cm x 4.47 cm x 1.88 cm (height x outer diameter x inner diameter). Its resonance frequency is 30 kHz, and it has a Transmitted Voltage Response (TVR) of 133 dB re 1μPa/V at 1m (see *Figure 2.10.a*) with omnidirectional directivity in the radial plane and toroidal in the axial plane (see *Figure 2.10.b*) [36]. In order to attach the transducer to the AB to use it at deep-sea, it is moulded and prepared, which consists in changing the connectors and adding a backing (see *Figure 2.9.b*).

(a) **(b)**

Figure 2.9: **(a)** Four FFRs SX30 newly acquired, before moulded. **(b)** The FFRs SX30 after moulded, ready to be mounted on the AB.

The moulding can affect the resonance frequency and the admittance of the transducer, for this reason, the electrical impedance Z and the admittance Y are measured before and after moulding (see *Figure 2.11*). These values will influence the performance of each source and it is important to ensure that the coupling between SEB and FFR is not negatively affected.

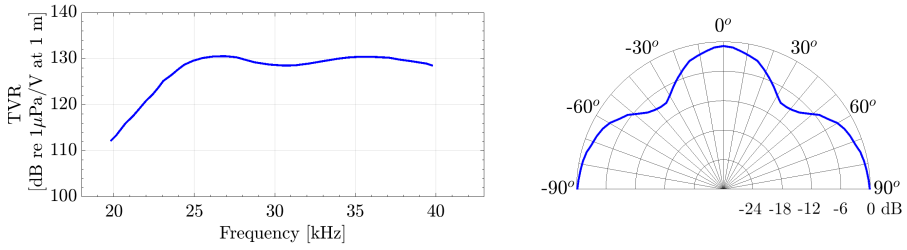

(a) **(b)**

Figure 2.10: The technical specifications provided by the manufacturer. **(a)** Emission sensitivity, TVR. **(b)** Radial plane directivity.

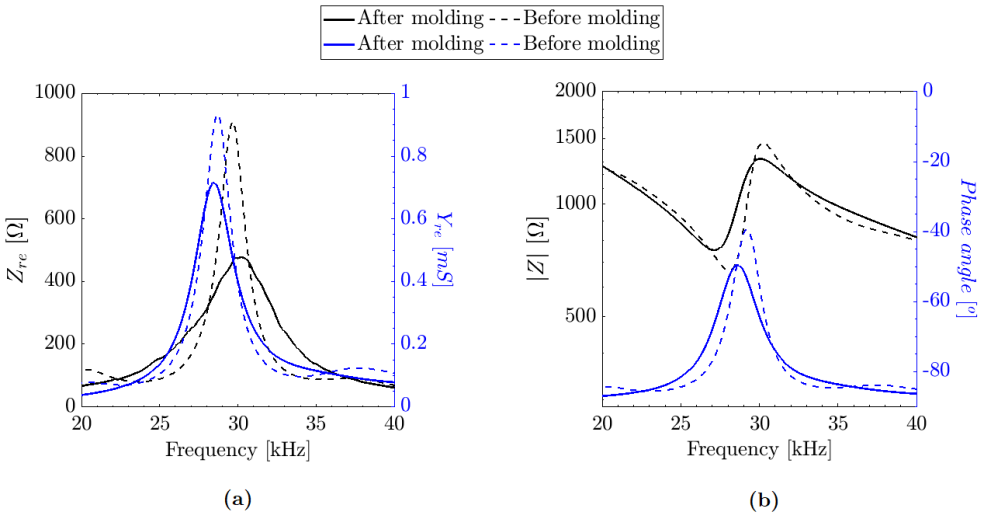

Figure 2.11: Measurement of the same FFR with the HIOKI IM3570 Impedance Analyzer, before and after moulding. **(a)** The real impedance Z_{re} and the real admittance Y_{re} to observe the antiresonance and resonance frequencies (respectively). **(b)** The module of impedance and the phase angle.

2.2.2 AB characterization

The final step in the production of an AB is its characterization, which consists of a series of measures to test and evaluate its performance before its use. The characterization process for a source is higly significant, since it indicates the quality, the power, and the functionality of the device. In Gandia's UPV Campus, the Institut d'Investigació per a la Gestió Integrada de Zones Costaneres (IGIC) has a tank and a pool which have a three-dimensional measurament system to characterize acoustic sensors, and it is where the ABs are measured. The characterization includes its power, directivity, and response delay. For this purpose, a series of measurements will be made, and these will be analyzed in order to be able to represent the characteristics of the AB. The measurements, their post-analysis, and the results for a specific AB are explained in this section.

The operation of an AB is simple: to turn it on you only have to supply it with 12 V. Then, with an RS232 connection and using a few commands you can configure and operate it. First, you configure the working emission mode, autonomous mode (it will wait for a duty cycle), trigger mode (it will wait

for a trigger signal), or manual mode (it will wait for a command). Then, the capacitor is charged according to the desired power (CVC). Finally, the type of signal to be emitted is indicated (or you can charge one) [37].

Experimental framework

To characterize acoustic sensors in emission and/or reception we use a PCI eXtensions for Instrumentation (PXI) terminal (NI PXI-1031). It has an arbitrary waveform generator with an output Digital-to-Analog Converter (DAC) channel resolution of 14 bits (NI PXI-5412) and a Data Acquisition (DAQ) system 8-Bit Digitizer with two channels (NI PXI-5102). This system permits emitting and recording synchronized with a sample frequency, f_s, until 20 MHz, so the idea is to generate a signal with the AB and record it with a calibrated hydrophone (in our case, a Teledyne RESON Hydrophone TC4034). Then, a post-analysis of this record allows obtaining the characterization parameters.

Once the experimental system is set and the AB configured, once triggered, the transducer is fed with the signal in voltage (V_{in}), which will convert it to a pressure signal (P_{out}) and propagate it through the medium, in this case, water. Once it arrives at the hydrophone, the pressure signal (P_{in}) is reconverted into an electrical signal (V_{out}). In the end, this is a DAC-ADC active acoustic system (see *Figure 2.12*). It should be noted that the V_{in} to P_{out} conversion will depend on the transmit sensitivity of the emitter transducer, the TVR, while the P_{in} to V_{out} conversion will depend on the receive sensitivity of the receiver transducer, the RVR.

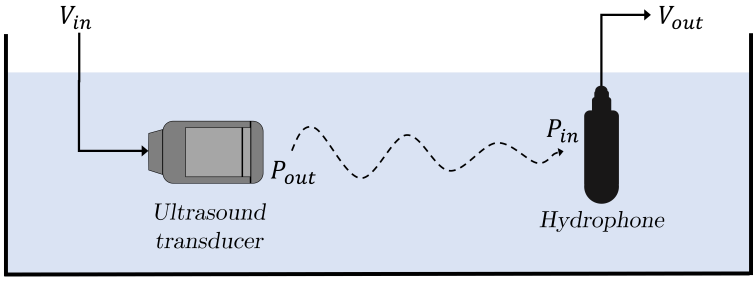

Figure 2.12: Sketch showing voltage and sound pressure values in a common acoustic active system setup DAC-ADC.

It is essential to consider the position of the hydrophone, which must be controlled relatively to that of the source. In our experiments, the hydrophone will be mounted on a motorized axis and will be moved in the axial plane of the AB (see *Figure 2.13.a*). This way, the Emitter-Receiver distance (distER) and the angle from the source are controlled. *Figure 2.13.b* shows a picture of an AB ready to measure in the tank and *Figure 2.13.c* is another in the pool.

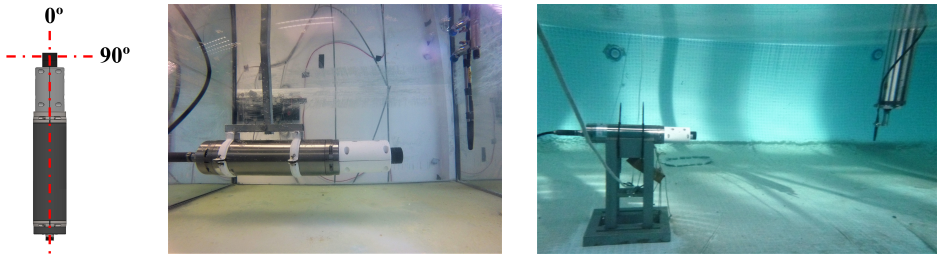

(a) **(b)** **(c)**

Figure 2.13: **(a)** Top view of hydrohphone position in AB measurament. **(b)** AB ready to measure in the tank of IGIC with hydrophone at 0 degrees. **(c)** AB ready to measure in the pool of IGIC with hydrophone at 0 degrees.

Before measuring any acoustic emitter, the characteristic distances of the transducer should take into account the near-field distance, L_r (distance at which notable non-linearities appear), and far-field distance, L_R (distance from which its use is recommended). For reliable measurements, therefore, one should always try to go beyond far-field. These distances depend on the frequency to be emitted and the radiating surface of the sensor. *Equation 2.2* estimates the far-field distance for a circular piezoceramic flat surface [38].

$$L_r = \frac{a^2}{\lambda} = \frac{a^2 f}{c} \tag{2.1}$$

where a is the radius of the surface, λ is the wavelength, which depends on emitted frequency f and sound speed propagation c.

$$L_R = \pi \cdot L_r \tag{2.2}$$

In the case of the transducer in an AB, some approximation can be attempted if the radiating surface is assumed to be flat, with a radius of 4.47/2 cm. In this case the far-field for 30 kHz and a sound speed of 1500 m/s would be

3.14 cm. In any case, measurements are always taken as far away from the emitter as possible, but considering the presence of the first reflections. Thus, in the tank the distER is 20 cm, while in the pool is 1 m. Notice that the further away from the source, the lower the Signal-to-Noise Ratio (SNR) of the captured wave.

Analysis of signals

Once the measurements have been made, each of the recorded signals must be analyzed in order to study the parameters of interest. In this case, the recorded wave will consist of background noise and the signal emitted by the AB, which will appear in a ToA equivalent to the Time of Flight (ToF). Different ways to estimate the ToA and amplitude of the desired signal automatically will be outlined below [37]. Obtaining the ToA and amplitude of the received signals will allow the characterization parameters for the AB to be calculated. Furthermore, when characterizing a transducer, these parameters usually refer to a distance of 1 meter. Since the tank is measured at a distance of 20 cm, an amplitude propagation process will be necessary to estimate the received amplitude at 1 meter, also explained in this section.

ToA calculation: There are several methods to obtain the ToA of signals, with greater or lesser precision and always depending on the type of signal sought:

- Threshold method. It is a plain process that is based on detecting the moment when the presence of the signal appears above a decided level. This method requires a good SNR and a study of the emitted signal in order to determine an optimal threshold level (minimum signal level), as filtering is often necessary to ensure that the signal of interest is recorded more accurately.
- Power Variation (Pvar) method. It is a process that also requires a good SNR, and sometimes it needs filtering and has two variants, the "Pvar cumulative" and the "Pvar saw".
    - Pvar cumulative: This variant calculates the cumulative frequency of the absolute values of the recorded waveform and is called $pvar_{cumulative}$. It shows an increasing trend of the values, which will change slope as the signal to be detected appears. This can be raised by a factor to make the change of slope more abrupt and to find the ToA more easily (see *Figure 2.14.a*).

- Pvar saw: subtracts to the $pvar_{cumulative}$ the average value of the recorded waveform, giving a saw-type signal ($pvar_{saw}$) in which the contribution of background noise is taken into account, perhaps avoiding the need for filtering. The ToA of the signal corresponds to the first change of slope that occurs in the $pvar_{saw}$ (see *Figure 2.14.b*).

- Correlation method. This method studies the similarity between the emitted signal and the recorded waveform, generating the correlation signal [39]. The amplitude peaks will start to be higher when the two signals coincide, providing the ToA at its maximum peak. One difference with the methods mentioned above is that this method is effective at low SNR (and without the need for filtering), and gives better results with sweep signals.

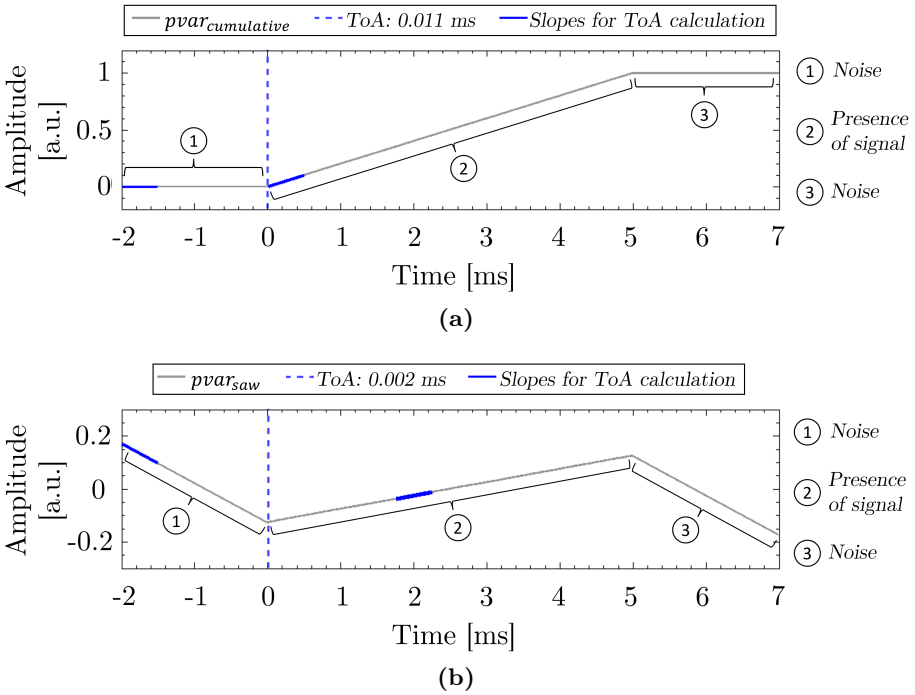

Figure 2.14: ToA calculation using the Pvar methods. The technique is applied to the signal in *Figure 2.2* with a 30 dB of SNR. The presence of signal and noise are noted. **(a)** Pvar cumulative. **(b)** Pvar saw.

Amplitude studies: Once the instant at which the signal arrives and the ToA receiver is known, its amplitude can be estimated. Three different methods are presented, and all of them giving the same value for an ideal signal (noise-free). Depending on the experimental case and the background noise, they will be some differences among them, but it is recommended to take all of them into account.

- Time. This analysis is the simplest, only the signal of interest is studied, where the offset is removed by subtracting its mean value, and then the peak amplitude is averaged.
- Frequency. It consists of transforming the signal of interest in the time domain to the frequency domain using the Fast Fourier Transform (FFT) and getting the amplitude value of the emitted frequency. This study is applicable to sinusoidal signals.
- Correlation. Using the peak value of the correlation signal (point of highest coincidence) in correlation units, it is possible to estimate the peak amplitude of the received signal expressed in volts [40].

Figure 2.18 shows two experimental examples where the amplitude is analyzed with these three methods. This is due to the fact that the ToA of the received signal has been previously calculated, and the study has been able to focus on the three intermediate cycles of the total five emitted (maximum stability).

Propagation effect It is possible to estimate the amplitude and shape of a signal propagated through any fluid. There are basically three attenuating effects that influence this process: spherical divergence (Div.), absorption (Abs.), and directivity (D.). The spherical divergence depends on the propagation distance, the absorption on the medium properties against the propagating wave, and the directivity on the receiver characteristics.

- Attenuated amplitude: Since the pressure (P_o) is a constant referenced to a distance (r_o), it is possible to estimate the pressure (P) at another point in the same space at distance r. As $\frac{A}{r}$ is the pressure amplitude of a wave, where A is a real constant [38]:

$$\left.\begin{array}{r} P(r) = \frac{A}{r}\ e^{-\alpha\ r} \\ P_o(r_o) = \frac{A}{r_o}\ e^{-\alpha\ r_o} \end{array}\right\} \Rightarrow P(r) = \frac{P_o\ r_o\ e^{\alpha\ r_o}}{r}\ e^{-\alpha\ r} = \frac{P_o\ r_o}{r}\ e^{-\alpha\ (r-r_o)} \tag{2.3}$$

where α represents the absorption coeffiecient of the wave in the medium. The most used model for the estimation of the absorption coefficient is the one proposed by François and Garrison [41], based on a large number of experimental results and theoretical studies.

If, in addition, it is desired to take into account the incident pressure on a receiving transducer (P_{in}), its directivity factor DI can be considered:

$$P(r,\theta) = P_o\ r_o \cdot \underbrace{\underbrace{\frac{1}{r}}_{\text{Div.}} \cdot \underbrace{e^{-\alpha\ (r-r_o)}}_{\text{Abs.}} \cdot \underbrace{10^{\frac{DI(\theta)}{20}}}_{\text{D.}}}_{\text{Attenuation}} \tag{2.4}$$

- Propagated signal: It is possible to simulate any signal propagated in the same medium. Knowing that attenuation does not affect all frequencies equally, it is necessary to work with the signal to be propagated ($Signal_{(t)}$) in the frequency domain (signal of pressure P_o at the reference distance r_o), using an FFT. The idea is to apply the *Equation 2.4* to each spectral content, so that when the iFFT (inverse FFT) reverts the signal to the time domain, the result will be the same signal but propagated at distance r ($Signal_{prop.\ (t)}$). *Figure 2.15* shows the scheme to follow.

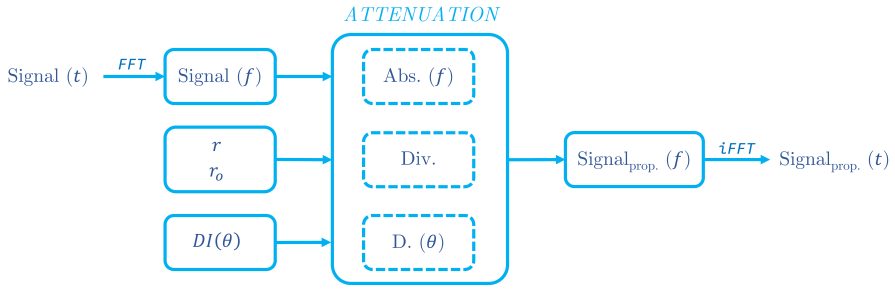

Figure 2.15: Diagram for simulating the attenuation of a signal.

Figure 2.16 shows a simulated sweep signal received 1 km from the source ($Signal$) and propagated to different distances ($Signal_{prop.}$). In the time and frequency representation, the drop in amplitude is observed, which is not the same for all frequencies (high frequencies are attenuated more).

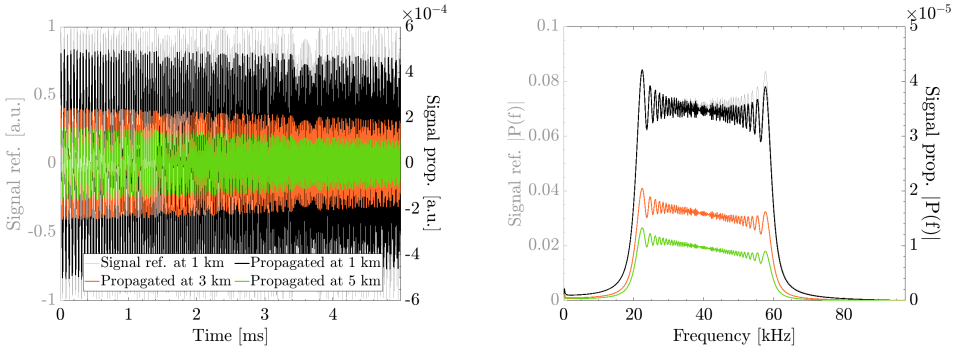

(a) **(b)**

Figure 2.16: Simulated sweep signal from 20 to 60 kHz during 5 ms received at 1 km of the source (in grey) and propagated at different distances. **(a)** Representation in time domain. **(b)** Representation in frequency domain.

SPL

Sound Pressure Level (SPL) measurements consist in putting the hydrophone at 0 degree orientation and at a known distance, and the AB emits tones (sinusoidal signals) every 2 kHz between 20 and 60 kHz. In addition, this test will be made for various CVC values. Each recorded waveform is then analyzed with the methods explained above, to estimate the ToA and to be able to analyze its amplitude in volts.

The SPL indicates the power emission of a source, because it is indicating the output in a specific distance. This spec is similar to a TVR, but the difference is that in a TVR measure it is necessary to control the input signal (V_{in}) to the transducer:

$$TVR = 20\ log_{10}\left(\frac{S}{S_{ref}}\right) = 20\ log_{10}\left(\frac{P_{out}/V_{in}}{P_{ref}/V_{ref}}\right) = 20\ log_{10}\left(\frac{P_{out}\ V_{ref}}{V_{in}\ P_{ref}}\right) \tag{2.5}$$

where P_{out} is the pressure emitted by the transducer, which is fed with an amplitude signal of V_{in} Volts. Furthermore, sensitivity measurements are always accompanied by reference voltage (V_{ref}) and pressure (P_{ref}) values, which in underwater acoustics are usually of 1 V and 1 μPa

The SPL is the parameter characterizable:

$$SPL = 20\ log_{10}\left(\frac{P}{P_{ref}}\right) \tag{2.6}$$

Since the SPL is obtained from the pressure incident to the hydrophone (where P is P_{in}), it is necessary to convert the amplitude value of the received signal in Volts to Pascals. For this purpose the value of RVR is needed:

$$RVR = 20\ log_{10}\left(\frac{S}{S_{ref}}\right) = 20\ log_{10}\left(\frac{V_{out}/P_{in}}{V_{ref}/P_{ref}}\right) = 20\ log_{10}\left(\frac{V_{out}\ P_{ref}}{V_{ref}\ P_{in}}\right) \tag{2.7}$$

where P_{in} is the pressure incident on the transducer expressed in Root Mean Square (RMS).

Figure 2.17 shows the SPL representation for an AB measured on the tank. In this case, the amplitude estimation has been done with the correlation method (it should be added that with the Frequency method, similar values were obtained but with the Time method, somewhat lower due to the filter effect).

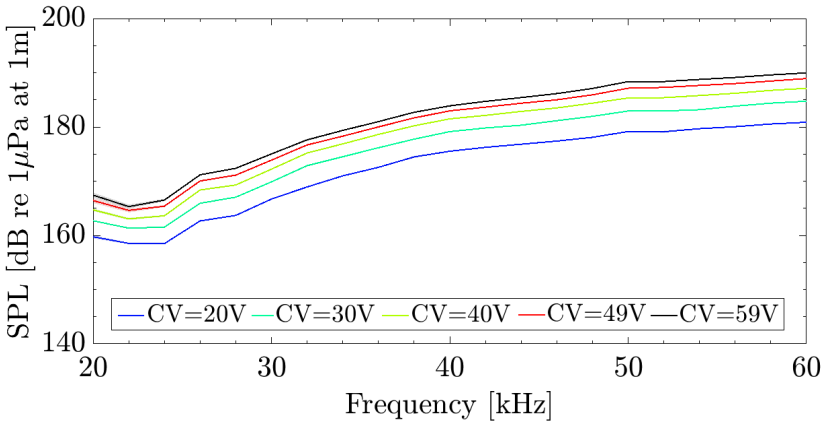

Figure 2.17: Measured SPL each 2 kHz in tank using the correlation analysis.

DIR

The directivity measure (DIR) shows the behavior in terms of received amplitude according to the angle of incidence in the horizontal plane (same distER). It is commonly presented as a relative measure since it indicates the drop in amplitude of the signal according to the angle measured from its maximum value at 0 degrees. So DIR measurements are nothing more than the same signal received at different angles, to represent its relative amplitude at each angle.

Figure 2.18 shows the same 30 kHz tone (five cycles) received and analyzed at two different angles. The ToA in both cases shows that they have been taken at the same distER. In grey it is the raw waveform, which appears much more intense at the 0 degrees angle than at the 90 degrees point. According to the analysis, this is not the case, because the amplitude of the tone at 90 degrees is higher than at 0 degrees. To demonstrate this visually, the interval of the three analyzed cycles filtered with a Butterworth low pass filter of order 8 with the cut-off frequency at 45 kHz is highlighted. This effect has an explanation: observing the FFT of the recorded signals (see *Figure 2.19*), it is demonstrated how the one received at 0 degrees has a lot of high-frequency content, while the one received at 90 degrees lacks such abrupt peaks. This is due to the fact that the PWM signal previously mentioned from the AB also propagates, as it is measured at short distances and at a centered angle, this signal is very noticeable. However, as it is a high-frequency signal (around 400 kHz), it is much more attenuated in lateral measurements. At longer distances where the AB will be used, the PWM contribution is expected to be significantly reduced, as high frequencies are much more absorbed.

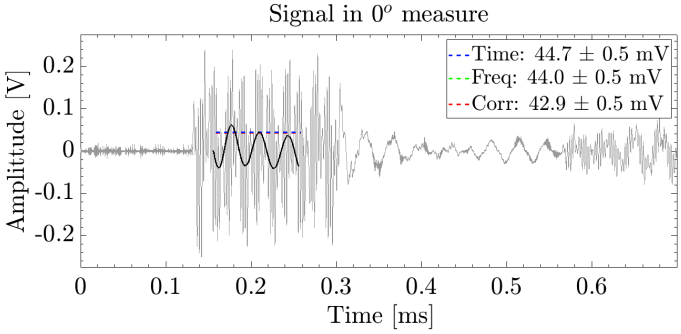

(a)

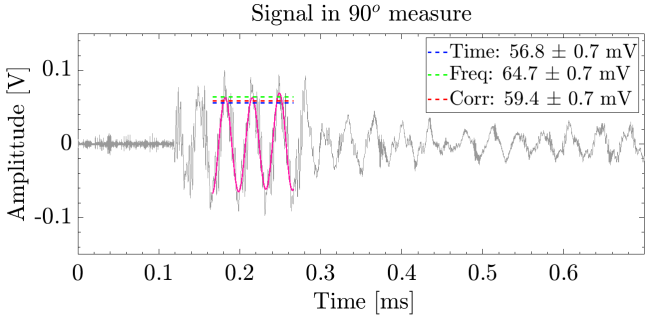

(b)

Figure 2.18: **(a)** Analyzed signal at 0 degrees. **(b)** Analyzed signal at 90 degrees.

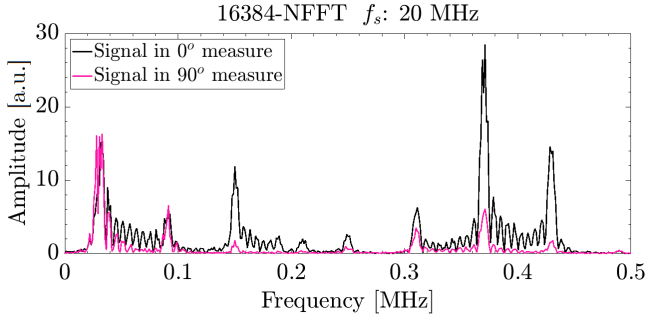

Figure 2.19: FFT of signal received at 0 and 90 degrees.

Below, *Figure 2.20* shows the directivity of an AB measured on the tank for four different frequencies. In this case, the result of the amplitude analyzed by correlation is presented, but any other method has similar results.

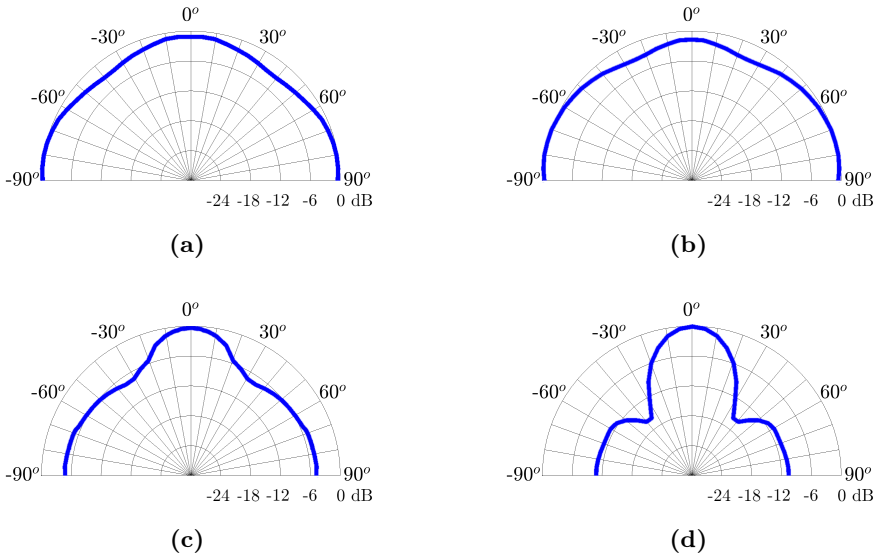

Figure 2.20: Measured directivity each 5 degrees in tank using the correlation analysis. **(a)** Directivity at 20 kHz. **(b)** Directivity at 30 kHz. **(c)** Directivity at 40 kHz. **(d)** Directivity at 50 kHz.

Delay

The delay is the time elapsed from the instant the device is commanded to emit until the signal appears on the medium. This parameter can be noticeable given the electro-mechanical-acoustic complexity of an AB. Thus, it can be taken into account to improve the accuracy of the APS in KM3NeT.

To assess the delay of an AB, attenuation measurements shall be made. This means that the same signal will be measured at different distances from the same axis at 0 degrees. Then, in the analysis of the recorded signals, the ToA of each signal is calculated and plotted against the actual distance. A linear fit can thereafter be made (see *Equation 2.8*), which will cross the horizontal axis (ToAs) revealing the delay value ($delay = -offset/c_{sound}$). To assess whether

the result is reliable, it is necessary to look at the value of the slope, which indicates the speed of propagation.

$$distER = c_{sound}\, ToA + offset \tag{2.8}$$

Below, *Figure 2.21* shows the attenuation measures to estimate the AB delay on the tank for a sweep from 20 to 60 kHz in 250 μs. In this case, the result of the ToA calculation by the correlation method is presented in measures between 5 to 30 cm every 5 cm.

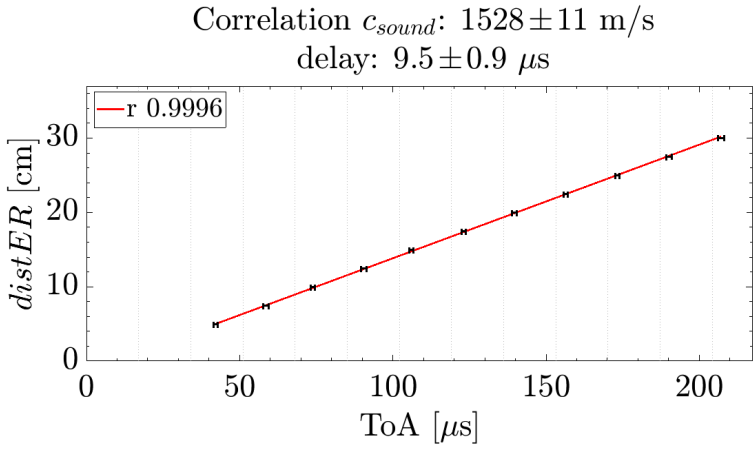

Figure 2.21: Delay measured using the correlation analysis.

During the course of this thesis, almost 40 ABs were measured, which has allowed us to obtain an experience capable of designing a characterization standard such as the last presented.

2.3 AB placement studies

Once the calibration and characterization have been successful, the AB is ready to be used in KM3NeT. As mentioned above, KM3NeT plans to use two types of ABs, autonomous (installed on a tripod and connected to a battery pack to emit at a predefined duty cycle) and triggered (installed on the DU bases and connected to the detector for power, time synchronization, and control).

2.3.1 Autonomous AB location. ORCA006 case

For ORCA006 (installation of the first 6 ORCA DUs) it was decided to install three autonomous ABs, but a good site had to be selected. From previous experience, it was known that at 250 m between DU and AB the signal was well received, but on this occasion, it was agreed to perform a simulation and ensure the expected range of pressures to be received by the DARs.

For this simulation, it is assumed that the SPL of an AB is around 180 dB re 1μPa at 1 m for 34 kHz, as can be seen in *Figure 2.17*. From the SPL, the P_{out} pressure at 1 meter is known, which allows propagating the emitted signal to each DAR using *Equation 2.4*, which takes into account the directivity of the AB (*Figure 2.20.b*), and the effective P_{in} received is estimated. The idea is to obtain a minimum good SNR level of around 20 dB, which means that the received signal should be more than 850 mPa [42]. Therefore, some possible locations were studied, and the positions were decided not only taking into account the expected received level, but all the surrounding logistics.

On the one hand, *Figure 2.22.a* represents the pressure received at each DAR of ORCA006 by a simulated AB, in Pascals and dB. On the other hand, *Figure 2.22.b* is a footprint of the detector with 6 DUs (in blue) and the proposal finally approved for the three autonomous ABs to install (in red). It shows how all the DUs fall within 250 m coverage of each AB.

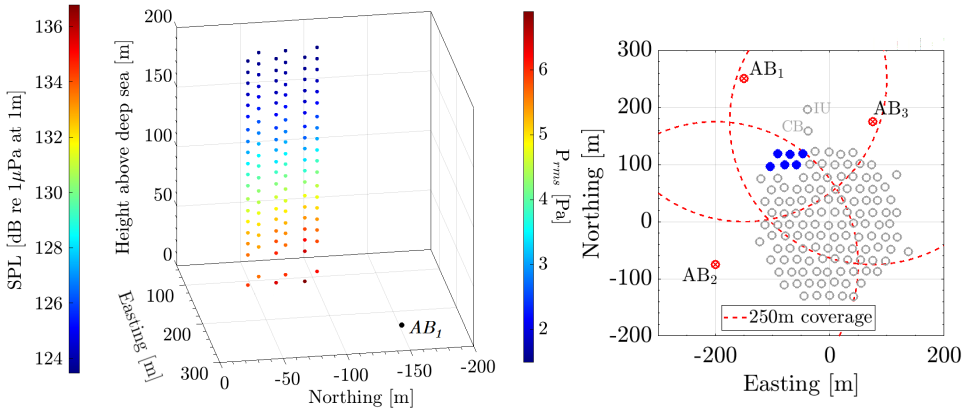

Figure 2.22: **(a)** Pressure received at each DAR of ORCA006 by a simulated AB, in Pascals and dB. **(b)** Footprint of the detector with 6 DUs (in blue) and the proposal finally approved for the 3 autonomous ABs to install (in red).

Table 2.1 shows the maximum and minimum pressures received by each simulated AB. In all cases, the highest piezoceramic receives the lowest amplitude in the line, while the hydrophone at each base receives the highest level. This is because at this distance, the predominant factor is the distER and not the directivity. In any case, the levels are always more than 1.4 Pa which will ensure a SNR greater than 20 dB.

ORCA006	$\mathbf{SPL}_{min}$	$\mathbf{SPL}_{max}$	$\mathbf{P}_{min}$	$\mathbf{P}_{max}$
AB_i	**[dB re 1μPa at 1 m]**	**[dB re 1μPa at 1 m]**	**[Pa]**	**[Pa]**
$\mathbf{AB}_1$	123.26	136.08	1.46	6.37
$\mathbf{AB}_2$	123.48	133.61	1.49	4.79
$\mathbf{AB}_3$	123.28	136.61	6.77	1.46

Table 2.1: Minimum and maximum amplitudes received by the DARs in ORCA006 by each simulated AB position. The simulation have into account the DIRs and the distER.

2.3.2 Triggered AB location proposal

As in the previous section, we have also made the first proposal for the plan to install the triggered ABs. This time for both telescopes, although from different construction phases (depending on what is already planned). In the case of ARCA, the proposal is for node 1 from September 2022, and in the case of ORCA from the completion of sector 1 in June 2023.

At the moment, a ratio of 1 AB for every 8 DUs (12.5%) is envisaged. ARCA plans to install one AB in each Junction Box (JB), as well as one in the Calibration Base (CB), and three more in DUs. With all this, ARCA would have a total of 7 ABs spread over 35 instrumentation units, which would make a ratio of 20%. ORCA, on the other hand, does have plans beyond what would be sector 1. In total, up to 4 phases are distinguished, which have been selected according to the planned order of installation. Only the first sector has AB installation planned (see *Figure 2.23*).

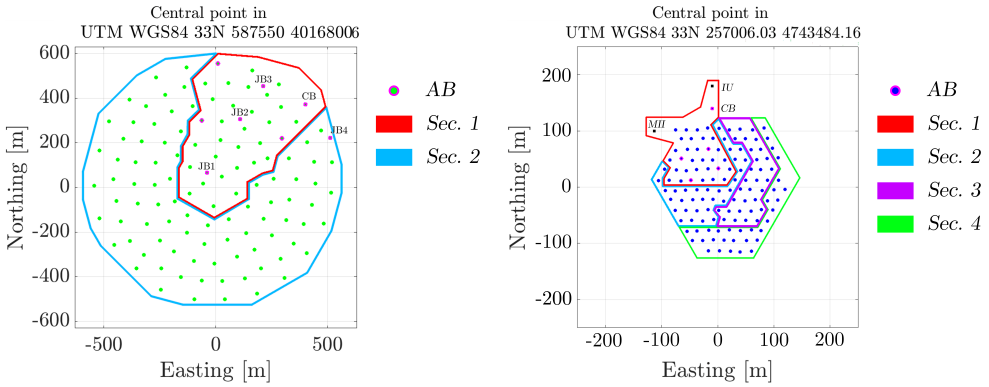

Figure 2.23: **(a)** Section ARCA deployment (block 1). Sector 1 is planned before September 2022, without further planning sectors. **(b)** Sections ORCA deployment. Sector 1 is planned before June 2023.

For ARCA, our proposal is to put a total of 16 ABs per node, which corresponds to 13.3%. For ORCA, our proposal is to put a total of 15 ABs spread over the 4 sectors (sectors are groups of 31 DUs selected according to the order of deployment), which corresponds to 12.0% (see *Table 2.2*).

ARCA	ABs / Instrumentation	Ratio
Sec. 1	7 ABs / 31 DUs + 3 JBs + CB	20.0%
Sec. 2	16 ABs / 115 DUs + 4 JBs + CB	13.3%

ORCA	ABs / Instrumentation	Ratio
Sec. 1	5 ABs / 31 DUs + CB	15.6%
Sec. 2	8 ABs / 62 DUs + CB	12.7%
Sec. 3	12 ABs / 93 DUs + CB	12.8%
Sec. 4	15 ABs / 124 DUs + CB	12.0%

Table 2.2: Number of triggered ABs proposal for KM3NeT.

Figure 2.24 shows the arrangement of each triggered AB in the proposed position. In principle, it seems better to choose the extremes so that the DUs find the ABs distributed in almost all directions and cover a greater variability of directions, otherwise, there may be cases where the acoustic signals arrive only from the same area with little variability, thus trilateration

difficult. For this reason, it is always planned to have three or four autonomous ABs distributed around the detector, to attempt to improve the triangulation of the DARs in the DUs at the border of the detector. Since autonomous ABs are operating with a battery pack, they will be replaced and installed depending on the detector's deployment status. Also, the state of the battery will play an important role in deciding its location.

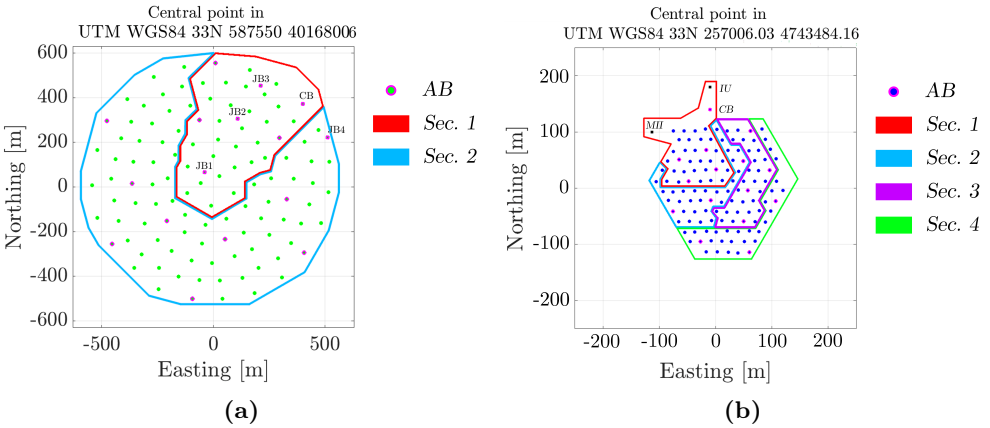

Figure 2.24: Triggered AB positions, first proposal. **(a)** Section ARCA deployment (block 1). **(b)** Sections ORCA deployment.

2.4 Performance operational in situ

Once the sensors have been installed in the detector, the emitter-receiver system functionality should be checked. This is done by taking one of the two parts as a reference value (direct comparison).

This section explains how to check the receiving sensitivity, RVR, of the DARs using a reference value in the transmitters part, and it explains how to check the transmitters, SPL, from the reference receivers value. This example uses three ORCA006 hydrophones and three autonomous ABs, but the example can be generalizd to the piezoceramic sensors and for the ARCA site as well.

2.4.1 Received Voltage Response of DARs

The RVR can be checked in situ too see if the value given by the manufacturer (-156 dB re 1 V/μPa at 1 m) has changed in operation. This is done by assuming a SPL on the part of the ABs of 170 dB re 1μPa at 1 m for the AB emissions (since they are used with a 30 V of CVC), and by looking at the RMS value received from each AB (V_{out}).

The steps to follow are:

1. Convert the reference SPL (or TVR) value to P_{out} using *Equation 2.6* (or *Equation 2.5*)
2. Attenuate the P_{out} value to convert it to P_{in} for each receiver using *Equation 2.4*
3. Calculate the RVR using *Equation 2.7*

Table 2.3 shows the result of the calculated RVR ($RVR_{calc.}$) and the difference from the RVR value provided by the manufacturer.

Hydro	AB	r [m]	α [Np/m]	V_{out} [mV]	$RVR_{calc.}$ [dB re 1V/μPa]	Diff. [dB]
DU2	14	234.6	$3.2616 \cdot 10^{-5}$	13.7	-160.8	-4.8
	16	151.1	$4.1565 \cdot 10^{-5}$	26.2	-159.0	-3.0
	24	232.9	$2.8651 \cdot 10^{-5}$	13.7	-160.9	-4.9
DU3	14	247.5	$3.2616 \cdot 10^{-5}$	10.9	-162.3	-6.3
	16	132.0	$4.1565 \cdot 10^{-5}$	16.8	-164.0	-8.0
	24	237.1	$2.8651 \cdot 10^{-5}$	10.9	-162.7	-6.7
DU9	14	212.9	$3.2616 \cdot 10^{-5}$	20.9	-158.0	-2.0
	16	169.7	$4.1565 \cdot 10^{-5}$	28.9	-157.1	-1.1
	24	213.9	$2.8651 \cdot 10^{-5}$	21.0	-157.9	-1.9

Table 2.3: Parameters and results in the RVR in situ calibration at ORCA006.

2.4.2 AB emitted Sound Pressure Level

The SPL calibration in situ is to check whether the installed ABs SPL correspond to the value meausred in the laboratory (170 dB re 1μPa at 1 m) when it is in operation. This is done by assuming an RVR on the part of the receivers of -156 dB re 1 V/μPa at 1 m, and by looking at the RMS value received from each AB (V_{out}).

The steps to follow are:

1. Convert the received amplitude V_{out} to presure value (P_{in}) using *Equation 2.7*
2. Amplify the P_{in} value to convert it to P_{out} for each receiver using *Equation 2.4*
3. Calculate the SPL using *Equation 2.6*

Table 2.4 shows the result of the calculated SPL ($SPL_{calc.}$) and the difference from the SPL measured in the laboratory. In this calculation, the directivity of the AB for 30 kHz shown in *Figure 2.20.b* has been taken into account.

AB	Hydro	r_o [m]	α [Np/m]	DI [dB]	V_{out} [mV]	$SPL_{calc.}$ [dB re 1μPa]	Diff. [dB]
	DU2	234.7	$3.2616 \cdot 10^{-5}$	-1.0	13.7	165.2	-4.8
14	DU3	247.5	$3.2616 \cdot 10^{-5}$	-1.0	10.9	163.7	-6.3
	DU9	212.9	$3.2616 \cdot 10^{-5}$	-1.0	20.9	168.0	-2.0
	DU2	151.1	$4.1565 \cdot 10^{-5}$	-1.0	26.2	167.0	-3.0
16	DU3	132.0	$4.1565 \cdot 10^{-5}$	-1.0	16.8	162.0	-8.0
	DU9	169.7	$4.1565 \cdot 10^{-5}$	-1.0	28.9	168.9	-1.1
	DU2	232.9	$2.8651 \cdot 10^{-5}$	-1.0	13.7	165.1	-4.9
24	DU3	237.1	$2.8651 \cdot 10^{-5}$	-1.0	10.9	162.7	-6.7
	DU9	213.9	$2.8651 \cdot 10^{-5}$	-1.0	21.0	168.1	-1.9

Table 2.4: Parameters and results in the SPL in situ calibration at ORCA006.

2.4.3 Auto system self-calibration

Naturally, the previous checks have given the same difference within the same emitter-receiver system. This shows that failure cannot be assumed to be caused by a single sensor as there are likely to be errors in other estimates such as absorption coefficient α value or distERs. However, there is more consistency in the differences for the hydrophones (-4.2 ± 1.1 dB in hydrophone of DU2, -7.0 ± 0.9 dB in hydrophone of DU3, -1.7 ± 0.5 dB in hydrophone of DU9). This is probably due to taking the manufacturer's RVR value rather than one measured in the laboratory. Consequently, if we want to perform a kind of self-calibration by feeding back the system, we should first correct the RVR of the hydrophones and then repeat the SPL calibration with these $\text{RVR}_{calc.}$, so that we would have a fully calibrated system in situ. In addition, a weekly calibration could be performed and it could be monitored if there has been any deterioration in some sensors or even anticipate battery charge decrease in the autonomous ABs.

2.5 Monitoring the Digital Optical Modules positions

Having presented all parts of the APS, now it will be explained how they are used to calculate the positions of the piezoceramic sensors. So far the ABs installed are autonomous, which means that they have been programmed to emit a one-minute pulse train every 10 minutes without any control of the ToE. This configuration is intended to triangulate the position of the piezoceramic sensors in constant movement every 10 minutes. Since the positions of the ABs and hydrophones are known, and the propagation velocity can be estimated, when a hydrophone records the ToA coming from an AB it will be straightforward to know its ToE (see *Equation 2.9*). The more hydrophones record the ToA of the same emission the more accurate the calculation of the ToE will be.

$$ToF = ToA - ToE \quad \Rightarrow \quad ToE = ToA - ToF = ToA - \frac{distER}{c_{sound}} \tag{2.9}$$

The speed of sound c_{sound} is estimated using the approximation proposed by Medwin and Makenzie [43]. The Sound Velocity Profle (SVP) estimated for KM3NeT is represented in *Figure 2.25* and even compared with experimental data extracted in three ORCA sea campaigns (September 2017, May 2019, and January 2020).

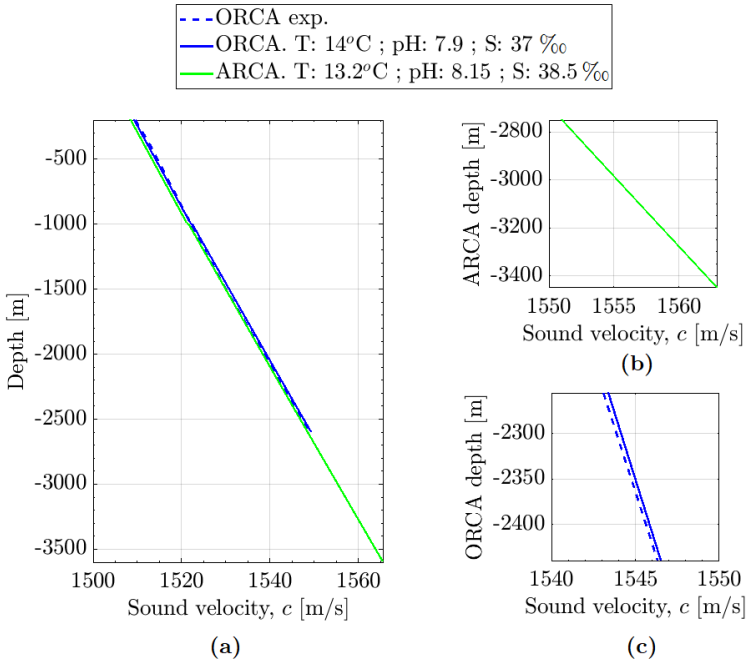

Figure 2.25: **(a)** SVP estimated for KM3NeT and compared with ORCA experimental data (sea campaigns in September 2017, May 2019, and January 2020. **(b)** Detailed for ARCA depth. **(c)** Detailed for ORCA depth.

Once the effective c_{sound} (this calculation should take into account the gradient of the pressure aalong its path between the emitter AB and the receiver) and ToE are known, the distER "measured" by the APS is calculated, which is necessary for trilateration.

Trilateration to produce the XYZ data

The trilateration method in acoustics requires a minimum of three sensors of known position to triangulate one of unknown position [29]. KM3NeT uses emitters in known positions to know the position of the receivers.

In order to locate a piezoceramic sensor (*piezo*), an equation system is created with one equation per emitter (AB_i). The *Equation 2.10* is used to generate it.

$$distER_i = \sqrt{(X_{AB_i} - X_{piezo})^2 + (Y_{AB_i} - Y_{piezo})^2 + (Z_{AB_i} - Z_{piezo})^2} \quad (2.10)$$

Figure 2.26 represents the triangulated position of a piezoceramic sensor with available data for an APS measure.

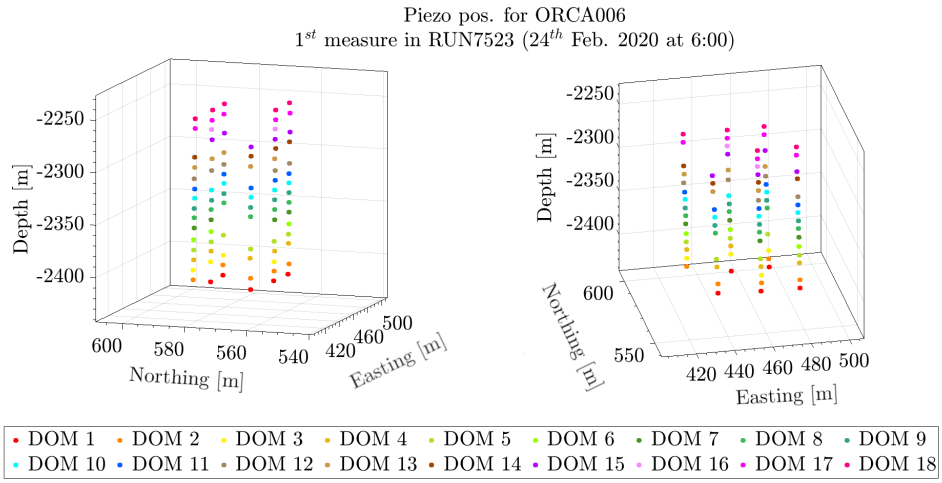

Figure 2.26: Localization of piezoceramic sensors on a measure of ORCA.

The DU line movements

In this section, the displacement of a DOM in ORCA is studied. This will be done by monitoring the position of the last DOM of a DU during a week of variable current.

Figure 2.27 shows the Instrumented Interface Module (MII) data at ORCA during the week of DOM monitoring. *Figure 2.27.a* shows how the sea current at the beginning is about 5 cm/s and reach a peak at 10 cm/s (high current for ORCA) on the second day, and then gradually relaxes to values below 5 cm/s. In turn, *Figure 2.27.b* shows how the direction measurement becomes much more stable during the high current period, while at small displacements the measurement becomes more inaccurate.

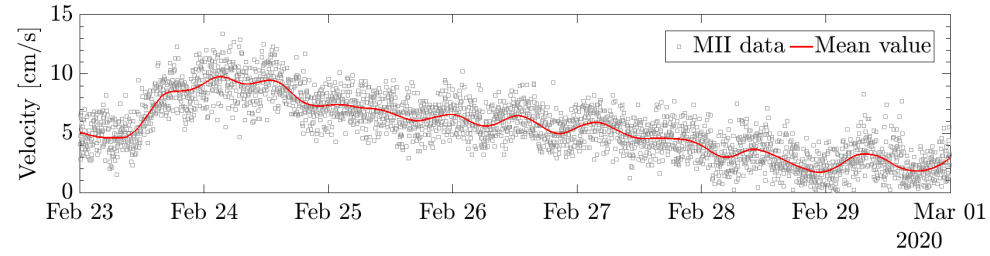

(a)

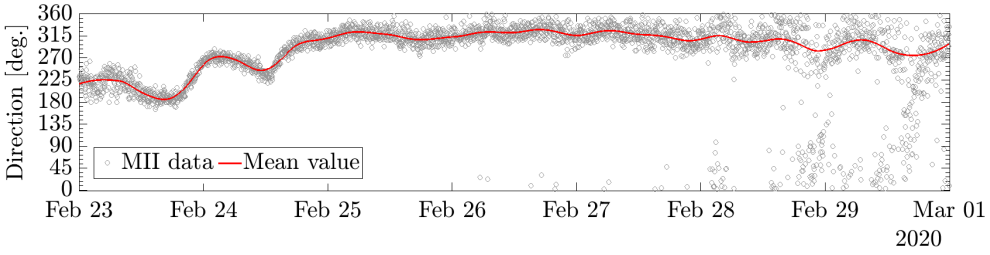

(b)

Figure 2.27: Sea current properties data for a week (Feb. 2020) provided by EMSO Ligure Ouest, *MII capteur AQUADOPP* [18]. **(a)** Sea current velocity. **(b)** Sea current direction.

Figure 2.28 shows the displacement of the DOM during the given week. It is noticeable how the period of high current causes a long displacement in a short time, while in the period of stable current it remains more still.

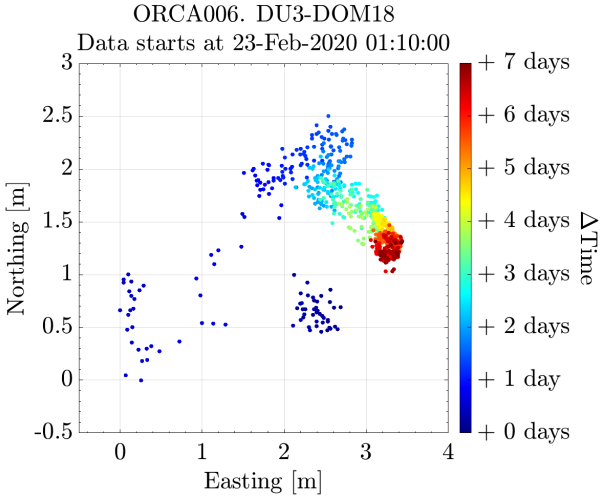

Figure 2.28: Piezoceramic movement on DOM18 of ORCA DU3.

The reconstructed DOM positions show that the DOMs move coherently and exhibit periodical movements in agreement with the expected period of the inertial motions induced by the Coriolis force, that at the latitude of KM3NeT site has a period of about 20 hours [44].

The APS is only able to detect the position of the piezoceramic sensor, but the orientation of the DOM is unknown. This is why it is necessary to have an AHRS. The AHRS combined with the APS can provide the position and orientation of the DOM, which would place in space each PMT, necessary for the reconstruction of a muon detected by them.

The next chapter discusses how this AHRS works and explains a combination of AHRS and APS data to eventually fit and improve the accuracy in the procedure of monitoring a DOM position.

2.6 Conclusions and future steps

Conclusions

The operation of the APS in KM3NeT is described and its elements are presented. It has been demonstrated that the sensitivity of hydrophones in the DU bases is higher than that of piezoceramic sensors in the DOMs (see

Figure 2.4 and *Figure 2.5*). Furthermore, it is explained how the ToA in the DB is triangulated to position each piezoceramic sensor.

Different methods of detection and analysis of the signals recorded by an acoustic receiver have been presented, as well as the process of simulating the propagation of any signal through any fluid taking into account its characteristics. Detection and analysis methods have been applied to characterize an AB. The propagation process has been implemented to simulate the signal received at any DAR of the detector, thus allowing to decide whether the location of any AB is correct or not.

The process of characterization of an AB in a laboratory is defined in detail (SPL, DIR, and *Delay*). This has permitted the creation of a more automatic process in measurements and analysis (as they are perfectly coordinate). The automatization has considerably reduced the time needed to complete the datasheet. This process could be modified to also characterize incoming DARs. By specializing in this field, it has been possible to develop a simple process to check the sensitivity values in situ in the emitter-receiver system (*section 2.4*).

Future steps

Based on the process for characterizing an AB in the laboratory prior to installation, a similar analog could be designed to characterize hydrophones in detail. As for the piezoceramic sensor, it is more unmanageable and not feasible to characterize the receiver inside the DOM, but some kind of quick check could be defined and tested in a selection of DOMs.

As for the in situ tests of acoustic sensors, they should also be applied to the piezoceramic sensors. This would check the variation between sensors of the same type manually glued to the glass of every DOM. In addition, if the detailed values of each AB measured in the laboratory prior to installation were applied, the difference between the expected sensitivity and the in situ measurement would be reduced. If the ADF were programmed to check each DAR periodically, the effect of noise on the results would be reduced and it would be possible to detect anomalies in the emitter-receiver system or to anticipate the imminent discharge of the battery pack in an autonomous AB.

Some kind of dynamic threshold level should be studied so that the ADF does not store so much disposable data (see *Figure 2.7*). Furthermore, the idea of saving the ToA in the DB is only for positioning, and the next step would be to store the XYZ data for every piezoceramic sensor. As it will be seen in *chapter 3*, this will not be the only data of interest to be recorded.

Chapter 3

The Detection Unit Line Fit

The Detection Unit (DU) Line Fit model idea was born from the need to control the positions and the orientations of the Digital Optical Modules (DOMs). Until now, they had always been treated independently. After the Acoustic Positioning System (APS) for the position part, presented in the last chapter, this chapter presents the Attitude and Heading Reference System (AHRS) for the DOMs orientation, an AHRS rotation matrix to analyze the position and orientation data, and in the end a Mechanical Model (MM) that permits a reconstruction of the DU line shape. This MM is taking into account the mechanical parameters of the DU elements along the line. Once the situation of the DOMs via experimental data is known, the MM can estimate an effective sea current properties (speed and direction) with the intention of using them later to determine positions from the MM. The DU Line Fit idea and relevance are explained in this chapter with an example of applicability using real data of the detector.

The *DU line fit* model is based on the KM3NeT positioning system: Acoustic Positioning System in *chapter 2*, Attitude and Heading Reference System in *section 3.1*, and a Mechanical Model in *section 3.2*. Making combinations of these (*section 3.3*), the *DU line fit* provides more accuracy, correction, and improvement of the positions and orientation of the DOMs. At the end of the chapter, experimental results of the DU Line Fit applied for a period of three hours of data are presented, and the chapter finalises with conclusions and some notes about future research.

3.1 The Attitude and Heading Reference System (AHRS) of KM3NeT

In the previous chapter (see *chapter 2*), the APS of the KM3NeT is presented. In this chapter, another part of the Positioning System in KM3NeT is given: the AHRS system, which serves to monitor the orientation of the DOM. Combining both parts, it is possible to know the position and orientation of each Photomultiplier Tube (PMT) in the DOMs of the detector [45].

3.1.1 AHRS using Compass and Tilt meter to produce the YPR data

The AHRS system uses Printed Circuit Boards (PCBs) which are installed inside each DOM (and an extra one on the DU base) to monitor the orientation of the elements along a DU. The PCBs use a compass sensor and a tilt meter to obtain the Magnetic field (H) and the Acceleration (A) in the three spatial components (x, y, and z). The PCBs are connected to the control station offshore, the AHRS data is 64-bit encoded and provided every 10 seconds.

From the AHRS components it is possible to calculate the Yaw (Y), Pitch (P), and Roll (R), which are the rotation around three perpendicular axes x, y and z for each DOM (see *Figure 3.2.a*). This rotation angles can be calculated as:

$$P = atan2\ (A_x, \sqrt{A_y^2 + A_z^2}) \tag{3.1}$$

$$R = atan2\ (-A_y, -A_z) \tag{3.2}$$

$$Y = atan2\ (-H_y\ \cos\ R + H_z\ \sin\ R, H_x\ \cos\ P + H_y\ \sin\ P \sin\ R + H_z\ \sin\ P \cos\ R) \tag{3.3}$$

Table 3.1 shows an example of the values for the calculated Y, P, and R provided by a particular DU in ORCA in a specific experimental measure. This data will be considered the raw YPR data, even though it has been calculated and calibrated previously.

	Raw YPR data		
	Yaw (Y) [deg.]	Pitch (P) [deg.]	Roll (R) [deg.]
DU base	121.7 ± 24.1	0.5 ± 0.1	177.7± 0.1
DOM 1	254.9 ± 0.5	1.8 ± 0.1	-5.6 ± 0.1
DOM 2	251.5 ± 0.4	-2.2 ± 0.0	-3.3 ± 0.1
DOM 3	261.1 ± 0.6	-3.3 ± 0.0	-4.8 ± 0.1
DOM 4	257.8 ± 0.6	-1.6 ± 0.0	-1.9 ± 0.1
DOM 5	253.6 ± 1.2	-1.0 ± 0.0	0.2 ± 0.1
DOM 6	-	-	-
DOM 7	-	-	-
DOM 8	250.7 ± 1.8	-0.7 ± 0.1	-3.2 ± 0.1
DOM 9	251.6 ± 1.6	-1.0 ± 0.1	-0.6 ± 0.1
DOM 10	-	-	-
DOM 11	244.9 ± 1.5	-3.6 ± 0.1	-0.2 ± 0.1
DOM 12	241.5 ± 1.7	-3.2 ± 0.1	-1.8 ± 0.1
DOM 13	242.5 ± 2.0	-1.8 ± 0.1	2.0 ± 0.1
DOM 14	243.6 ± 2.2	-3.0 ± 0.1	1.1 ± 0.2
DOM 15	244.9 ± 2.4	-2.0 ± 0.1	1.2 ± 0.2
DOM 16	239.6 ± 2.2	-2.0 ± 0.1	-0.3 ± 0.2
DOM 17	253.3 ± 1.3	-2.9 ± 0.1	5.5 ± 0.2
DOM 18	240.3 ± 2.4	-4.6 ± 0.1	-1.5 ± 0.2

Table 3.1: Raw YPR data (from AHRS) by ORCA-DU3 for the first measure in RUN 7523 (24^{th} Feb. 2020 at 6:00). The data have been rounded to s decimal place for better presentation.

YPR data corrections

Yaw fitting Given the structural disposition of a DU, it is expected that the Y value between DOMs has some progressive fluctuation of a few degrees due to the possible torque effect produced by the ropes and DOMs situation. However, in the raw YPR data presented at the *Table 3.1*, the Y values have small unexplained variations between DOMs (in *Figure 3.1* is visually appreciated in blue dots). Consequently, this might be corrected using a linear fit between them. Moreover, considering this fit, it is possible to predict the Y values in order to complete the missing DOMs (DOMs on the 6th, 7th, and 10th floors).

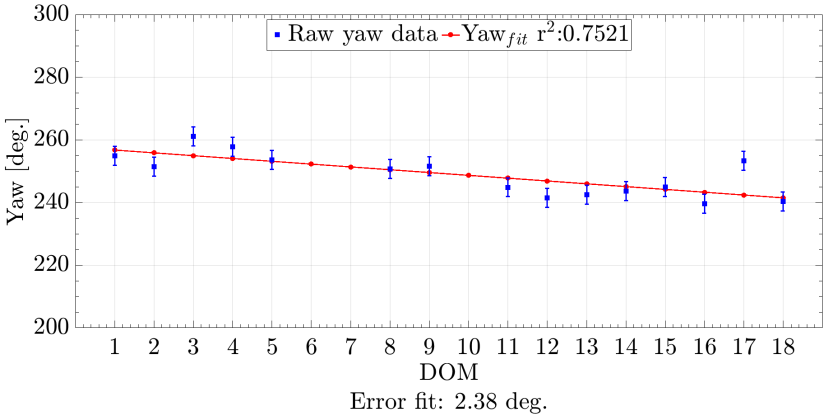

Figure 3.1: Fitting the raw Yaw (Y) data. The raw Y data is the same presented in *Table 3.1*, and the error bar is 3^o based on the laboratory calibration (previous to their installation in KM3NeT).

Pitch and Roll offsets After monitoring and analyzing the raw YPR data for diverse studies, it has been concluded that they need a correction (especially for P and R). The possibility of calculating the inclination of the DOMs (*zenith* angle) was being studied respect their position in vertical, but it was not possible to obtain good results prior to these corrections (see *subsubsection 3.1.2* and *Figure 3.3*). The correction consists of determining an average value during really calm periods of the sea current and treating them as an offset. The hypothesis is that in extremely quiet periods of sea current, the DU line stands upright in a vertical position and the P and R values should be around zero.

Table 3.2 provides an example of the P and R offsets for a particular DU in ORCA calculated during three detected quiet sea periods.

ORCA DU3	Pitch offset [deg.]	Roll offset [deg.]
DOM 1	2.826 ± 0.040	-5.683 ± 0.040
DOM 2	-1.170 ± 0.029	-3.333 ± 0.027
DOM 3	-2.341 ± 0.027	-4.806 ± 0.025
DOM 4	-0.670 ± 0.000	-1.981 ± 0.000
DOM 5	-0.028 ± 0.000	0.009 ± 0.000
DOM 6	-	-
DOM 7	-	-
DOM 8	0.189 ± 0.027	-3.337 ± 0.030
DOM 9	-0.135 ± 0.025	-0.808 ± 0.026
DOM 10	-	-
DOM 11	-2.705 ± 0.017	-0.446 ± 0.018
DOM 12	-2.306 ± 0.009	-1.979 ± 0.009
DOM 13	-1.067 ± 0.018	1.776 ± 0.018
DOM 14	-2.247 ± 0.012	0.911 ± 0.009
DOM 15	-1.314 ± 0.018	0.847 ± 0.018
DOM 16	-1.354 ± 0.027	-0.546 ± 0.018
DOM 17	-2.252 ± 0.009	5.199 ± 0.008
DOM 18	-4.057 ± 0.000	-1.789 ± 0.000

Table 3.2: Pitch (P) and Roll (R) offsets for ORCA-DU3. The measure was for RUNs (7900 - 8021 - 8247) with low sea speed current. Orange indicates that the values come from less than 10 valid measures in the data. The data have been rounded to 3 decimals placed for better presentation.

The *offset* application is shown in an experimental reconstruction using *TILT analysis* in *subsection 3.3.1* (see *Figure 3.3*). The YPR corrections are applied for *Table 3.3*, as an example.

3.1.2 The AHRS matrix for YPR data analysis

From the previously commented idea of calculating the inclination (*zenith* angle) of the DOMs with respect to their vertical, the first step is to use a matrix rotation to set each DOM into the same reference system. The solution has been to use the *AHRS matrix* (*Equation 3.4*), with YPR data so to express the DOM's orientation in the same unitary axes system (see *Figure 3.2.b*).

$$\begin{pmatrix} u_x \\ u_y \\ u_z \end{pmatrix} = \begin{pmatrix} \cos(\psi)\cos(\theta) & -\sin(\psi)\cos(\phi) - \cos(\psi)\sin(\theta)\sin(\phi) & \sin(\psi)\sin(\phi) - \cos(\psi)\sin(\theta)\cos(\phi) \\ \sin(\psi)\cos(\theta) & \cos(\psi)\cos(\phi) - \sin(\psi)\sin(\theta)\sin(\phi) & -\sin(\psi)\sin(\theta)\cos(\phi) - \cos(\psi)\sin(\phi) \\ \sin(\theta) & \cos(\theta)\sin(\phi) & \cos(\theta)\cos(\phi) \end{pmatrix} \begin{pmatrix} 0 \\ 0 \\ -1 \end{pmatrix} \tag{3.4}$$

In this equation, θ and ϕ correspond to P and R values respectively, and the ψ corresponds to $90 - Y$ value, it is a correction applied to convert from the reference system on the PCB to the reference system of the KM3NeT detector (see *Figure 3.2.b*). The u point is the Cartesian coordinates for the DOMs in this East, North, Up (ENU) reference system.

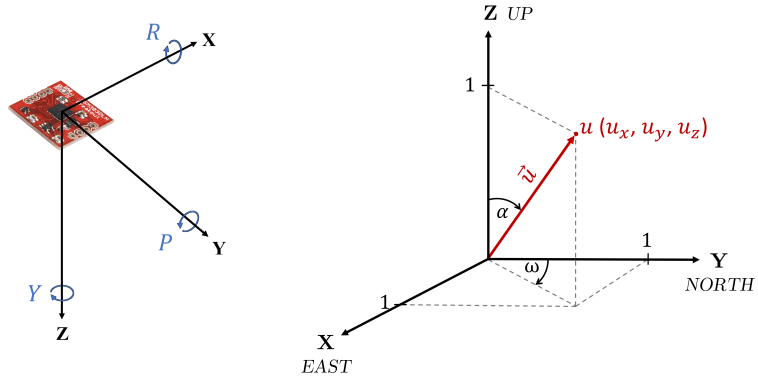

(a) **(b)**

Figure 3.2: **(a)** The PCB axis system in each DOM (relative coordinate system) and Yaw (Y), Pitch (P), and Roll (R). **(b)** The absolute coordinate system for a DU uses a unitary vector ($\vec{u}$) to locate the orientation of the DOMs.

The *AHRS matrix* (*Equation 3.4*) is used for two different objectives: to estimate the zenith angle α of the DOMs and the sea current direction ω, and to translate the piezoceramic detected location to the center of the DOM ($XYZ_{piezo} \rightarrow XYZ$).

Zenith angle estimation for every DOM

Using the u_z component, after the *AHRS matrix rotation* application (*Equation 3.4*), it is possible to estimate the zenith angle α for any DOM along the DU line (see *Figure 3.2.b* and *Equation 3.5*):

$$\cos(\alpha) = u_z \tag{3.5}$$

	YPR data and Zenith			
	Yaw (Y) [deg.]	Pitch (P) [deg.]	Roll (R) [deg.]	Zenith (α) [deg.]
DOM 1	257.651	-0.998	0.055	0.999
DOM 2	256.754	-1.019	0.071	1.021
DOM 3	255.856	-0.977	0.017	0.977
DOM 4	254.958	-0.980	0.046	0.981
DOM 5	253.061	-0.987	0.160	1.000
DOM 6	253.163	-	-	0.973
DOM 7	252.256	-	-	0.943
DOM 8	251.368	-0.906	0.136	0.916
DOM 9	250.470	-0.849	0.163	0.865
DOM 10	249.572	-	-	0.881
DOM 11	248.674	-0.871	0.211	0.896
DOM 12	247.777	-0.904	0.166	0.919
DOM 13	246.879	-0.764	0.242	0.802
DOM 14	245.981	-0.794	0.210	0.821
DOM 15	245.084	-0.658	0.301	0.723
DOM 16	244.186	-0.612	0.289	0.677
DOM 17	243.288	-0.622	0.315	0.698
DOM 18	242.391	-0.525	0.253	0.583

Table 3.3: Corrected YPR data of *Table 3.1* after corrections (Y fitting and PR offsets application) and the estimated zenith by the *AHRS matrix rotation* employment. Marked in orange are the values provided by Y fitting in missed data, and marked in red are the values interpolated from adjacent DOMs. The data have been rounded to 3 decimals placed for better presentation.

Table 3.3 shows an example where using the correct YPR data (after the *Yaw fit* and offsets application), DOMs' zenith angle, α, can be estimated. The zenith angle in missing DOMs is completed with other adjacent DOMs values, marked in red. Another possibility would be to complete them with an interpolation between α and the height of the DOM.

The possibility to monitor DOMs' zenith angle α along the DU line is interesting to learn and know its behaviour when subjected to sea currents.

Sea current direction from YPR data

Predicting the sea current direction, ω, on the KM3NeT environment is possible if the DU line shape is known: the sea current will tilt the DU in its same direction. In strong sea current periods, the displacement of the DOMs from their vertical position will be larger, and the accuracy of the sea current prediction will increase.

Using the u_x and u_y (*AHRS matrix rotation* components from *Equation 3.4*), which represent the position of the CLB on the unitary reference system from a top view, see *Figure 3.2.b*, it is easy to predict the direction of the force that produced the displacement:

$$\omega = atan2\ (u_x, u_y) \tag{3.6}$$

Although not all DOMs in the same DU present the same ω clearly (these discrepancies can be produced by the accuracy on the YPR data taking), the average value of them which can be used as an effective sea current direction.

DOMs position from the piezoceramic location

Knowing the sphere radius of the DOM, r_{DOM} , the piezoceramic location from the APS ($XYZ_{\ piezos}$ data), and the orientation of the DOM from the AHRS (YPR data), it is possible to estimate the centre position of any DOM applying the *AHRS matrix rotation*:

$$\begin{aligned} X_{DOM} &= X_{piezo} - u_x \cdot r_{DOM} \\ Y_{DOM} &= Y_{piezo} - u_y \cdot r_{DOM} \\ Z_{DOM} &= Z_{piezo} - u_z \cdot r_{DOM} \end{aligned} \tag{3.7}$$

3.1.3 Positioning DOMs from YPR data

It is possible to reconstruct the position of the DOMs (XYZ) taking the inter DOM distances, $interDOMdist$, the YPR data, and the DU base location. The principles that govern the reconstruction are the *AHRS matrix* parameters (*Equation 3.4*). The position of the DOM_j depends on the previous one (DOM_{j-1}), starting the reconstruction from the DU base position:

$$
\begin{aligned}
X_{j\ rec.} &= X_{j-1} + u_x \cdot interDOMdist \\
Y_{j\ rec.} &= Y_{j-1} + u_y \cdot interDOMdist \\
Z_{j\ rec.} &= Z_{j-1} + u_z \cdot interDOMdist
\end{aligned} \tag{3.8}
$$

This means that from the YPR data (only using the AHRS) it is plausible to obtain an estimation about the positions of the DOMs (XYZ_{rec} by an *AHRS positioning*). This procedure is extremely sensitive and requires corrected input data since any change in the input can modify considerably the output result.

Figure 3.3 shows how the *AHRS positioning* is applied for a DU in ORCA detector. On this occasion, the reconstruction is applied using the raw YPR data of *Table 3.1* directly (*Figure 3.9.a*) and corrected YPR data of *Table 3.3* (*Figure 3.9.b*) to show the impact of the corrections into the analysis. It is clear than the corrections for the YPR data are highly important. Thus, it is necessary to be careful when taking maximum accuracy in any parameter, and if any DOM has missing data, it is required to fill it with the adjacent DOM data.

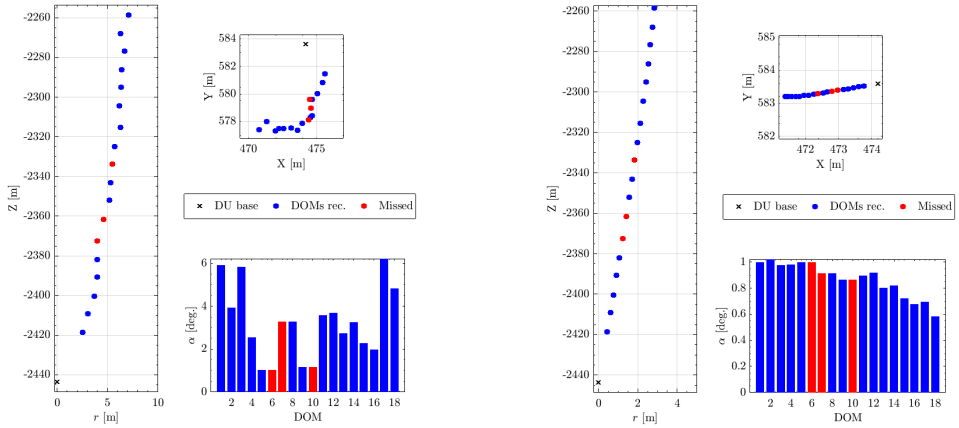

Figure 3.3: Positioning from YPR data (*AHRS positioning*). The profile and top views of the DU line, and the estimated zenith angle are represented. **(a)** Before YPR data corrections applied (using the raw data in *Table 3.1*). **(b)** After YPR data corrections applied (using the corrected data in *Table 3.3*).

Sea current direction from XYZ data

Once the XYZ data is known, like in *subsubsection 3.1.2*, an effective sea current direction can be estimated from the positions of the DOMs. It is possible to estimate the DOMs direction considering only the X and Y Cartesian values to calculate their differences, $Diff$, from the first DOM (the lowest with data), or from DU base position (independently). On this occasion, a linear fit is used to obtain ω:

$$Diff_y = Diff_x \cdot \omega \tag{3.9}$$

3.2 The Mechanical Model (MM) for KM3NeT

Based on the *line shape* model used for the ANTARES detector [46], the *DU line fit* of KM3NeT uses a Mechanical Model (MM). This MM reduces the complexity of the problem to a simple scheme of the DU, which is composed by a string of spheres (DOMs) connected by a simple rope between them (cable), with a cylinder on top (Top buoy), and anchored to the floor (DU base). It studies the forces supported (buoyancy and drag) for each element to predict the vertical displacement of the DOM, see *Figure 3.4* [47].

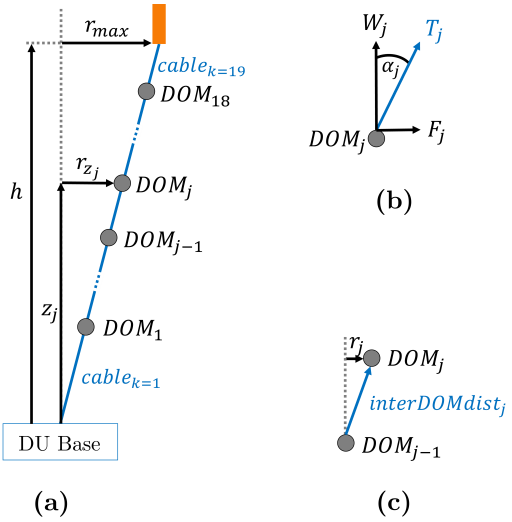

Figure 3.4: A DU line scheme for Mechanical Model equations on KM3NeT. **(a)** Complete DU in profile view. **(b)** Forces supported by a DOM and zenith angle. **(c)** r_j displacement and $interDOMdist_j$.

The tangent of zenith angle, α, at a given height z, of the line is given by the ratio of horizontal drag force, F, and a vertical buoyancy, W. This is the resultant of forces summed over all the line elements above this height z:

$$\tan(\alpha) = \frac{dr}{dz} = \frac{F(z)}{W(z)} \tag{3.10}$$

$$F(z) = f(z)\ v^2 = \left\{ \left[\sum_{k=1}^{18} \left(f_{DOM} + f_{cable_{k+1}} \right) + f_{cable_1} \right] \left(\frac{h-z}{z} \right) + f_{top\ buoy} \right\} v^2 \tag{3.11}$$

where $F(z)$ represents the drag force at height z of the line (being h the maximum height of the DU). This depends on the *drag parameter* f of the different elements (*Equation 3.13*) and on the sea current velocity v.

$$W(z) = \left[\sum_{k=1}^{18} \left(W_{DOM} + W_{cable_{k+1}} \right) + W_{cable_1} \right] \left(\frac{h-z}{z} \right) + W_{top\ buoy} \tag{3.12}$$

where $W(z)$ represents the vertical force that depends on the buoyancy force W of all elements along the DU.

It is possible to determine the *drag parameter* f_i for each element (see *Table 3.4*):

$$f_i = \frac{1}{2}\, C_{D_i}\, A_i\, \rho \tag{3.13}$$

where f_i represents the *drag parameter* on the element j that depends of its drag coefficient C_D, its cross section area A and the density of the environment ρ.

The *drag parameter* f depends on the values of C_D, which in KM3NeT elements can change because of the direction of the drag force F. This change is especially noticeable in the case of DOMs. As they have two supports on each side, the axisymmetry is destroyed. In addition, the tension of the cables will be affected differently also by the orientation in which the DU base was installed [48].

Table 3.4 presents the values of the f (*Equation 3.13*) and the buoyancy W (*Equation 3.12*) for the KM3NeT elements along the DU line for an F incidence direction of 0 degrees.

Detector	**Property**	**Element** i		
		DOM + support	$cable_1$	**Top Buoy**
ARCA	f $[N\ s^2/m^2]$	51.65	659.51	312.95
	W $[N]$	125.57	0	1030.05
ORCA	f $[N\ s^2/m^2]$	51.65	252.28	312.95
	W $[N]$	125.57	0	1226.25

Table 3.4: Mechanical properties of the elements in a DU line of KM3NeT.

The *drag parameter* for the inter DOM cables ($cables_{\ 2-18}$) is 377.07 ± 4.47 and 95.56 ± 6.67 $\mathrm{Ns^2/m^2}$ for ARCA and ORCA respectively, depending on the cable length between DOMs. The upper cable ($cable_{19}$, between the top buoy and last DOM) *drag parameter* is 52.73 $\mathrm{Ns^2/m^2}$ in both detectors.

3.2.1 Mechanical equations for the model

The equations of the MM seek to be simple and direct, as they are linear equations. The MM of KM3NeT develops two different analyses, depending on the origin of their variables: the *TILT* for the α data, and the *POS* for the XYZ data analysis.

Both analysis consider that the total *drag* and buoyancy forces contributed to the DU line by each floor j (η_j and ξ_j) depend on these parameters for the element and its bottom (see Equation 3.14). Therefore, the *TILT* and the *POS* analysis are reconstructing the shape line floor by floor (from low to up).

$$\begin{aligned} \eta_j &= f_{cable_j} + f_i \\ \xi_j &= W_{cable_j} + W_i \end{aligned} \tag{3.14}$$

Equation for a TILT analysis

To study the estimated α by DOMs, and based on *Equation 3.10*, the next equation is necessary:

$$\mathbf{tan(\alpha_j)} = \frac{f_j}{W_j} \cdot v^2 = \frac{\eta_j + \eta_{j+1}}{\xi_j + \xi_{j+1}} \cdot v^2 = \boldsymbol{Mech_{tilt_j} \cdot v^2} \tag{3.15}$$

In the end, this linear fit equation considers a *mechanical constant*, $Mech_{tilt}$, which depends on the different floor j and the squared effective sea current velocity (v^2) as an independent variable.

Since the coefficient $Mech_{tilt_j}$ is known (see *Table 3.6* and *Figure 3.5*), it is a matter of getting one of the other two variables (α_j or v^2) as inputs so that the remaining one becomes an output directly.

Equations for a POS analysis

The basic MM scheme in *Figure 3.4* shows how the displacement r_j (displacement radial relative between two consecutive DOMs $_{j-1} \rightarrow _j$) is estimated from the inter DOM distances and the sinus of zenith angle. Since the α values are expected to be less than 3.5 degrees (in a normal situation it is less than 1 degree, see *Figure 3.6* and *Figure 3.7*), the approximation $\sin(\alpha) \cong \tan(\alpha)$ can be done. Then, the r_j displacement using the mechanical parameters, and the effective sea current velocity v can be estimated:

$$
\begin{aligned}
r_j &= \sin(\alpha_j) \cdot interDOMdist_j \cong \tan(\alpha_j) \cdot interDOMdist_j = \\
&= \frac{f_j}{W_j} \cdot v^2 \cdot interDOMdist_j = \\
&= \frac{(\eta_j + \eta_{j+1}) \cdot interDOMdist_j}{\xi_j + \xi_{j+1}} \cdot v^2 = mech_{pos_j} \cdot v^2
\end{aligned}
\tag{3.16}
$$

Therefore, the radial displacement accumulated at height z_j corresponds to the accumulative value of the r_j displacements in the previous DOMs:

$$
\boldsymbol{r_{zj}} = \sum_{i=1}^{i=j} r_i = (mech_{pos_j} + mech_{pos_{j_{-1}}}) \cdot v^2 = \boldsymbol{Mech_{pos_j} \cdot v^2} \tag{3.17}
$$

where i represents the floor of the element to calculate its accumulated radial displacement.

In the same way that the *TILT* analysis, the equation for a *POS* analysis consists in considering a dependent variable (r_{zj}), and the squared effective sea current velocity (v^2) as an independent variable. The coefficients are the formerly studied $Mech_{pos}$ (see *Table 3.5* and *Figure 3.5*). Since the $Mech_{pos}$ constants are already known, it is a matter of getting one of the other two variables (r_{zj} or v^2) as inputs so that the remaining one becomes an output directly.

In addition, since the DU bases are not positioned with an accuracy greater than 1-2 meters when they are geolocated during the deployment marine campaign with the Remotely Operated Vehicle (ROV), an option is to leave the $offset_r$ parameter free, which will represent the radial displacement from the DU base and the DOM in the first floor:

$$
r_z = Mech_{pos} \cdot v^2 + offset_r \tag{3.18}
$$

Mechanical constants

The mechanical constants for *TILT* and *POS* analysis ($Mech_{tilt}$ and $Mech_{pos}$) are presented in *Table 3.5* and *Table 3.6* respectively. Since in ORCA006, the DU9 has no Top Buoy (it had to be cut due to a failure during its deployment), its mechanical constants are also calculated.

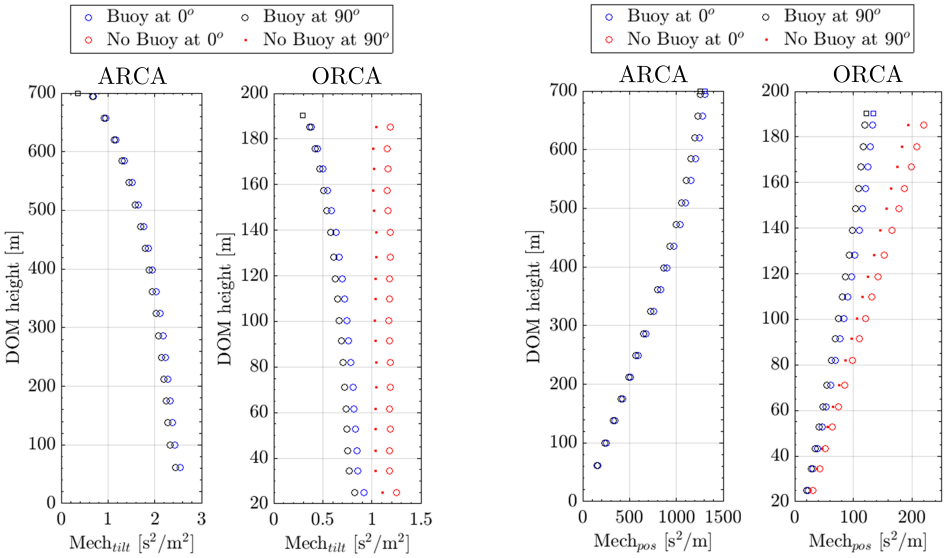

Figure 3.5: Mechanical constants for the DU Line Fit analysis. The representations are for 0 and 90 degrees of sea current incidence. In the case of ORCA, they show the values for a DU with and without the top buoy. **(a)** $Mech_{tilt}$. **(b)** $Mech_{pos}$.

	POS analysis $Mech_{pos}$ [s^2/m]					
	ARCA		ORCA			
	Top Buoy		Top Buoy		No Top Buoy	
Incidence in DOM:	**0 deg.**	**90 deg.**	**0 deg.**	**90 deg.**	**0 deg.**	**90 deg.**
DU base	0.000	0.000	0.000	0.000	0.000	0.000
DOM 1	157.578	151.473	22.797	20.487	31.140	27.576
DOM 2	249.784	240.006	31.033	27.851	42.467	37.530
DOM 3	339.911	326.548	38.493	34.527	52.875	46.677
DOM 4	425.939	409.163	46.477	41.682	64.202	56.634
DOM 5	511.664	491.500	53.686	48.149	74.610	65.783
DOM 6	594.884	571.444	61.379	55.062	85.946	75.752
DOM 7	674.864	648.291	69.984	62.805	98.906	87.150
DOM 8	754.163	724.502	77.288	69.384	110.163	97.037
DOM 9	830.180	797.578	83.813	75.271	120.500	106.115
DOM 10	902.010	866.650	90.697	81.500	131.767	116.015
DOM 11	971.536	933.537	96.793	87.030	142.112	125.104
DOM 12	1036.922	996.471	103.164	92.832	153.410	135.038
DOM 13	1097.251	1054.578	110.072	99.148	166.293	146.365
DOM 14	1153.800	1109.095	115.702	104.316	177.373	156.081
DOM 15	1204.197	1157.742	120.496	108.745	187.499	164.955
DOM 16	1246.554	1198.706	125.269	113.199	198.587	174.682
DOM 17	1281.731	1232.845	129.146	116.863	208.683	183.527
DOM 18	1306.943	1257.484	132.755	120.346	219.934	193.420
Top Buoy	1308.789	1259.331	134.306	121.897	-	-

Table 3.5: Mechanical constants for POS analysis in the DU Line Fit. For ORCA, it is taken into account the case of DU9 that does not have Top Buoy.

	TILT analysis $Mech_{tilt}$ [s^2/m^2]					
	ARCA		ORCA			
	Top Buoy		Top Buoy		No Top Buoy	
Incidence in DOM:	0 deg.	90 deg.	0 deg.	90 deg.	0 deg.	90 deg.
DU base	0.000	0.000	0.000	0.000	0.000	0.000
DOM 1	2.540	2.442	0.916	0.823	1.252	1.108
DOM 2	2.425	2.329	0.860	0.769	1.182	1.039
DOM 3	2.381	2.287	0.847	0.758	1.182	1.038
DOM 4	2.334	2.241	0.835	0.748	1.185	1.042
DOM 5	2.286	2.196	0.820	0.736	1.184	1.041
DOM 6	2.231	2.143	0.806	0.725	1.188	1.045
DOM 7	2.172	2.087	0.789	0.710	1.188	1.045
DOM 8	2.108	2.026	0.764	0.688	1.178	1.034
DOM 9	2.034	1.955	0.742	0.670	1.176	1.033
DOM 10	1.952	1.877	0.722	0.653	1.181	1.038
DOM 11	1.863	1.792	0.695	0.631	1.180	1.036
DOM 12	1.760	1.694	0.669	0.609	1.187	1.044
DOM 13	1.643	1.582	0.636	0.582	1.186	1.043
DOM 14	1.510	1.456	0.591	0.543	1.164	1.021
DOM 15	1.352	1.305	0.548	0.506	1.157	1.014
DOM 16	1.166	1.128	0.502	0.469	1.167	1.024
DOM 17	0.952	0.924	0.444	0.420	1.157	1.013
DOM 18	0.685	0.670	0.381	0.367	1.187	1.044
Top Buoy	0.355	0.355	0.298	0.298	-	-

Table 3.6: Mechanical constants for TILT analysis in the DU Line Fit. For ORCA, it is taken into account the case of DU9 that does not have Top Buoy.

3.2.2 DOMs position estimation from sea current properties

The *mechanical equations* for the *POS* analysis (*Equation 3.17*) help to reconstruct the DU line shape forced by the sea current. If realistic sea current properties (effective velocity v and direction ω) are applied, the DU line shape could be reconstructed:

$$\begin{aligned} X_{j\ rec.} &= DU_x + \sin(\omega) \cdot r_{zj\ rec.} \\ Y_{j\ rec.} &= DU_y + \cos(\omega) \cdot r_{zj\ rec.} \\ Z_{j\ rec.} &= DU_z + \sum_{i=1}^{j} interDOMdist_{\ i_{-1} \rightarrow i} \end{aligned} \tag{3.19}$$

where DU represents the DU base position in its Cartesian coordinates.

Using the $XYZ_{rec.}$ of *Equation 3.19*, the cumulative radial displacement $R_{j\ rec.}$ (*Equation 3.20*) and zenith angle $\alpha_{j\ rec.}$ (*Equation 3.21*) can be predicted for every DOM.

$$R_{j\ rec.} = \sqrt{X^2_{j\ rec.} + Y^2_{j\ rec.}} \tag{3.20}$$

$$\tan \alpha_{j\ rec.} = \frac{R_{j\ rec.}}{Z_{j\ rec.}} \tag{3.21}$$

So *Figure 3.6* and *Figure 3.7* represent the reconstructed shape of a DU in ARCA and ORCA respectively. They show the DOM displacement $R_{j\ rec.}$ and tilt $\alpha_{j\ rec.}$ for different sea currents. This is possible by applying *Equation 3.17* to the sea current velocities, reconstructing the XYZ positions with *Equation 3.19* and applying *Equation 3.20* and *Equation 3.21*.

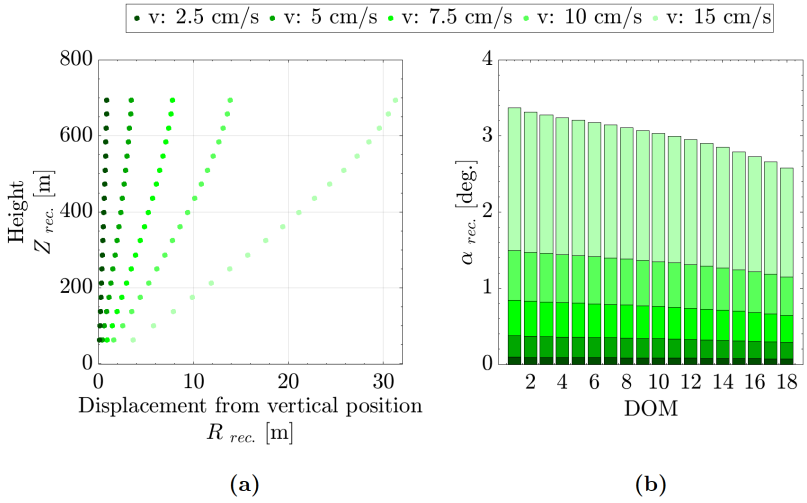

(a) **(b)**

Figure 3.6: MM applied to different sea current velocities in ARCA **(a)** Radial displacement accumulated at DOMs height estimation. **(b)** Tangent of zenith for each DOM estimation.

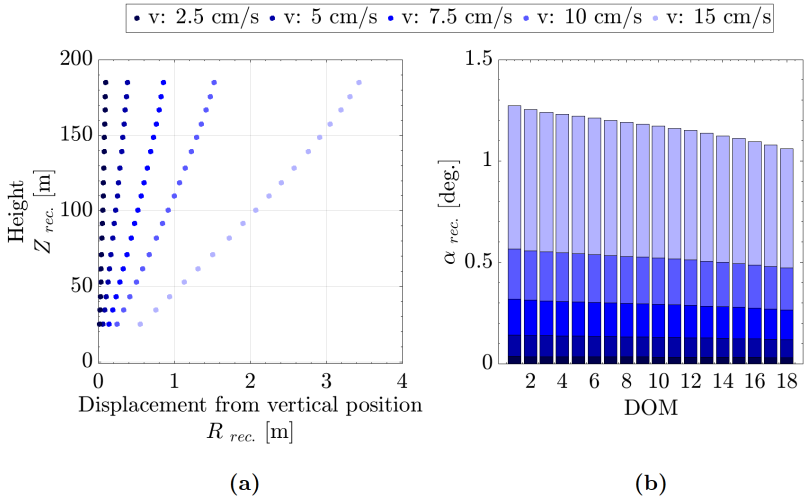

(a) **(b)**

Figure 3.7: MM applied to different sea current velocities in ORCA **(a)** Radial displacement accumulated at DOMs height estimation. **(b)** Tangent of zenith for each DOM estimation.

ARCA is shown to be more sensitive to the movement produced by the sea current, as it moves the line more from its axis at rest than ORCA (see *Figure 3.6* and *Figure 3.7*). This is to be expected given the difference in height of the DUs. While in ORCA the top buoy moves 0.86 m with a current of 7.5 cm/s (maximum zenith angle of first DOM 1 at 0.32 degrees), in ARCA it displaces 7.82 m (maximum zenith angle of first DOM at 0.84 degrees). Moreover, given the shape of the DU, the zenith angle of the DOM decreases gradually as they move away from the base.

3.3 MM application to the reconstruction: the DU Line Fit

The DU line fit consists of different analyses of different data to obtain a reconstruction in the position and the orientation of the DOMs, improving the precision of classical methods for this purpose [49]. *Figure 3.8* summarizes the internal processes of the DU Line Fit according to the different data to be analyzed: the original data is processed, the DU Line Fit applies the MM to obtain effective sea current properties (velocity and direction), and it uses these parameters to reconstruct the positions of the DOMs.

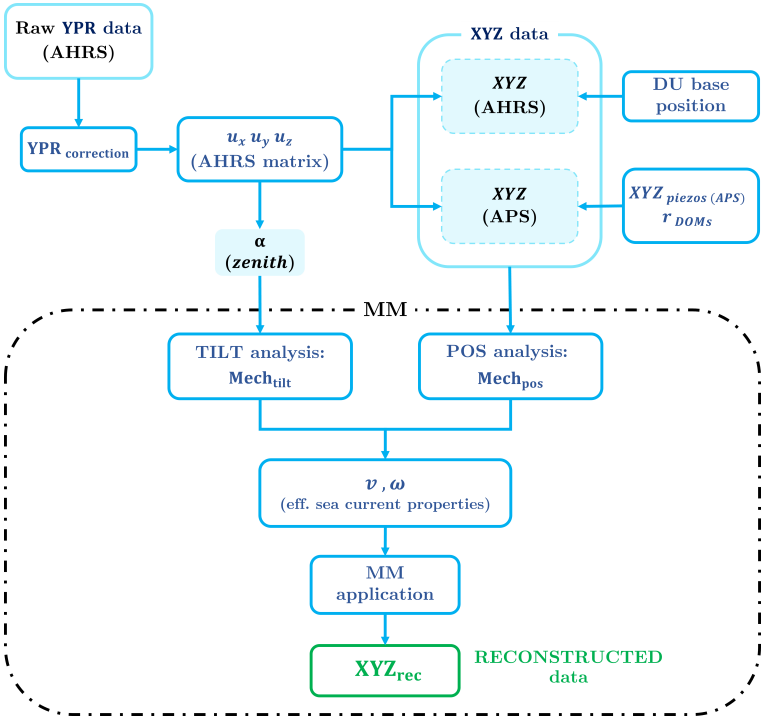

Figure 3.8: Internal DU Line Fit process to calculate the reconstructed positioning data from different data type (XYZ or YPR).

3.3.1 TILT analysis

The *TILT* analysis procedure of the DU Line Fit studies the α data. This data is provided by the DU Line Fit analysis in the YPR data (see *Equation 3.5*). The idea of this analysis is to obtain an effective sea current speed (v) and an effective sea current direction (ω) for the determination of DOM positions.

Considering the *tilt mechanical constants*, $Mech_{tilt}$, of the floors and the tangent of the zenith angle (tan α) provided by each DOM along the DU line. The *Equation 3.15*, the v^2 parameter can be obtained from a linear fit. The ω is calculated projecting the xy components of the *AHRS matrix* and fitting a line giving through the origin (see *Equation 3.6*).

Figure 3.9 shows the processes calculated to obtain the effective sea current speed and direction, using the values from the *Table 3.3* after *AHRS matrix* calculation. The goodness of effective sea current estimation is controlled by the error in the fitting value and the squared correlation coefficient (r^2).

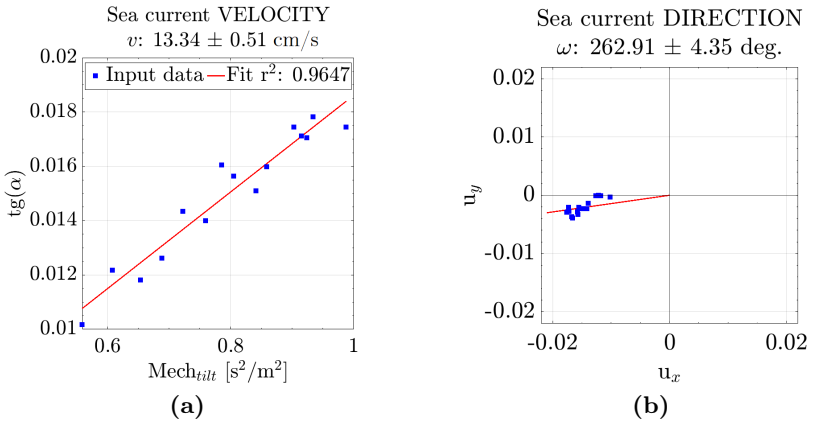

Figure 3.9: *TILT* analysis applied to the data on *Table 3.3*. **(a)** Fit to obtain the effective sea current velocity v according to *Equation 3.15*. **(b)** Fit to obtain the effective sea current direction ω according to *Equation 3.6*.

Once the effective sea current parameters are estimated, the final step is to use the MM again to reconstruct the DOMs positions (see *Equation 3.19*) and fit the DU Line shape.

3.3.2 POS analysis

The *POS* analysis procedure of the DU Line Fit is applied to the XYZ data. It does not matter where the *position data* comes from (APS, with the piezoceramic translation to the center of the DOM, or AHRS with the correction and transformation). This analysis, like the *TILT* analysis, also consists of estimating effective sea current speed, v, and direction, ω, studying the input data, and then applying an MM reconstruction with these parameters. The ω is calculated projecting the $Diff\ xy$ components of the data and fitting a line giving through the origin (see *Equation 3.6*).

Figure 3.10 shows the processes calculated to obtain the effective sea current properties using the $XYZ_{rec.}$ values from the *Table 3.3* using *Equation 3.8*. At

all times, the effective sea current estimation is controlled by the error in the fitting value and the correlation coefficient (r^2).

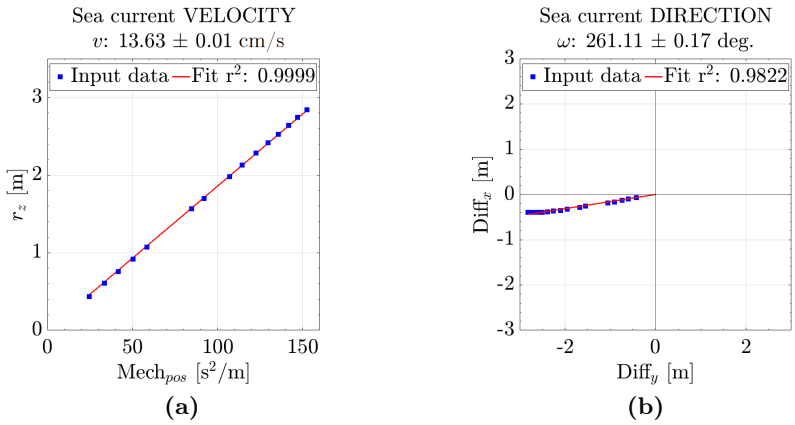

Figure 3.10: *POS* analysis applied to the data on *Table 3.3* after $XYZ_{rec.}$ calculation using *Equation 3.8*. **(a)** Fit to obtain the effective sea current velocity v according to *Equation 3.18*. **(b)** Fit to obtain the effective sea current direction ω according to *Equation 3.9*.

Once the effective sea current parameters are estimated, the final step is to use the MM again to reconstruct the DOMs positions (see *Equation 3.19*).

3.3.3 Mechanical reconstruction

Figure 3.11 shows how the MM reconstruction is applied for the DU3 in ORCA detector using the mean effective sea current parameters estimated in the *TILT* and *POS* analysis.

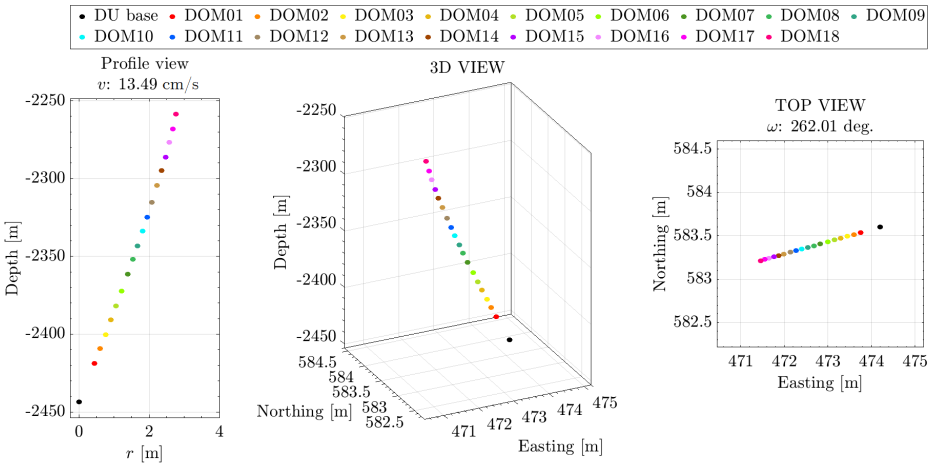

Figure 3.11: Mechanical reconstruction from the mean value of the sea current properties by the two different analysis. Profile, 3D, and top views of the reconstructed DU line.

Results

With the intention of conveying the capabilities of the DU Line Fit application, a complete experimental *POS* analysis (3 hours of data taking) is carried out in this section. On this occasion, the example is applied for ORCA006: RUN 7523 (24^th Feb. 2020 from 6:00 to 9:00).

During this period, the raw YPR was downloaded from the PCBs. Then, the DU Line Fit procedure splits the data in measures of 10 minutes and calculates their average values for the analysis. The DU Line Fit is applied measure by measure, in an independent way: it corrects the data, it transforms them into positions, and it applies the MM to save the reconstructed data as an output method. The 4 next figures (*Figures 3.12*, *3.13*, *3.15*, and *3.14*) represent these outputs of the DU Line Fit application in the analyzed period.

Figure 3.12 is a top view of the detector, with the reconstructed DOMs positions during the period. In the figure, it can be observed how a DU (called *DU*9) has a different displacement. It is because it does not have top buoy, and behaves differently when facing sea current changes.

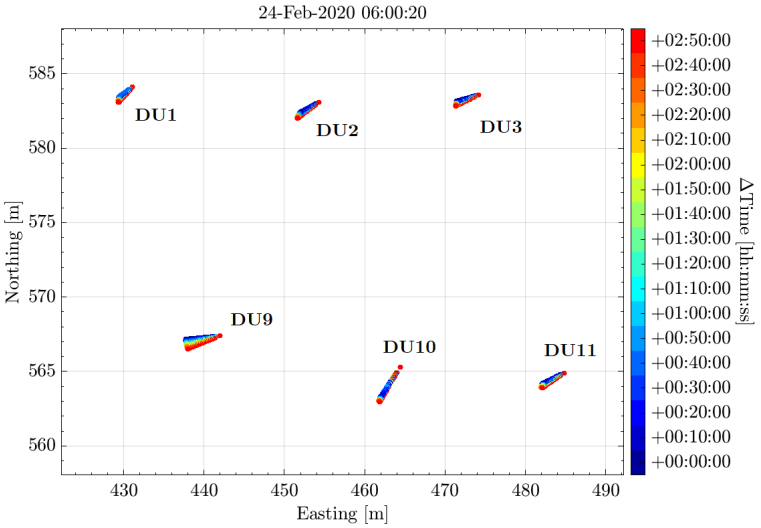

Figure 3.12: Top view of ORCA006 after DU Line Fit model application during 3 hours of analysis.

It can be appreciated how the sea current produces slight movements in the DOMs. *Figure 3.13* shows a profile view for each DOM, to appreciate the DU line shape and the maximum displacement for each one. Here the difference in tilt between DUs with and without top buoy is more noticeable.

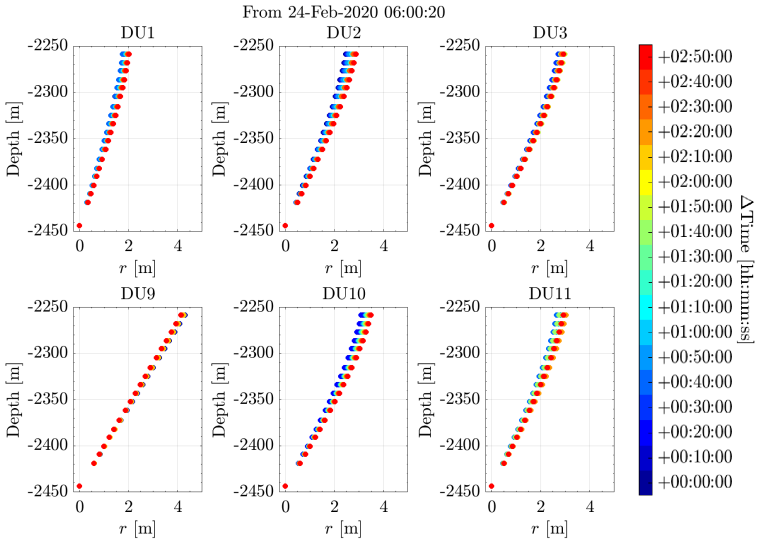

Figure 3.13: Profile view of the DUs in ORCA006 after DU Line Fit model application during 3 hours of analysis.

For a more direct comparison of the direction of the DUs, in *Figure 3.14* there is a top view of the reconstructed DUs with respect to base at the start, in the middle, and at the end of the period. The sea current properties derived from the three measures, and used for the MM reconstruction are also shown.

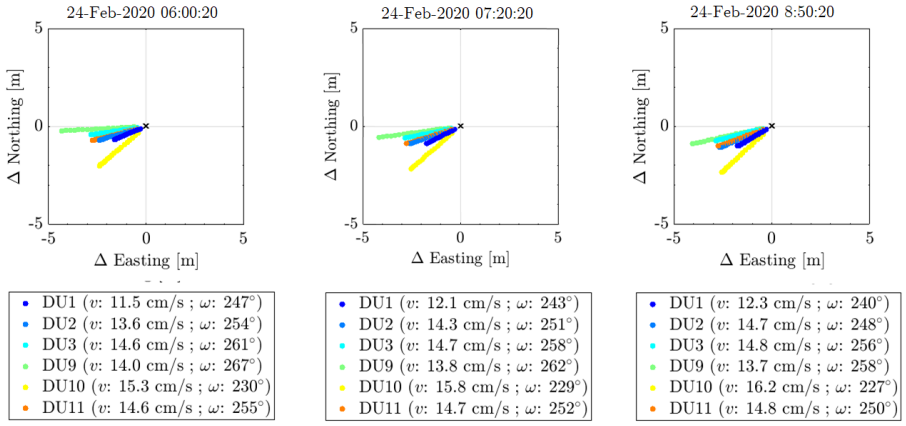

Figure 3.14: DU Line Fit application for the first, middle and last measure in RUN 7523 of ORCA006.

Finally, *Figure 3.15* shows the effective sea current properties estimated from the analysis of the positions of the DOMs (after transformation from YPR data) and used in the previous MM reconstructions. This data seems to have less deviation between DUs than those provided by the European Multidisciplinary Seafloor Observatory (EMSO) Instrumented Interface Module (MII) Acoustic Doppler Current Profiler (ADCP) in ORCA site.

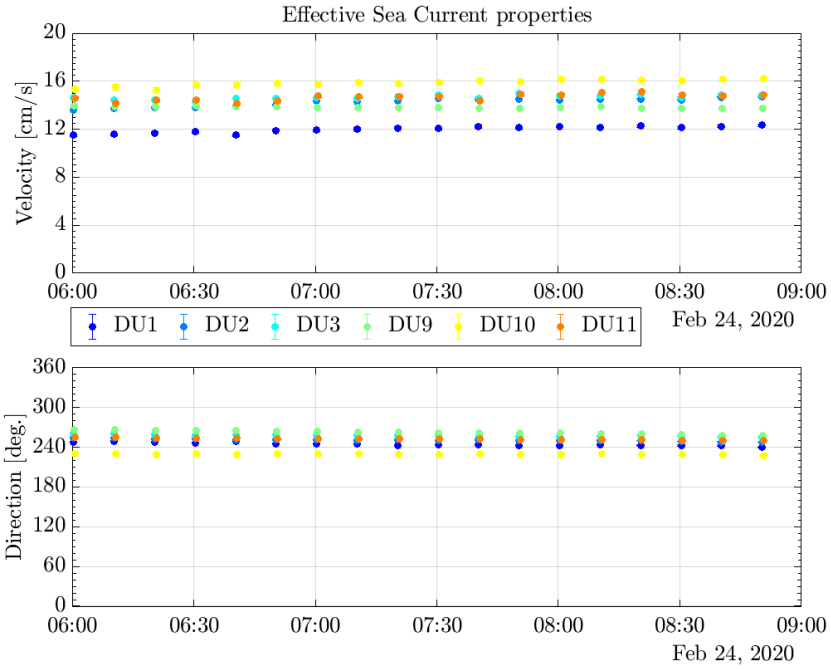

Figure 3.15: Effective sea current properties estimation (velocity on top and direction on bottom) during the RUN 7523 of ORCA006 using the DU Line Fit model.

3.4 Conclusions and future steps

Conclusions

The DU Line Fit process is defined in detail and it is ready for its application. It is set to treat the data provided by the AHRS or a combination of AHRS and APS, allowing the DOMs position and orientation monitoring. Moreover, it solves the question of how a line without a top buoy behaves and can take into account this anomaly on the DU.

The DU Line Fit analysis allows to reconstruct the DU shape improving the accuracy of the individual DOM positioning methods during strong sea current periods. It is demonstrated how both methods (*TILT* and *POS*) have similar results, as shown in *Figure 3.9* and *Figure 3.10*.

The idea of the DU Line Fit application is to control the movement and to understand the shape of the AHRS lines (monitoring the position and orientation of the DOMs). This method can be integrated automatically into the detector process and its output can be registered so to take it into account for the analysis of triggered events and the reconstruction of the direction of particles generated, tracks, or showers.

Future steps

As it has been noted, the DU Line Fit is very sensitive to the input data in the AHRS matrix (XYZ data). Thus, the application of the offset for its correction is a step that requires caution. These offsets should be as accurate as possible to ensure the best of the DU Line Fit model. For this reason, it is advisable to continue studying more calm periods, and to study in detail the offsets and the DU Line Fit application. The study and the identification of calm periods could be automatized programming an alert in the YPR data monitoring.

Until now, the DU Line Fit has been applied and it has been useful for strong sea current periods (critical situations) in its current version. However, it would be appropriate to calibrate the reconstruction model to estimate the DU line shape in sea current calm periods.

Part II

Acoustic Signal Analysis for Unknown Sources. Studies for Acoustic Neutrino Detection

Chapter 4

Full Acoustic Calibration of Underwater Neutrino Telescopes using a Compact Array Transducer

The idea of this chapter is to describe a calibration technique for an underwater telescope's acoustic system. The calibration system requires synchronization between the emission-reception step and the subsequent analysis. The calibration process will consist in emitting a known and characterized signal from the source, then analyzing the recorded raw acoustic data on the sensors and detecting it. In KM3NeT, this would be done during a marine campaign using a transducers array designed to emit high power over a wide range of frequencies and direct the beam from a ship. The calibration method will not only allow us to study the response of the system to each acoustic signal emitted but it can also be used to develop new analysis techniques to detect less common signals such as neutrino interactions. The possibility to realize an acoustic neutrino detection requires the presented techniques to study its viability.

The parametric effect allowing to generate of low frequencies with narrow directivities, proposed for the emission of Bipolar Pulses, is explained in *section 4.1*. Then, *section 4.2* proposes a complete calibration of the detector (*subsection 4.2.1*) using one of the arrays designed for this purpose (*subsection 4.2.2*) and following three different calibration steps (*subsection 4.2.3*, *subsection 4.2.4*, and *subsection 4.2.5*).

So far underwater neutrino telescopes are equipped with an Acoustic Positioning System (APS). This positioning system opens up many possibilities. While its main goal is to monitor the position of the light detectors, it opens up a whole range of secondary acoustic studies, thanks to the receivers used: bioacoustics, ship noise monitoring, environmental noise control, acoustic neutrinos detection, etc. The acoustic detection of neutrinos is one of the most promising possibilities to extend the neutrino telescopes to the Ultra High Energy (UHE) range. In fact, having a hybrid underwater neutrino telescope (optical-acoustic) is the only possibility to extend the energy range detection beyond 100 PeV, with a reasonable number of sensors (see *Figure 1.10*). The acoustic neutrino detection technique is based on the discovery of the pressure pulse generated by the heating of the water by the hadron cascade after the interaction of the neutrino (see *Figure 4.1.a*). The particularities of the radiated pulse (high-directivity bipolar pulse with axial symmetry) would allow, on the one hand, to distinguish it from other types of signals much more abundant, and on the other hand, to determine the source direction with a few degrees of resolution.

To discriminate this singular little neutrino signature with the highest precision, as the light sensors, the acoustic sensors need to be calibrated. As seen in *chapter 2*, the sensors of the APS are already calibrated and characterized before deployment, but it is once they are installed on the seabed that their response to the background noise in the environment should be studied. For this reason, this chapter proposes an in situ calibration of the positioning system's acoustic receivers. The aim of this process is to determine the response of the system already in operation, which may be affected by the passage of time or depend on the background noise at the given time. It will not only allow us to study the sensitivity of the different sensors, but it can also be used to see the feasibility of developing an UHE neutrino detector. If we are able to emit and capture such a unique signal, we will be able to experiment with new analysis techniques to detect them.

4.1 Using the Parametric Effect to Reproduce the Acoustic Neutrino Signature

The main special feature of the neutrino acoustic signature is that it is a kind of acoustic bipolar pulse propagated in a very narrow beam (less than 5^o), which turns out to be a very directive low-frequency range signal (less than 100 kHz), a very rare phenomenon in nature.

Over the last decades, different experimental techniques have been developed to reproduce it. One of the proposals for its reproduction has been to take advantage of the so-called parametric effect that arises from the natural propagation of an acoustic wave in a non-linear medium to obtain low-frequency signals with pronounced directivity.

In this section, the acoustic neutrino signature and the theoretical principle of the acoustic parametric effect are explained. In *subsection 4.2.2*, the prototypes of acoustic emitters developed to date with the intention of reproducing a Bipolar Pulse (BP), will be presented. The last two prototypes were already intended to take the advantages of the parametric effect to generate it.

4.1.1 The Acoustic Neutrino Signature

When a UHE neutrino interacts with a non-linear fluid (such as water or ice) and produces a muon (see *subsection 1.1.1*), an acoustic signal is generated in turn. The acoustic pulse generated sits in a "pancake" perpendicular to the original neutrino direction along 1 km. Their typical opening angle is less than 5 degrees [7] (see *Figure 4.1.a*). Along the path of the neutrino energy deposition, the temperature increases immediately. The corresponding acoustic pulse shape is defined by the double derivative (with respect to time) of this temperature profile. This gives rise to a characteristic acoustic wave which is bipolar in shape (see *Figure 4.1.b*) and has a typical frequency of 10–50 kHz [21, 22] (see *Figure 4.1.c*). This type of signal would also be produced by the interaction with the rock that forms the earth's crust, although its amplitude is estimated with an order of greater magnitude [50].

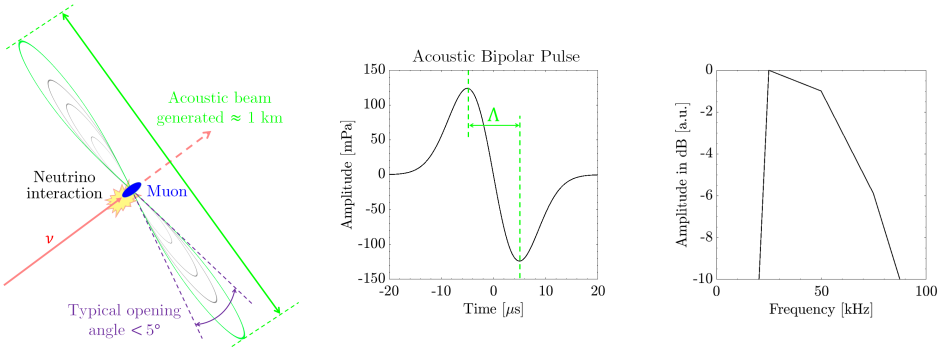

(a) **(b)** **(c)**

Figure 4.1: **(a)** Acoustic "pancake" beam generation from a neutrino interaction. **(b)** Acoustic BP simulating the signal after neutrino interaction on a fluid. The amplitude is from a neutrino deposition of 10^{11} GeV of thermal energy at 1 km and 0 degrees. For this example, the Λ value is 10 μs, and the maximum pressure is 124 mPa [51]. **(c)** Acoustic BP in frequency domain (f_s = 20 MHz). The -3 dB decay occurs between 20 and 60 kHz.

There are several equations to simulate a BP from the interaction of a neutrino in fluid. On this occasion, it has been chosen to simplify the generation of a $BP(t)$: by deriving a normal distribution $g(t)$.

$$g\left(t\right) = e^{-\frac{1}{2}\left(\frac{t}{\sigma}\right)^2} = e^{\frac{-t^2}{2\sigma^2}} \tag{4.1}$$

where the σ represents the standard deviation at a confidence interval of ~68%.

To control the width of the BP, the inter-peak value Λ should be equivalent to 2σ:

$$BP\left(t\right) = \frac{dg}{dt} = -\frac{t}{\sigma^2} \cdot e^{\left[\frac{-t^2}{2\sigma^2}\right]} \quad \xrightarrow{\Lambda=2\sigma} \quad BP\left(t\right) = \frac{-4t}{\Lambda^2} \cdot e^{-2\left(\frac{t}{\Lambda}\right)^2} \tag{4.2}$$

Therefore, the acoustic neutrino signature is an exotic signal that contains a range of low frequencies (less than 70 kHz).

4.1.2 The Acoustic Parametric Effect

The parametric effect is a non-linear physical phenomenon that appears in the propagation of intense waves. In acoustics, it may result in the appearance of "new" frequencies that were not present in the emitted signal during its propagation. It corresponds to combinations of existing frequencies, such as sum, difference frequencies, and harmonics. This effect permits to produce a differential frequency, 2^{nd} beam, between two adjacent tones of high frequencies during the propagation of the high-intensity wave, the 1^{st} beam (see *Figure 4.2*).

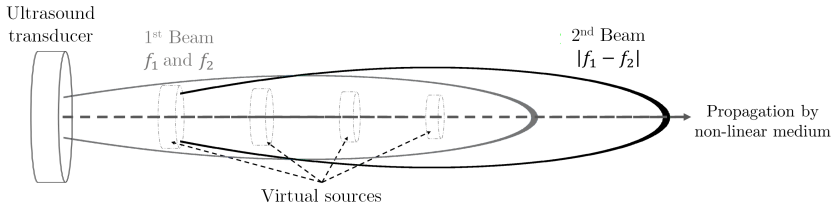

Figure 4.2: Generation of the parametric frequency-difference effect in a non-linear medium. In grey, the 1^{st} beam, which corresponds to the signal emitted by the transducer. In black, the 2^{nd} beam, which corresponds to the parametric signal generated along the propagation through a non-linear fluid of the 1^{st} beam.

The theoretical studies have determined that the shape of this 2^{nd} beam (the "new" signal) corresponds to the second derivative of the square envelope of the 1^{st} beam (the emitted signal) [52, 53]. The waveform and the amplitude of this parametric effect is determined by the following equation:

$$p\left(x,t\right) = \left(1 + \frac{B}{2A}\right) \frac{P^2 S}{16\pi\rho c^4 \alpha x} \frac{\partial^2}{\partial t^2} \left[E\left(t - \frac{x}{c}\right)\right]^2 \tag{4.3}$$

where p is the pressure of the 2^{nd} beam in x position at time t, $\frac{B}{A}$ is the non-linear medium parameter, P is the pressure of the 1^{st} beam, S the surface of emitter transducer, ρ the medium density, c the propagation sound velocity in the medium, α the sound absorption medium coefficient, and E the envelope function of the emitted signal.

Another characteristic of the parametric effect, being a non-linear phenomenon, is that the intensity of the parametric signal (2^{nd} beam) does not increase linearly with the intensification in the intensity of the emitted signal (1^{st} beam).

This technique of being able to broadcast low frequencies in a directive (i.e. more directed) way has opened up the possibility of research into new underwater communications techniques [25, 26, 54, 55].

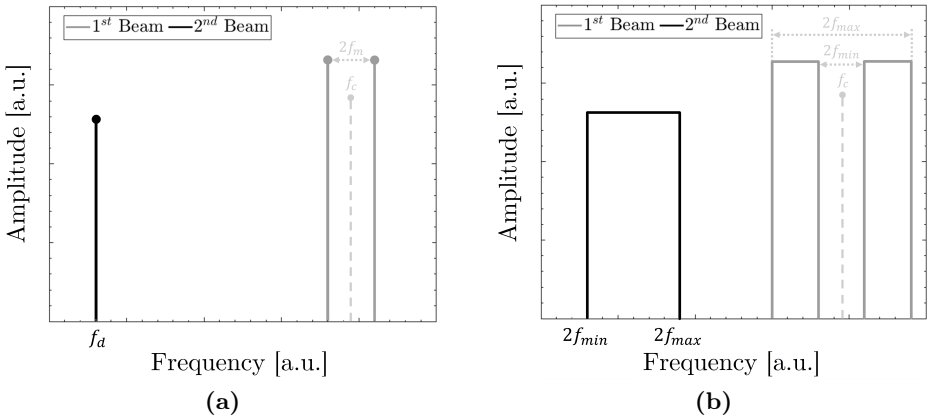

Figure 4.3: (a) Non-linear effect using a parametric sinusoidal signal in frequency domain. **(b)** Non-linear effect using a parametric sweep signal in frequency domain.

For this second calibration step, two types of parametric signals are defined: sinusoidal and sweep. This type refers to the envelope wave (E) in the linear modulation process to produce it. The modulation used is an AM DSB-SC (Amplitude Modulation Double Side Band–Suppressed Carrier), where the lower frequency signal (modulating signal, which will act as an envelope with f_m frequencies) is multiplied with a high-frequency signal (sinusoidal carrier signal of f_c Hz) [56].

By using this modulation it is possible to control the parametric effect (2^{nd} beam) that will be created, since it generates a signal of spectral content around the f_c that depends on the frequency in the modulating signal, f_m: the emitted signal will contain spectral information in $f_c - f_m$ (Lower Side Band) and $f_c + f_m$ (Upper Side Band), which will be the 1^{st} beam, and the frequency difference f_d ($f_d = 2f_m$) will be the one that will appear during its propagation due to the parametric effect, the 2^{nd} beam. Then, if we are talking about a parametric sine (see *Figure 4.3.a*), the frequencies of both beams will be point-like. However, if we assume a parametric sweep (see *Figure 4.3.b*), the 1^{st} beam will have spectral content from $f_c - f_{max}$ to $f_c - f_{min}$ and $f_c + f_{min}$ to $f_c + f_{max}$, and the 2^{nd} beam will be a sweep from $2f_1$ to $2f_2$, where f_1 is the initial frequency and f_2 is the final frequency of the sweep.

4.2 Acoustic Calibration of Underwater Neutrino Telescopes

Laboratory calibration is important for acoustic neutrino detection, but in situ calibration should be labeled as essential. A good calibration should monitor the detection system by checking the sensitivity and response of each acoustic sensor individually (see *section 2.4*). From this, to have knowledge about the overall sensitivity and response of the whole system (full acoustic calibration in *subsection 4.2.1*), to test and validate the acoustic neutrino detection technique by studying the signal/background separation, reproducing some kind of events (with the help of a special array designed for this purpose in *subsection 4.2.2*) and determining the reliability of the system. For this purpose, it would be better to have a system with easy and versatile operation in hard environments, such as the deep sea KM3NeT [57]. In the end, calibration is a stage that requires the connection between the emitters to be used, the receivers to be characterized, and the signals to be emitted, and given its requirements, the best way is to develop these technologies as a whole, integrated on the same system (a challenging task).

4.2.1 The full calibration for KM3NeT

Prior to using any sensor, they should be characterized and calibrated in order to know its behaviour and response to different possible scenarios. KM3NeT has a powerful acoustic positioning system for Digital Optical Modules (DOMs) location. However if you want to raise the level of exigency in this system, and take advantage of its full potential by exploring all its possibilities, it is necessary to know how it responds once installed in depth. To this end, this chapter proposes a complete calibration of the acoustic sensors in underwater neutrino telescopes in order to characterize the response of the detector in all its frequency bands and for all its possible uses. This calibration is intended to be performed using an array of sources like the formerly presented prototypes. This section will refer to the use of the last presented array.

The full calibration process has been divided into three steps, depending on the type and the level of complexity. Each level will emit a type of signal, with the idea of detecting it later in the signals recorded by the sensors and analyzing its reception (amplitude and frequency response):

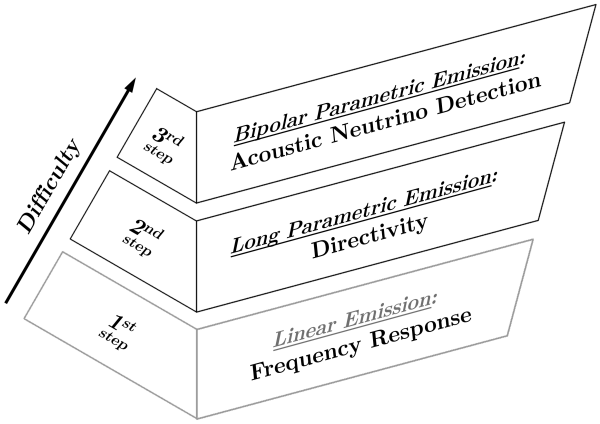

Figure 4.4: Strategy for the full calibration with the compact array.

The combination of the three in one unique tool, the compact array, not only increases the versatility and functionality of the two but also paves the way towards the most difficult task. The first step consists of low-frequency linear emission with the array, the other two steps are directive non-linear emissions using the parametric effect.

4.2.2 The compact array transducer prototype: the bipolar pulse emitter

During the last few years of the development of deep-sea neutrino telescopes, experiments have been carried out to create a powerful array of transducers capable of emitting acoustic signals from the ship to the telescope during a marine campaign. The main particularity these emitters have is that they are able to produce the particular signal by the interaction of a UHE neutrino, a BP, apart from being able to emit the most common signals over a wide range of frequencies. There are two ways of trying to reproduce this signature with acoustic emitters. One possibility is to use a long linear array, like the first developed prototype transducer for this purpose. Another is to use a compact array where the aim is to provoke the appearance of the BP thanks to the parametric effect produced by the propagation of the emitted wave itself (see *subsection 4.1.2*) [58]. For this reason, up to three different array prototypes have been developed and are presented below. All of them have been designed and assembled within the framework of a doctoral thesis (referenced in the

text). But it is the last prototype the only one that has been handled during the work of this thesis [59].

The first prototype of this kind of calibrator arrays had 8 emitters along 8 m of length. It was designed according to simulations with the purpose of generating a coherently BPs at 23 kHz using a phased emitter array. In the last step to validate it, it was tested in ANTARES during a sea campaign, but due to some technical problems, the results were not conclusive [60, 61].

The second array designed was a compact array with 3 emitters along 40 cm of length. This prototype included a specific electronic part to obtain enough power for parametric generation [34]. It tried to reproduce the acoustic neutrino's signal too, but using parametric techniques [62]. It was tested for large distances (110–115 m). It was operative in linear emissions, but it presented low efficiency of parametric generation and a misalignment in the emitters [63, 64].

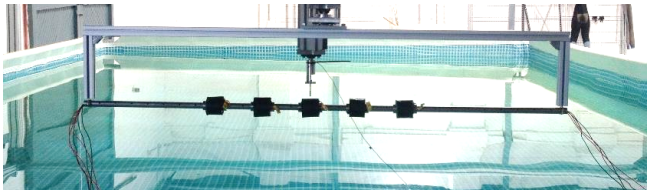

Figure 4.5: The last one developed so far compact array transducer prototype.

The third prototype array is the last one developed so far (see *Figure 4.5*). The successful deployment and operation of this compact array transducer was demonstrated in studies with one emitter element and some simulations [65]. The prototype array is assembled with 3 emitters in the first studies, but the final idea is to use it with 5 elements along 70 cm to increase the parametric BP directivity [66]. The resonance frequency of their elements is 380 kHz and they can be used serial or parallel [59]. Since their Transmitted Voltage Response (TVR) is until 160 dB re 1 μPa/V at 1 meter, it is possible to emit acoustic signals with an amplitude larger than 10 kPa, which is sufficient energy to produce a noticeable non-linear effect able to create the directive signals at low frequency [67].

4.2.3 1st step: Linear Emission for Frequency Response Calibration

The compact array allows emitting sine and sweep signals directly in low frequency. The TVR for one element is about 135 dB re 1 μPa/V at 1 m in the 10–100 kHz region. The final design of the array with 5 elements and the adequate electronics, aims to reach easily 180–190 dB re 1 μPa/V at 1 m. This power will be capable to extend the detector a few km away with positive Signal-to-Noise Ratio (SNR). Therefore, it is possible to use these linear emissions to check the status of the acoustic receiver and get knowledge about the propagation of signals in situ. Moreover, signals used for the APS of the KM3NeT could be done, benefiting from the procedures and protocols for detecting these signals at the same time as being an independent cross-check for that system. The idea would be to apply the same process as in *section 2.4* but emitting the desired signals with a characterized array as a reference from a ship.

An important feature of this step is that the emission is for all receivers because the linear emission in low frequencies produces a non-directivity wave, and thus, an accurate orientation of the array with respect to the telescope is not needed.

This first step could be an easy calibration to acoustic studies about noise environment, bioacoustics (whistles detection), checking the status of the APS, or other marine sciences.

4.2.4 2nd step: Long Parametric Signal Emission for Directivity Calibration

The first non-linear emission to calibrate the acoustic receivers in KM3NeT uses a long parametric directive signal. A long signal provides less difficulty on detection when the signal is received thanks to signal processing techniques, such as cross-correlation [40]. In this context, a long duration signal (of the ms order) is considered to determine the response of the telescope to very directive signals (a few degrees) with cylindrical symmetry [59]. This allows the calibration of the different sensors throughout all frequency regions, but including the directivity component. For this second calibration step, two types of parametric signals are defined: sinusoidal and sweep.

Figure 4.6 shows an example of a parametric sinusoidal signal, where the f_c is 400 kHz (resonant frequency of the transmitting array) and the envelope has an f_m of 20 kHz, which will produce a parametric signal with f_d of 40 kHz.

Note that the maximum value of the 2^{nd} beam has an amplitude of about -38 dB relative to the maximum of the 1^{st} beam (only taking into account the waveform).

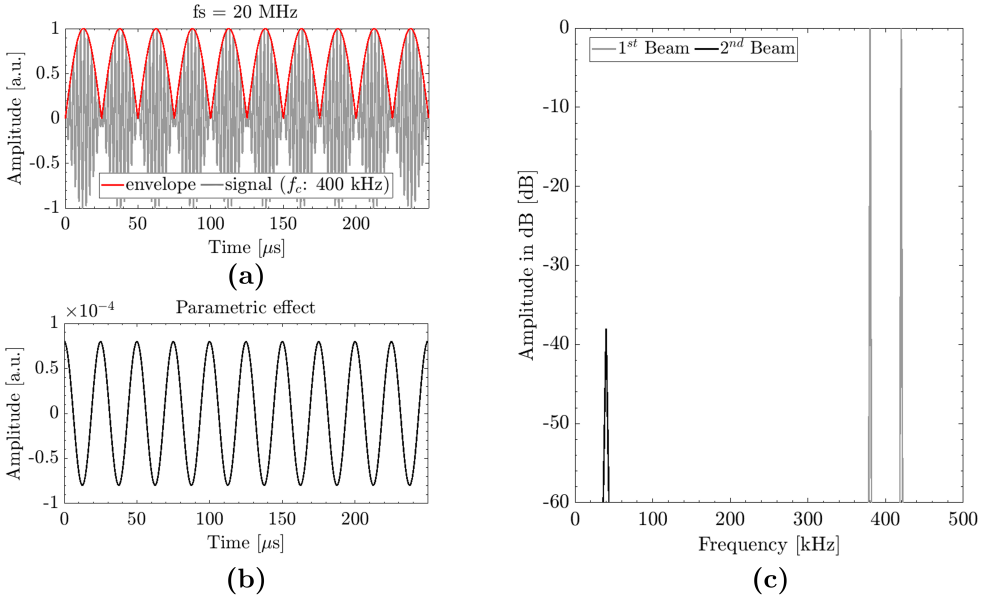

Figure 4.6: **(a)** The signal to be emitted is shown in grey (1^{st} beam). In red its envelope (calculated by the Hilbert transform). **(b)** Resulting parametric signal (2^{nd} beam). **(c)** Frequency domain for 1^{st} and 2^{nd} beams in a sinusoidal parametric signal.

In the case of a parametric sweep signal, the second derivative of the squared envelope solved analytically shows how the amplitude of the signal varies as a function of time (see *Equation 4.4* and *Figure 4.7.a*). This makes it difficult to control, but produces a directive signal with a wide frequency range. The latter feature, in a neutrino telescope, may be more interesting since a possible bipolar pulse generated by the interaction of a neutrino in the non-linear fluid would have a bandwidth (see subsection 4.1.1).

$$P_d \sim \frac{\partial^2}{\partial t^2} E^2 = 4\pi \left\{ \frac{|f_2 - f_1|}{T} \cdot \sin\left[4\pi t \left(\frac{|f_2 - f_1|}{T} \cdot t + f_1\right)\right] + 2\pi \left(2 \cdot \frac{|f_2 - f_1|}{T} \cdot t + f_1\right)^2 \cdot \sin\left[4\pi t \left(\frac{|f_2 - f_1|}{T} \cdot t + f_1\right) + \frac{\pi}{2}\right] \right\} \tag{4.4}$$

where P_d is the pressure of the 2^{nd} beam in a parametric sweep signal and E is its envelope. E is a sweep from f_1 to f_2 frequency in a transition time of T.

Figure 4.7 shows an example of a parametric sweep signal, where the f_c is 400 kHz (resonant frequency of the transmitting array) and the envelope is a linear sweep from 10 kHz (f_1) to 50 kHz (f_2), which will produce a parametric sweep signal with f_d between 20 kHz to 100 kHz. In this case, the maximum value of the 2^{nd} beam has an amplitude of between -32 dB (at 93 kHz) and -67 dB (at 20 kHz) relative to the maximum of the 1^{st} beam (only taking into account the waveform).

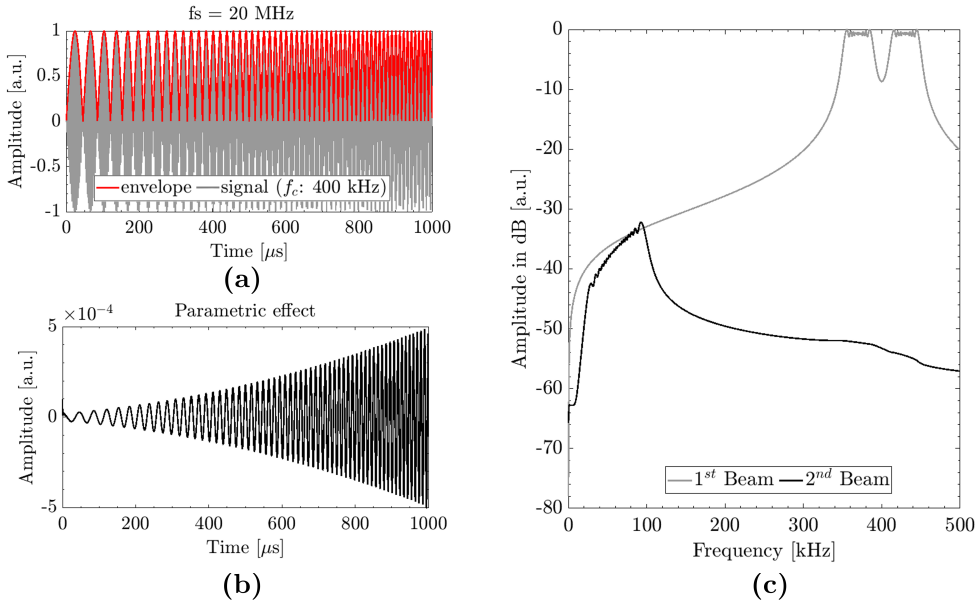

Figure 4.7: **(a)** The signal to be emitted is shown in grey (1^{st} beam). In red its envelope (calculated by the Hilbert transform). **(b)** Resulting parametric signal (2^{nd} beam). **(c)** Frequency domain for 1^{st} and 2^{nd} beams in a sweep parametric signal.

The parametric sinusoidal and the parametric have a narrower directivity (characteristic of high frequency) that allows us to direct the beam to a specific sector of the sensor array on the telescope and characterize them. Combining the information of all the sensors determines the directivity of the source, thus being able to discriminate the signal from other more frequent less-directive acoustic signals. This information is then critical to improve the performance of the facility and determine its sensitivity.

This second step could be a calibration for acoustic studies about bioacoustics (echolocation), low frequencies directivity responses (parametric effect), other directivity signals to positioning sources, etc.

Experimental analysis of a parametric acoustic process. Sweep signal case

Calibration of acoustic transducers in a moderate-sized laboratory water tank can be an arduous task. This is due to the complexity of recording a pure signal (reflections free), since it is difficult to move the emitter farther away than half or one meter from the receiver, and large depths are not available. Using the parametric signals presented above, a process that could be used to characterize these sensors at low frequencies (10–100 kHz) without a complicated analysis of the recorded signals has been studied [68].

On this occasion, the ultrasound transducer characterized by the proposed parametric process is the commercial sensor Teledyne RESON Transducer TC3027 (see *Figure 4.8.a*). It will be used as an emitter, to evidence the parametric effect generation during the process.

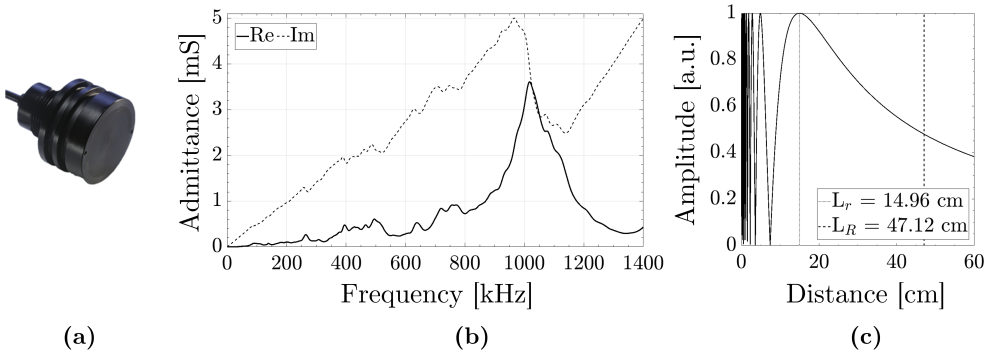

Figure 4.8: **(a)** Teledyne RESON Transducer TC3027. **(b)** Admittance (real and imaginary) measure by HIOKI IM3570 Impedance Analyzer. **(c)** The characteristic distances of the transducer indicating the near-field distance (L_r) and far-field distance (L_R) for 1 MHz calculated by *Equation 2.1* and *Equation 2.2* respectively.

The resonance frequency is noticeable in an admittance measure, in this case, verification is needed to ensure that it is a 1 MHz transducer (see *Figure 4.8.b*). Studying the characteristic distances of the transducer indicate the near field distance, L_r, and far-field distance, L_R, the Emitter-Receiver distance (distER) must therefore be at least about 48 cm (see *Figure 4.8.c*).

The receiver in this experiment will be the Teledyne RESON Hydrophone TC4014, which comes with a preamplifier. This hydrophone has been characterized in the tank laboratory following the same process as explained in *subsection 2.4.1* and using as reference an AIRMAR P19 for the low frequencies and the same Teledyne RESON Transducer TC3027 for the high frequencies (see *Figure 4.9.a*). Now that the sensitivity in reception (RVR) is known, both in high and low frequencies, they will be taken into account for the analysis in the parametric emission.

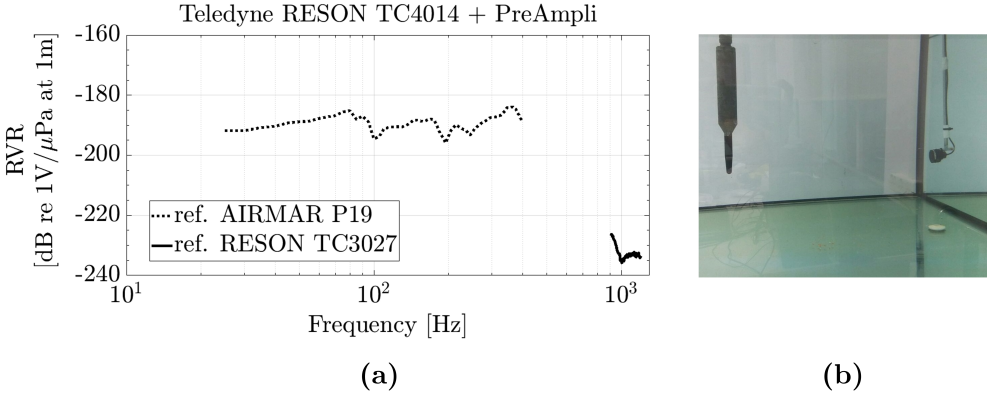

Figure 4.9: **(a)** Experimental measurement of RVR for the RESON TC4014. **(b)** RVR measure on laboratory tank for the RESON TC4014 using as emitter of reference the RESON TC3027.

In this experiment, both transducers were placed at distER of 50 cm in a laboratory water tank (see *Figure 4.9.b*). In order to receive the signal with a positive SNR, a signal amplifier (*Electronics & Innovation 2100L*) was placed between the signal generator and the emitter transducer. The signal emitted is the presented parametric sweep in *Figure 4.7*. The system works with a frequency sample, f_s, of 20 MHz.

Once the experimental setup is ready, a test signal is emitted and recorded, which is analyzed to verify that the expected parametric effect is produced. A simple spectrogram is enough to evidence its emergence. In this case, *Figure 4.10* represents a spectrogram using a Fast Fourier Transform (FFT) length of 2000 samples with an overlap of the 50% to calculate the Power Spectral Density (PSD) of the receiver signal. The received signal in the spectrogram is easily distinguishable, since the Time of Flight (ToF) is as expected (with a distER of 50 cm) and it is consistent with the frequency range

of the 1^{st} beam. As it can be seen, the parametric effect is not instantaneous, it needs a moment to generate the 2^{nd} beam. In addition, the most intense reflection produced (the one behind the receiver), and its mixing with the direct signal, can be appreciated too. This would be avoidable in a bigger tank.

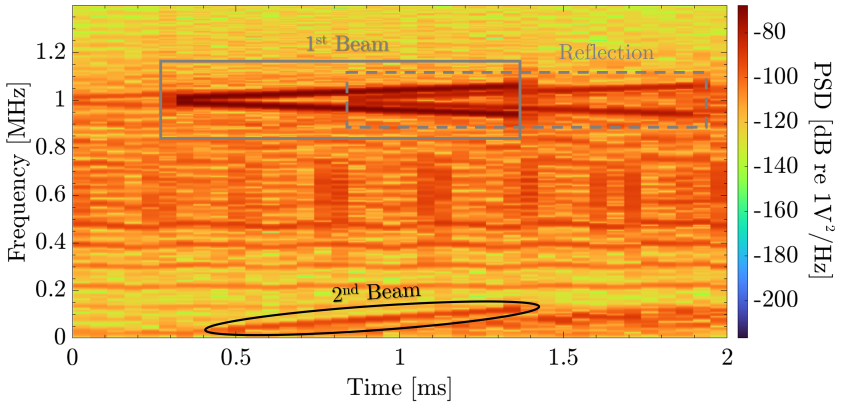

Figure 4.10: Zoom in Y–axis of the spectrogram between 0 and 1.4 MHz to visualize the parametric sweep recorded. The 1^{st} beam have spectral content from 950 kHz ($f_c - f_{max}$) to 990 kHz ($f_c - f_{min}$) and 1.01 MHz ($f_c + f_{min}$) to 1.05 MHz ($f_c + f_{max}$), while the 2^{nd} beam is a sweep from 20 kHz ($2f_{min}$) to 100 kHz ($2f_{max}$).

Now that the ability to generate the parametric effect in a controlled manner has been demonstrated, it is time to detect it and proceed with the characterization of the transducer. For this purpose, correlation analysis is tested in *Figure 4.11*. Since this is a sweep signal, the resulting correlation shows a clear peak in the Time of Arrival (ToA) of the 1^{st} beam. The second little correlation peak for the 1^{st} beam corresponds to the order 2 reflection, produced behind the receiver. The order 1 reflections created by the bottom and the surface water are not visible (probably due to the directivity of the emitting transducer itself). About the 2^{nd} beam correlation, it is produced by the correlation between the second derivative of the square of the received signal envelope and the theoretical parametric effect defined in *Equation 4.4*. In this case, there are more peaks appreciable, but the first one is clearly distinguishable and marks the ToA of the parametric signal. Then, the parametric effect is characterizable with a simple correlation process.

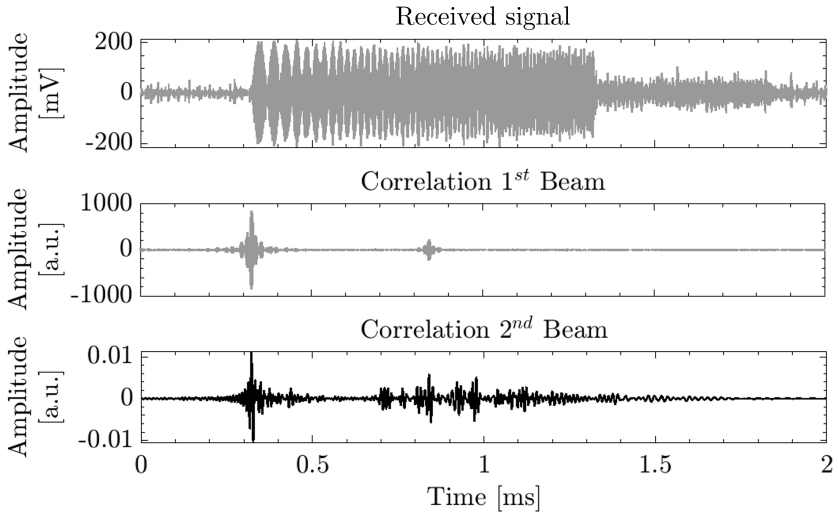

Figure 4.11: The figure at the top shows the recorded signal received by the hydrophone Teledyne RESON Hydrophone TC4014. The figure at the center shows the 1^{st} Beam correlation, the signal result of the correlation between the received and the emitted signals. The figure at the bottom shows the 2^{nd} Beam correlation, the signal result of the correlation between the second derivative of the square of the received signal envelope and the theoretical parametric effect defined in *Equation 4.4*.

As it has already been demonstrated how to detect both beams in the received signal, the non-linear effect between both is shown. For this purpose, measurements are made by varying the amplitude of the signal to be emitted prior to the amplifier, and the amplitude received is plotted (see *Figure 4.12.a*).

Finally, the directivity of the transducer is measured for both beams, and it is verified that the low-frequency secondary beam presents a narrow directivity similar to that obtained with the high frequency of the first beam (see *Figure 4.12.b*).

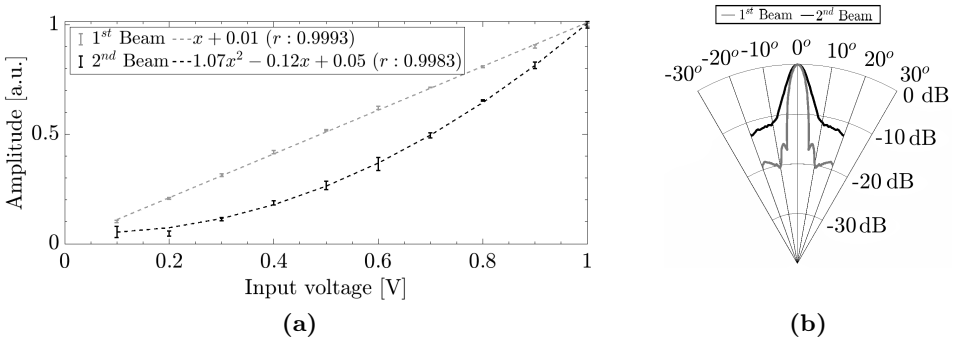

(a) **(b)**

Figure 4.12: **(a)** Amplitude variation in the input voltage to evidence the parametric effect apparition. The amplitude on the Y–axis corresponds to the normalized values of the peak amplitude of each beam-correlation with respect to its maximum. **(b)** Directivity pattern in dB obtained through the normalized values of the peak amplitude of each beam-correlation with respect to its maximum. The directivity of 1^{st} Beam is in grey, where the -3 dB decay occurs from $\pm$ 2^o and the -6 dB decay occurs from $\pm$ 3.5^o. The directivity of 2^{nd} Beam is in black, where the -3 dB decay occurs from $\pm$ 3^o and the -6 dB decay occurs from $\pm$ 5^o.

4.2.5 3rd step: Bipolar Parametric Signal Emission for Acoustic Neutrino Detection Calibration

For a final characterization of the receivers to the acoustic neutrino's detection and test, the viability of the technique is essential to be able to reproduce its acoustic signature. Unlike the previous step, the signal to be emitted will be very short, which will make it difficult to detect in the post-analysis and will require a system capable of recording these kinds of signals. The signal consists of a BP similar to that generated by the interaction of a neutrino in water. This pulse spectrally contains a wide low-frequencies range but with a really narrow directivity (see *Figure 4.1*). This means that the parametric effect is necessary to achieve it.

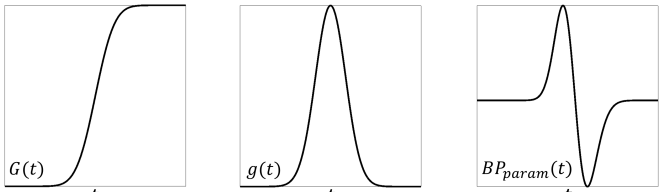

(a) **(b)** **(c)**

Figure 4.13: **(a)** Envelope $G(t)$ of the signal to be emitted to produce a bipolar pulse generated from the parametric effect during its propagation in the non-linear fluid. It corresponds to Gaussian bell integral. **(b)** Gaussian bell $g(t)$ from which the enveloping signal $G(t)$ is deduced. **(c)** Created BP from the propagation of a signal with the envelope $G(t)$ in a non-linear medium. It corresponds to the second derivative of the square of the envelope $G(t)$.

With this aim, a parametric BP signal is generated using the compact array. Similarly to the parametric sweep signal, the carrier signal is a sine with the resonance frequency of the emitter element, but in this case, the envelope signal is $G(t)$, defined by *Equation 4.6*, that corresponds to the integral of the Gaussian function $g(t)$, defined by *Equation 4.5*. The second derivative of the square $G(t)$ corresponds to a BP, the BP_{param}, defined in *Equation 4.7*. Therefore, the 1^{st} beam will be the parametric BP signal that owns a peak in the f_c frequency, and the 2^{nd} beam will be a BP_{param} that owns a wide range of low frequencies such the neutrino's acoustic signature in water (see *Figure 4.14*).

$$g(t) = \frac{1}{\sigma\sqrt{2\pi}} e^{-\frac{1}{2}\left(\frac{t-\mu}{\sigma\sqrt{2}}\right)^2} \tag{4.5}$$

where σ is the standard deviation of the distribution, which is centered in μ position.

$$G(t) = \int g(t)\ dt = \frac{1}{2}\left(1 - \frac{2}{\sqrt{\pi}} \int_{\frac{x-\mu}{\sigma}}^{\infty} e^{t^2}\ \mathrm{d}t\right) \tag{4.6}$$

$$BP_{param}(t) = \frac{\partial^2 G(t)}{\partial t^2} \tag{4.7}$$

To take control in the generation of a BP_{param}, the interval time peak-to-peak defined as Λ is equivalent to the 30.85% of $\frac{\sigma}{2}$, and μ represents the instant where BP_{param} is ideally going to appear. However, it presents the problem that the amplitude of $G(t)$ starts with zero and it remains constant without decreasing to zero. It is necessary to transitory relax the transducer and not create abruptness. At first, it was decided to create a linear or exponential degradation, but finally, it was decided to use a drop equal to the rise, which would cause a second inverted BP_{param}. This duality can be used to facilitate its detection since it is expected to be followed by another inverted BP one at a controlled (and known) time distance.

Figure 4.14 shows a designed parametric BP signal where the aim is to create a BP_{param} with Λ of 10 μs. The μ value is 0.3 ms and the drop is distanced 2μ from the rise. Note that the maximum value of the 2^{nd} beam has an amplitude of between -61 dB (at 12.5 kHz) and -115 dB (at 93 kHz) relative to the maximum of the 1^{st} beam (only taking into account the waveform). Although the FFT is calculated for the complete displayed signal, it would be more correct to cut only the signal of interest.

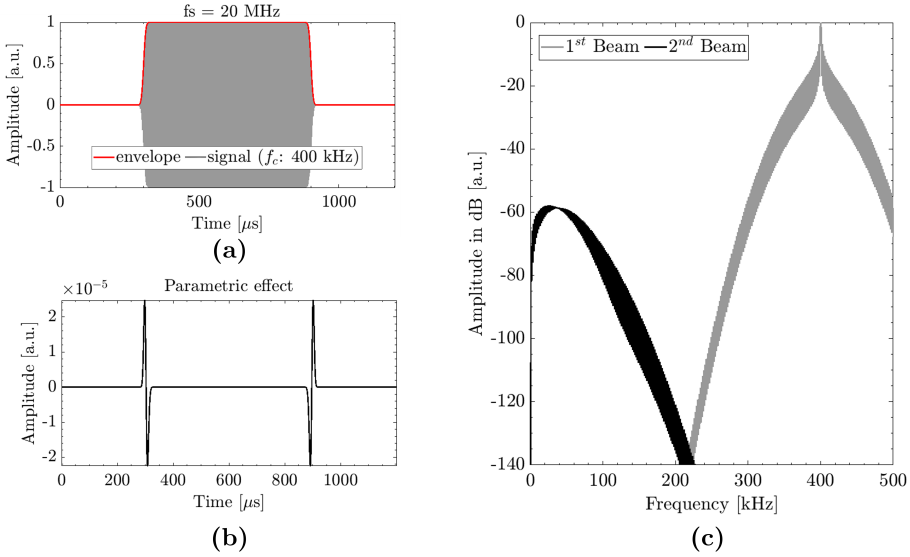

Figure 4.14: **(a)** The signal to be emitted is shown in grey (1^{st} beam). In red its envelope (calculated by the Hilbert transform). **(b)** Resulting parametric signal (2^{nd} beam). **(c)** Frequency domain for 1^{st} and 2^{nd} beams in a BP parametric signal.

Figure 4.15 shows a zoom in the BP_{param} generation to note the both shapes (normal and inverted) in the parametric effect.

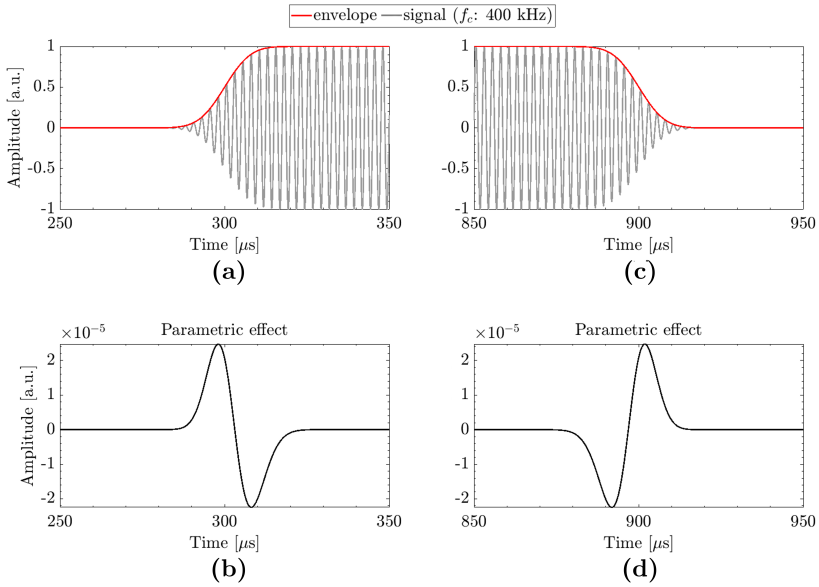

Figure 4.15: **(a)** Zoom in the rise of parametric BP signal. In grey is the signal to emit (1^{st} beam). In red its envelope (calculated by the Hilbert transform). **(b)** Zoom in the parametric effect produced by the rise in the parametric BP signal, a normal BP_{param}. **(c)** Zoom in the drop of parametric BP signal. In grey is the signal to emit (1^{st} beam). In red its envelope (calculated by the Hilbert transform). **(d)** Zoom in the parametric effect produced by the drop in the parametric BP signal, an inverted BP_{param}.

This last step of the calibration will be a valid calibration for the UHE acoustic neutrino detection techniques, both to evaluate the response of the detector to this type of signal, and to develop the necessary post-analysis to detect them.

The parametric BP emission directivity with the last transducer array prototype

In the course of the complete characterization of an individual element of the latest transducer array prototype (during the design process), the directivity of a parametric BP (2^{nd} beam) was experimentally measured [65]. The directivity was obtained at 60 cm of distER, far-field of the transducer, in a laboratory water tank [69]. This has made it possible to simulate the directivity that the array would have with the 5 elements of the final design. These elements are equispaced by 14 cm, and the directivity of the 2^{nd} beam has been estimated for a range of $\pm 30^{o}$ at different distER (see *Figure 4.18*).

Figure 4.16 shows the signal received at a point 1 km away and 2 degrees from the center of the array. First, the signal received by each element of the transducers array (*Source 1* is the central one, *Source 2* and *Source 3* are the adjacent ones, and *Source 4* and *Source 5* are both extremes) is taking into account the attenuation estimated by *Equation 2.3*, to finally add them up in a coherent way (see *Figure 4.16*).

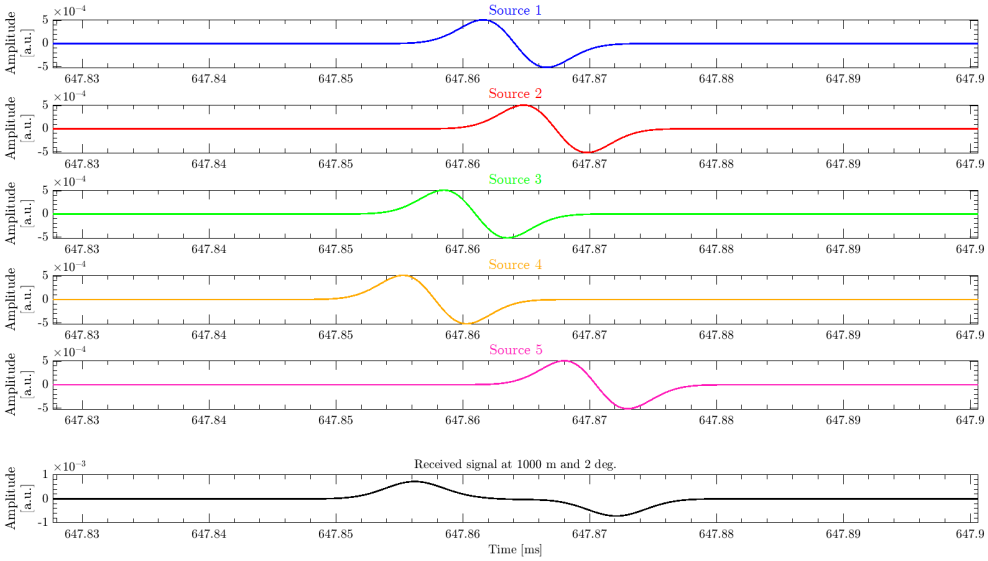

Figure 4.16: Received signal from each source of the array in a point at 1 km and 2 degrees from the central point.

Figure 4.17 shows some examples of signals received at different angles, to appreciate the directivity effect on the simulated received signal.

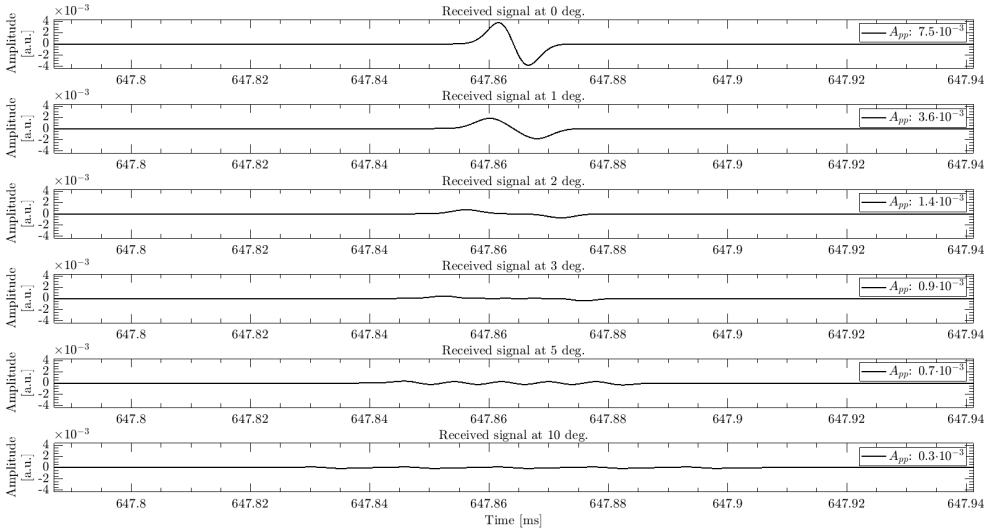

Figure 4.17: Received signal at 1 km and different degrees from the central point.

Thus, *Figure 4.18.a* shows the directivity measured experimentally in the laboratory of one element of the array, while *Figure 4.18.b* shows the result of simulating the directivity of 5 elements like the previous one mounted on the array.

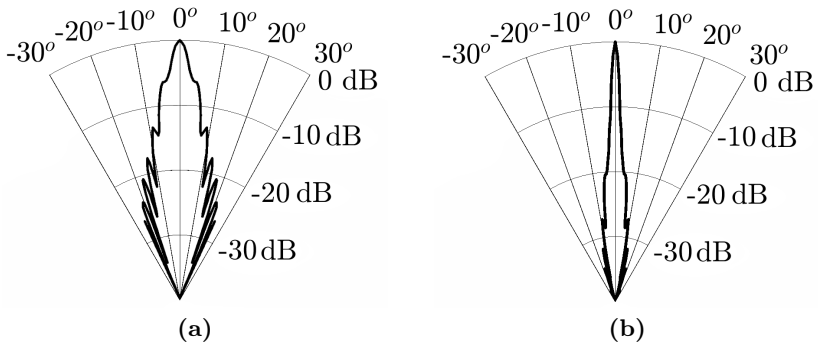

Figure 4.18: **(a)** Experimental directivity of a single element at 60 cm. **(b)** Simulated directivity of the array at 1 km.

In fact, the simulation permits to observe that at a distance of 1 meter the contribution of the 5 elements would still be distinguishable, so it would be advisable to measure it as an array at a greater distance.

Table 4.1 shows the decay values for −3 and −6 dB at different *distER*. In the end, from a distance of 10 meters, the directivity of the array is already invariable. The resolution in the simulation is 0.5 degrees.

	1 element (experimental)	**5 elements (simulation)**			
Distance *distER*	**60 cm**	**1 m**	**3 m**	**10 m**	**1 km**
-3 dB decay	2.0^o	10.0^o	6.0^o	1.0^o	1.0^o
-6 dB decay	3.5^o	22.0^o	6.5^o	1.5^o	1.5^o

Table 4.1: Decay values for −3 and −6 dB in the experimental and simulated at different distances directivity.

4.3 Conclusions and future steps

Conclusions

The history of existing arrays for calibrating neutrino underwater telescopes has been presented. To date, three prototypes have been developed, of which the last two ones are intended to be able to act as parametric emitters. The last one has shown good efficiency in emitting a parametric bipolar pulse on a single element during its characterization. Its directivity has allowed estimating the directivity of the complete array in its final design, as shown in *Figure 4.18*. This encourages further development of emission technologies in order to achieve a robust calibrator with its integrated electronic amplifier stage.

It has been demonstrated the possibility of controlling the acoustic generation of the parametric effect with the design of specific signals: sinusoidal, sweeps, and bipolar. However, there is a level of complexity in its generation, given the relationship between the amplitude of both beams (1^{st} and 2^{nd}), which makes it very difficult to detect and study the 2^{nd} beam. Moreover, it has been shown that the parametric sine signal has the best ratio, with a difference of –38 dB, followed by the parametric sweep, whose frequencies of the 2^{nd} beam

are difficult to control, and has a difference of between –32 and –67 dB. Finally, the defined parametric BP, which has a difference of between –61 and –115 dB. Even so, these signals provide a lot of possibilities by achieving low frequencies with the typical directivity of high frequencies.

A full calibration technique for acoustic sensors in a neutrino telescope has been proposed in three different steps: linear, long parametric, and bipolar parametric emission. Following this, the exploration of additional uses that can be made of common APS on these telescopes is possible, from environmental noise monitoring or control of absence/presence of animal life, to the possibility of developing technology for the acoustic detection of UHE neutrinos.

Future steps

As for the latest array prototype, there is already evidence that it is well on its way to becoming a good tool to operate as a calibrator. So far it has not been possible to measure as an array, since only three elements are operational, and each one has a different sensitivity. So before treating it as a whole system, it is recommended to redo the elements that compose it, with greater care to achieve real equality between elements. Once you have them, it is time to measure them as an array in a laboratory water pool and characterize it.

The next stage will be doing some tests in situ to check the emission and reception for all the steps of the calibration plan, in order to have a complete characterization of the array, and evaluate its feasibility as a robust calibrator. Before that, the electronics of the array should be designed for parametric use and thus be able to produce high-level acoustic signals that reach large distances (∼km) with enough intensity to be detected by the sensors of the telescope.

Once the calibrator-telescope connection is achieved, analysis techniques must be developed to search for the emitted pulses. If parametric BPs are recorded, the simple fact of detecting them will be enough to start developing a real automatic acoustic neutrino detection algorithm that generates alerts in case of finding them. *Chapter 5* develops this last idea and will attempt to make it viable.

Chapter 5

Proposal of a Trigger for Acoustic Neutrino Detection

For the neutrino acoustic detection, a first trigger level to be implemented in KM3NeT is proposed. It looks for coincident events that can be originated by a Bipolar Pulse, such as the one that would be generated by the interaction of a neutrino in water. The spectrogram is used as an analysis of the signal received, and up to three parameters are calculated to indicate the presence of a possible event of interest. In case of coincidence between receivers, the event would be recorded as a Bipolar Pulse candidate. For the first trigger test, the hydrophones in ORCA006 are used, previously "configurated" for its application. Finally, the efficiency of the detector is evaluated thanks to the insertion of an artificial Bipolar Pulse between the experimental data.

Section 5.1 presents the spectrogram analysis as a detector of interesting signals, in this case, a Bipolar Pulse. *Section 5.2* then looks at the recorded data available to ORCA006 and decides which ones to use to test the first level of the trigger to be proposed. *Section 5.3* discusses how to evaluate the efficiency of the trigger to be applied and the need to pre-configure each receiver. *Section 5.4* shows the proposed Bipolar Pulse detector to be implemented, and shows its first results in *section 5.5*.

As in any process of installing state-of-the-art scientific and technological infrastructure, as much data as possible is collected for further analysis. As this procedure requires massive storage space, data from a representative period is usually studied in order to develop analysis techniques that allow the automation of saving the most interesting and representative parameters of this massive data. This preprocessing optimizes resources, allowing the raw data received from every sensor to be discarded directly, exponentially reducing the volume of memory needed to monitor the data with the required temporal resolution.

In the Acoustic Positioning System (APS) of KM3NeT, the preprocessing of the received acoustic signals permits saving the Digital Optical Module (DOM) positions (XYZ data) every 10 minutes. This chapter aims to develop analysis techniques in search of Bipolar Pulses (BPs) (possible signals originating from the interaction of a neutrino in water) to make a supplementary preprocessing to the current APS and to realize a possible acoustic neutrino detector. Raw acoustic signals from the KM3NeT-ORCA006 hydrophones have been studied to define possible parameters and alerts that could help to distinguish the neutrino acoustic signature. In this chapter, the studies done for the proposal of a trigger for acoustic neutrino detection in KM3NeT are presented.

5.1 Analysis technique: the spectrogram

The spectrogram is a basic representation tool used for the analysis of electrical signals, communication signals, and any audiovisual signal in its frequency content. It is a representation in three dimensions: time, frequency, and amplitude of the energy distribution of a signal. The X–axis represents the time, the Y–axis the frequency, and the Power Spectral Density (PSD) is coloured coded.

The spectrogram divides the signal into bins (bins of N_{bin} samples of the signal) to calculate the Fast Fourier Transform (FFT). It is common to use a bin overlap, to improve its representation, a Hamming window is used in the FFT calculation to soften the edge effect. In acoustics, they are often used to visualize signals that in the time domain are masked by the background noise itself or below another recorded signal (reduced Signal-to-Noise Ratio (SNR)), but they are appreciable in the frequency domain.

It should be noted that the time and frequency resolution, T_{bin} and f_{bin} respectively, of a spectrogram is limited by the preselected N_{bin} and the sampling rate f_s of the recorded signal:

$$T_{bin} \geq \frac{N_{bin}}{f_s} \longrightarrow N_{bin} \leq T_{bin} \cdot f_s \tag{5.1}$$

$$f_{bin} \geq \frac{f_N}{N_{bin}} = \frac{f_s}{2N_{bin}} \longrightarrow N_{bin} \geq \frac{f_s}{2f_{bin}} \tag{5.2}$$

Therefore, a compromise between T_{bin} and f_{bin} exists. In order to correctly appreciate the signal in the frequency domain, it must be taken into account that at least two complete cycles of the signal must fit in a bin length, T_{bin} [70]. Thus, when making a spectrogram, *Equation 5.3* must be considered.

$$2T_{valid} \lesssim T_{bin} \longrightarrow 2 \cdot \frac{1}{f_{valid}} \lesssim \frac{N_{bin}}{f_s} \longrightarrow f_{valid} \gtrsim \frac{2f_s}{N_{bin}} \tag{5.3}$$

The spectrogram as a detector

A spectrogram is a good tool that can be used as a signal detector. The idea is to apply an alert level that indicates the presence of the signal of interest in the spectrogram. This is achieved by averaging the energy concentrated in the frequency bands of interest. When this level is above the background noise during a time compatible with the length of the signal, a candidate will be detected. Thus, the spectrogram detection will be conditioned by the time resolution T_{bin}, the frequency resolution f_{bin}, and the threshold level. These characteristics shall be adjusted to the particularities of the signal.

Acoustic neutrino detection is not easy because it is a very short signal (high temporal resolution), with a large spectral component, and of very low energy (which entails very small amplitudes). One of the characteristics of spectrogram detection is that it does not depend as much on the waveform as on the energy concentrated at certain frequencies during a specific time duration. This presents some advantages over the classical correlation method where the shape of the signal must be known. As a drawback, its application requires more computational cost.

5.2 The raw acoustic data

This section aims to analyse the raw acoustic data from KM3NeT to study if it is feasible to develop a possible acoustic neutrino detector using its current APS. The data recorded with the hydrophones will be studied, as they have higher sensitivity and stability than the piezoceramic sensors on the DOMs. Since ORCA was at the time of performing the analysis the detector node with the largest number of operational hydrophones (three, the minimum to be able to position the source of a detected event), its data will be examined, which will help to filter out possible neutrino candidates if no coincidence is found between them.

5.2.1 Noise in the data

Concerning the KM3NeT acoustic system, given its location and the possibility to obtain data from many sensors, it can be considered a unique scientific infrastructure because it is equipped with highly sensitive hydrophones streaming data in real time continously, which allows a large amount of information to be stored. Highly sensitive hydrophones have a downside: they "listen to" everything. For this reason, it is important to know the environment and whether the signal of interest will be distinguishable/detectable (e.g. with an in situ calibration tool as presented in the previous chapter). Anything else than the signal of interest will be understood as background noise. If the SNR is insufficient to detect it in the temporal domain, the possibility of studying it using the frequency domain or a spectrogram should be considered, and this is where you can really see all the information that KM3NeT can collect in the different nodes of the array that constitute the hydrophones.

Signals recorded by electronic devices are usually a combination of the signal received by the hydrophone plus some signals generated by electronic devices. Long the raw acoustic data registered in KM3NeT, the recorded signals on ARCA present less electronic noise partly due to the use of a 600 Hz high-pass filter in the hydrophones. However, ORCA has a lot of electronic inputs, as it is shown below.

Figure 5.1 is an spectrogram of 2 seconds recorded data by a hydrophone on ORCA site with a N_{bin} of 4096 samples (which means that it has a T_{bin} of $\sim$20.97 ms and a f_{bin} of $\sim$23.84 Hz, but f_{valid} from $\sim$97.66 Hz). It shows a continuous electrical signal between 85 and 90 kHz and other at 48 kHz (in the case of ARCA this type of noise is also observed from 85 to 90 kHz, and from 70 kHz to 95 kHz). Then, an impulsive electric noise every

∼100 ms is observed. Finally, the unique natural two signals appreciated in the spectrogram as non-perfect horizontal lines are two emitted whistles by dolphins (these bioacoustics are remarked in a square).

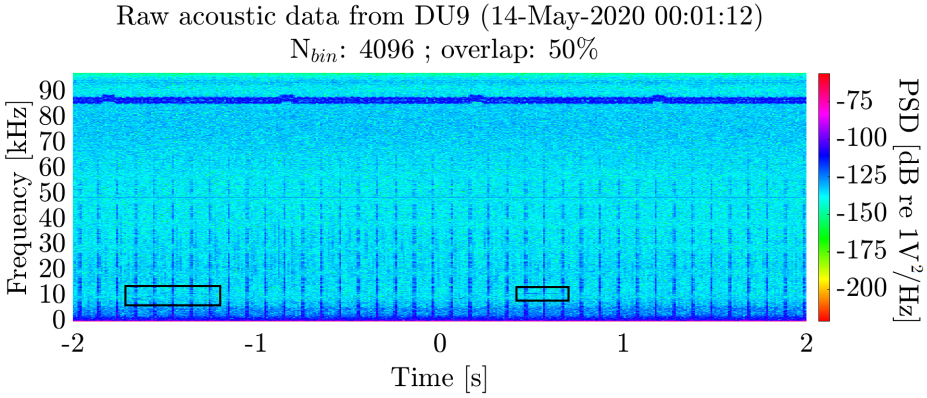

Figure 5.1: Spectrogram of raw acoustic data from the hydrophone in ORCA-DU9. The timestamp corresponds to 14-May-2020 at 00:01:12. The spectrogram shows 4 seconds of signal with a N_{bin} of 4096 samples and an overlap of 50%. Two dolphin whistles are remarked in the squares.

Figure 5.2 shows the signal represented in the previous spectrogram on the temporal domain. It can be seen how the electricity network signal of 50 Hz (and its upper harmonics) of high amplitude is mixed with the rest. Being such a relative low frequency, it is easy to remove them with a high-pass filter. The two remarked pieces with a square correspond to the electric impulsive noise shown in *Figure 5.1*.

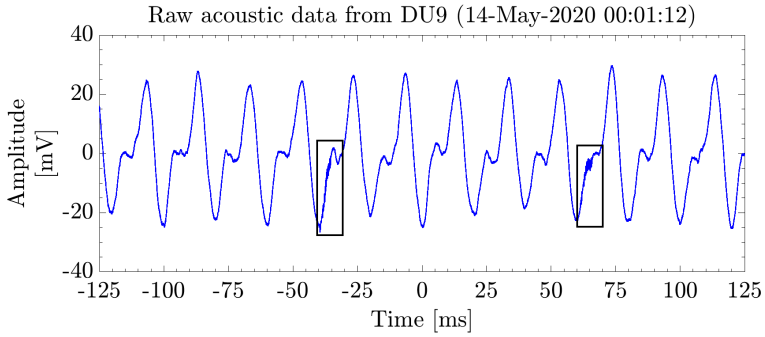

Figure 5.2: Recorded signal with 250 ms of raw acoustic data from the hydrophone in ORCA-DU9. The timestamp corresponds to 14-May-2020 at 00:01:12. The signal shows how the electricity network signal of 50 Hz (and its harmonics) of high amplitude is mixed with the rest of the signal. Two Digital Penetrations (DPs) are remarked into the squares.

Figure 5.3 shows a zoom-in from *Figure 5.2* to the second marked square where this electronic noise is desplayed in detail. A more detailed study concluded that they are DPs, ones or zeros in binary, from the conversion Alternating Current to Direct Current (ACDC) in some device that are generated. It has a work cycle of $\sim$100 ms with a baud rate of 9600 during $\sim$4 ms. These DPs do not represent a problem for the APS operation but they are very tedious for other studies. It must be noted that the level of DPs in the hydrophone of DU9 is especially more noticeable than in the others, it has higher SNR. Some actions have been discussed to mitigate this problem in future DUs to be deployed, by checking this cross-talk is not produced. Also, for the DUs in operation, the reading interval time of the ACDC will be increased from 0.1 s to 10 s, so as to reduce the noise by a factor of 100.

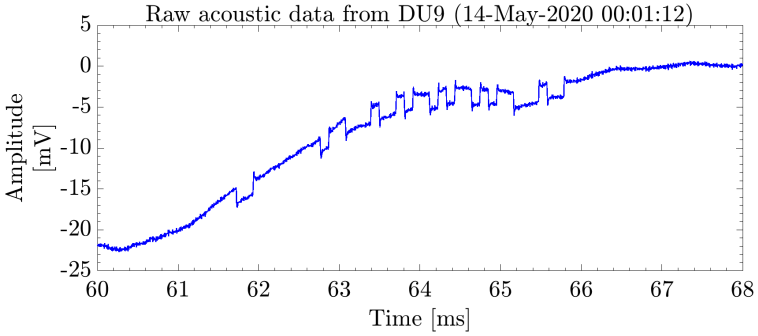

Figure 5.3: Recorded signal with 8 ms of raw acoustic data from the hydrophone in ORCA-DU9. The timestamp corresponds to 14-May-2020 at 00:01:12. The signal is a zoom-in from *Figure 5.2* to the second marked square to show in detail a DP.

Consequently the acoustic signal captured by the acquisition system (the raw acoustic data) is composed of electronic noise and the signal recorded directly by the transducer. This last one is composed of bioacoustics (environmental noise produced by ocean currents, animal noise, such as whistles or echolocations by dolphins and whales, and other natural sources, such as neutrino interactions, etc.) and anthropogenic signals (noise from ships, sonar, ABs, etc.).

5.2.2 Data selection for the experiment

First of all, it is necessary to assess the data available. In ORCA006 there are two periods of almost 24 days recorded continuously in two consecutive years, for this reason it was decided to use these data to carry out this first study. In this data, the Sound Pressure Level (SPL) contained in the 1/3 octave of 31.6 kHz (a frequency of interest in a BP) was evaluated. To do so, the FFT of every two seconds of the signal was calculated and the spectral content belonging to the 1/3 octave was added, obtaining the SPL. Finally, these values are averaged every thirty minutes. Thus, the heatmaps shown in *Figure 5.4* are obtained.

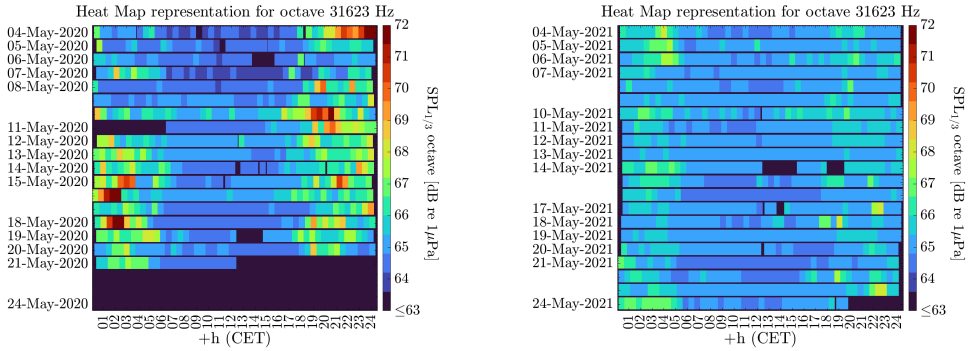

Figure 5.4: Heat Map representation for a long-time monitoring SPL for the octave around 30 kHz in the hydrophone of ORCA-DU3. The period shown is 20 days, where each pixel corresponds to the mean level in a half hour. Weekdays are indicated, the two unlabelled days correspond to the weekend, and the corresponding times in Central European Time (CET). The black regions are due to a gap in data [71]. **(a)** May of 2020. **(b)** May of 2021 [*Credits: Guillermo Lara, IEO*].

Figure 5.4 shows a clear change in SPL from one year to the next one, which is thought to be due to a reduction in shipping traffic during the COVID-19 pandemic restrictions. In addition, gaps in the data can be observed. In any case, *Figure 5.4* evaluates the situation of the noise level and helps to distinguish between noisy and quiet periods for our detector.

The first trial used 6-hour chunks of data (the longest RUNs in KM3NeT). Firstly, two totally opposite RUNs were evaluated, the extremely noisy RUN8018 and the very quiet RUN8019. The study was then extended to 10 more randomly selected RUNs, on the condition that they lasted around 6 hours.

Table 5.1 shows the date and time at which each RUN starts, the total SPL for the 1/3 octave bands of 25.1, 31.6, 39.8, and 50.2 kHz (frequencies between 22.3 kHz to 56.3 kHz), and the SPL level at the 25, 50, and 75 quartiles and at the 99th percentile.

RUN	Date + 6H	SPL_{22-56} kHz [dB re 1μPa]			
		$Q25\%$	$Q50\%$	$Q75\%$	$PCTL99\%$
8008	14/05/2020 00:01	64.4	64.8	65.5	80.4
8015	15/05/2020 06:01	64.0	64.0	64.1	80.2
8018	16/05/2020 00:01	64.3	65.1	68.0	80.4
8019	16/05/2020 06:01	64.0	64.0	64.1	79.9
8021	16/05/2020 18:01	64.9	65.5	66.0	80.4
8027	18/05/2020 06:01	63.7	63.7	63.8	80.3
8042	19/05/2020 18:01	64.3	64.7	65.4	80.0
8048	21/05/2020 06:01	63.7	63.7	63.8	80.1
9901	05/05/2021 00:00	64.2	64.7	65.4	79.5
9907	06/05/2021 12:00	63.7	64.0	64.3	79.4
9913	08/05/2021 00:00	64.1	64.2	64.3	79.5
9919	09/05/2021 12:00	64.1	64.2	64.3	79.5

Table 5.1: Total SPL for first three quartiles and 99th percentile values for the frequencies between 22.3 kHz to 56.3 kHz on the data recorded by the hydrophone in DU3.

In order to visualize it better, *Table 5.1* is represented in boxplots (see *Figure 5.5.a*). The semi-interquartile range, $(SPL_{Q75\%} - SPL_{Q25\%})/2$, is calculated to observe the dispersion in the noise of each RUN (see *Figure 5.5.b*).

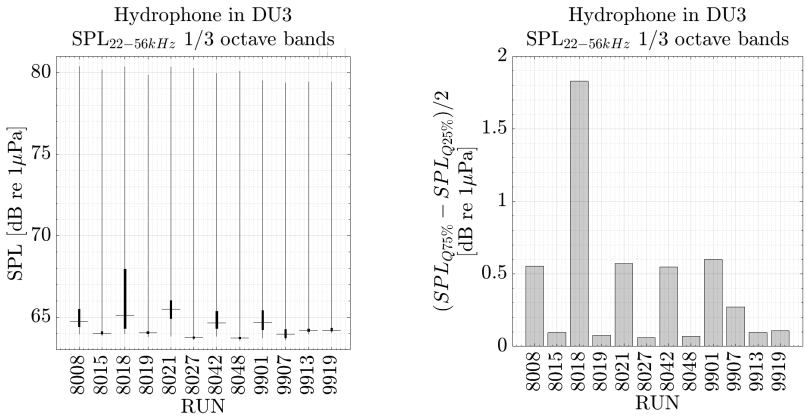

Figure 5.5: SPL (noise) in the data recorded by the hydrophone in DU3 for the triggered tested. **(a)** boxplots representing the total SPL for the frequencies between 22.3 kHz to 56.3 kHz. **(b)** The semi-interquartile range, $(SPL_{Q75\%} - SPL_{Q25\%})/2$, calculated to observe the dispersion of this noise.

5.3 The detector procedure

Once the analysis technique has been chosen and the data for the study has been selected, it is necessary to stablish the method to trigger a possible BP event.

The idea is to analyze the data from every hydrophone with an adaptive threshold level to activate the trigger alert. This will be modified according to the noise in the section of the data being analyzed. In this case, each part of data will correspond to one second. The main objective will be to reduce the data to less than one candidate (event) per second. In order to have "true" events, an artificial BP is created to simulate the pulse after the interaction of a neutrino in water and its reception by the hydrophones of KM3NeT. Considering the RVR *Equation 2.7*, it is possible to convert from P_{in} to V_{out}. *Figure 5.6* shows the BP, the "true" event generated by a neutrino interaction. The signal is from a neutrino of 10^{11} GeV of thermal energy at 1 km and 0 degree orientation from the acoustic "pancake". This artificial BP will be added to the raw acoustic data previously analyzed, at a ratio of one every minute.

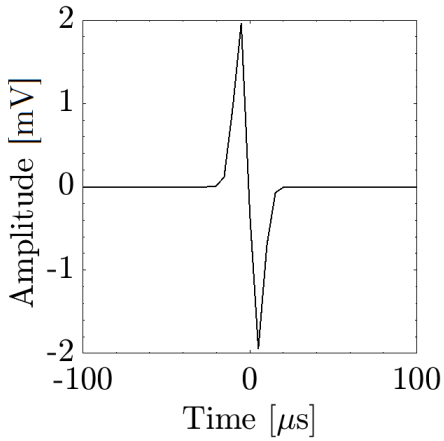

Figure 5.6: Acoustic BP simulating the signal in KM3NeT hydrophones after neutrino deposition of 10^{11} GeV of thermal energy at 1 km and 0 degree orientation. For this example, the inter-peak value is 10 μs, and the maximum pressure is equivalent to 124 mPa [51].

5.3.1 Evaluation

Adding an artificial BP to every minute (0.02 ev/s) of data will allow to evaluate the behavior of the detector. On the one hand, its accuracy (*Precision*, *Equation 5.4*) can be calculated, and on the other hand, its efficiency (*Recall*, *Equation 5.5*) can be calculated. So a BP will be added to all data to analyze. At a distance of 1 km from the midpoint between the three hydrophones, a point will be randomly selected, which will simulate the position where a Ultra High Energy (UHE) neutrino interacts. Then the ToA and amplitude are calculated for each hydrophone corresponding to that event, and finally, the artificial BP is added to the signals before they are analyzed by the detector.

When a detected event corresponds to an artificial BP, it will be a True Positive (TP). If the candidate is not an artificially added BP, it will be considered as False Positive (FP). In addition, a BP added and not detected shall be a False Negative (FN). Thus,

$$Precision = \frac{TP}{TP + FP} \tag{5.4}$$

$$Recall = \frac{TP}{TP + FN} \tag{5.5}$$

5.3.2 Configuration

Being able to evaluate the method can serve as a kind of calibration for the application of the cuts. For this first trigger level, three parameters will be considered:

- $P1$: to control the energy. It is the mean PSD value between 20 and 60 kHz of a sample time (around 50 μs).
- $P1w$: to control the duration. It corresponds to the width to 80% of the $P1$ peak.
- $P2$: to control the duration too. It is the difference between $P1$ value of 1 sample and the $P1$ value of the $\pm$ 50 samples surrounding it (around 5 ms)

A dynamic threshold shall be applied to $P1$. This threshold shall be composed of a level corresponding to a percentile ($pctl$) of $P1$ in the data plus an extra threshold level (th). If any candidate exceeds this dynamic threshold of $P1$, $P1w$ and $P2$ will be calculated. If the event also passes their respective threshold levels, it will be considered a BP candidate.

To select the threshold levels, some tests were made with the most extreme data (RUN8018 and RUN8019), so the percentile of the dynamic threshold was decided for each hydrophone: 95% for DU2, 90% for DU3, and 85% for DU9. In addition, it was decided to limit the $P1w$ to 200 μs and avoid the majority of long candidates that can slip.

Regarding the rest of the values to be configured (extra threshold in $P1$ and threshold in $P2$), a study was carried out during a neutral RUN (RUN7790) adding an artificial BP every 5 seconds. First, the threshold for $P2$ was set to 10 dB, and the precision, recall, and the number of events per second were studied with different values of the extra threshold of $P1$ (see *Figure 5.7.a*, *Figure 5.7.b*, and *Figure 5.7.c*). Observing the results, the extra threshold of $P1$ was set at 7 dB for the hydrophone in DU2 and 5 dB for the rest. The next step was to repeat the study, but now varying the value of the threshold at $P2$ (see *Figure 5.7.d*, *Figure 5.7.e*, and *Figure 5.7.f*). Finally, it was set at 15 dB for the hydrophone in DU2 and 10 dB for the rest.

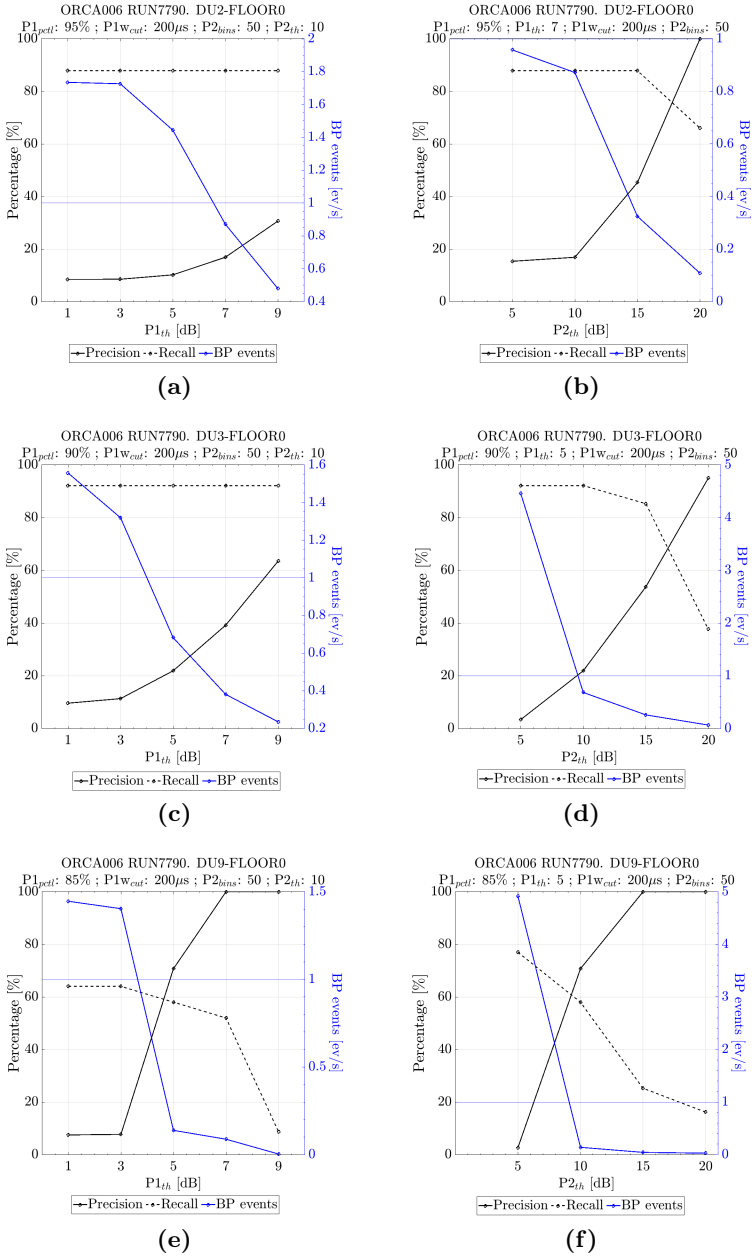

Figure 5.7: Hydrophone settings in detector parameters, observing the *Precision*, the *Recall*, and the BP events: **(a)** $P1_{th}$ in hydrophone of DU2. **(b)** $P2_{th}$ in hydrophone of DU2. **(c)** $P1_{th}$ in hydrophone of DU3. **(d)** $P2_{th}$ in hydrophone of DU3. **(e)** $P1_{th}$ in hydrophone of DU9. **(f)** $P2_{th}$ in hydrophone of DU9.

5.4 Trigger proposal to implement in KM3NeT

As already explained, the trigger for BP detections in KM3NeT is intended to work on each second of data independently from each receiver (see *Figure 5.8*). From its spectrogram of 20 samples per bin and 50% overlap (time resolution of about 50 μs and frequency resolution of 5 kHz), the parameter $P1$ is calculated. This parameter sets the dynamic value of the percentile per second, which together with the threshold level, marks the first cut. The parameters $P1w$ and $P2$ are then calculated for those who have exceeded it, and the second and third cuts take place from a limit value in the detection for $P1w$, and from a threshold level in the case of $P2$. In this way, a BP event is collected. However, if it coincides with the reception of any AB signal, it will be disregarded, as its high power may affect the detector result giving a FP.

Then, the ToAs of the events collected by each sensor will be compared. Taking into account that in KM3NeT the position of each receiver is known, an ideal time window where the events should coincide can be estimated. If matches are found, they will be considered BP candidates. Our proposal for KM3NeT is to implement this analysis and automatically save the ToA, the detection values ($P1$, $P1w$, and $P2$), and the part data with the event ($\pm$ 5 ms) to enable a post-analysis. In the postanalysis the recorded signal could be studied in detail (amplitude, waveform). The ToA could be used to find a periodic pattern comparing it with the rest, or it could be used to estimate the source location by the trilateration method. This is done to either discard that the BP candidate was being produced by the interaction of a neutrino in water or to determine the properties of the candidate event. Furthermore, the RUN could be ranked according to the number of candidates found.

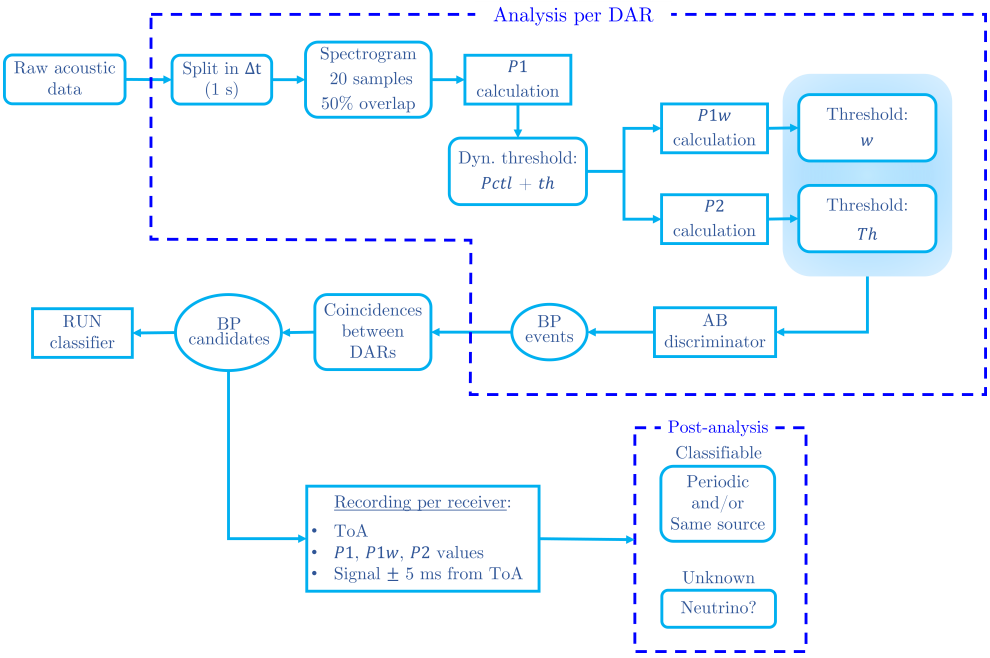

Figure 5.8: Workflow of the first proposal BP trigger for KM3NeT.

5.5 Results

5.5.1 BP events and BP candidates

In this first study, the proposed BP detector has been applied to the RUNs mentioned above. In total there have been 12 RUNs with an executed time of 6 hours per RUN. During its operation, the effect of each cut has been monitored. Thus, *Table 5.2* shows the number of BP events that have passed the different cuts studied ($P1$, $P1{+}P1w$, $P1{+}P2$, and $P1{+}P1w{+}P2$) in each hydrophone, and presents the value of BP candidates once the coincidence between them has been studied.

Hydro in DU	Time analyzed	Cut P1	P1+P1w	P1+P2	P1+P1w+P2	**Coinc.**
2	2.79 days	5.18 M	3.33 M	2962.88 k	2191.09 k	
3	2.87 days	4.03 M	1.73 M	717.10 k	464.63 k	41.16 k
9	2.79 days	5.53 M	3.18 M	232.67 k	199.65 k	

Table 5.2: Number of BP events that have passed the different studied cuts: $P1$, $P1{+}P1w$, $P1{+}P2$, and $P1{+}P1w{+}P2$. Coincident BP events (Coinc.) in hydrophones are called BP candidates.

The difference between the number of BP events per hydrophone seems to be related to the SNR level of the DPs (higher in DU9) and their RVR sensitivity (difference demonstrated in *subsection 2.4.1*). The effect of each cut is also depicted more graphically in *Figure 5.9*.

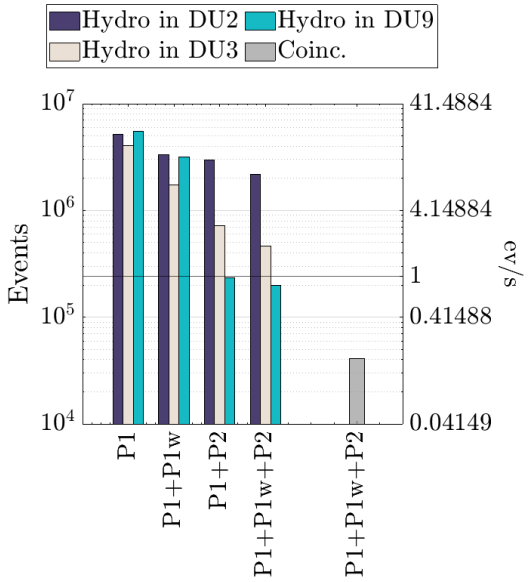

Figure 5.9: Number of BP events and BP candidates in ev/s for the different studied cuts.

It is worth noting that an artificial BP has been added to the data every minute (0.02 ev/s), so the TP, FP, and FN of the experiment are known. This provides the possibility to evaluate the detection method. *Table 5.3* shows the *Precision* and the *Recall* values of each hydrophone for the BP events and for the coincident BP candidate.

DU-Hydro	Events [ev/s]	Precision [%]	Recall [%]
2	9.08	0.15	79.97
3	1.87	0.72	81.42
9	0.83	1.13	56.41
Coinc.	0.17	3.9	39.34 ± 0.63

Table 5.3: Value of *Precision* and *Recall* for BP events and BP candidates (coincidences).

Consequently, the increase of ev/s (background) produces lower *Precision* but delivers higher *Recall* (efficiency). However, if the study is applied by RUNs, it is shown that this statement is not always true. It is therefore thought that the SPL (noise) also has a role on this, and it is studied in the *Figure 5.10*.

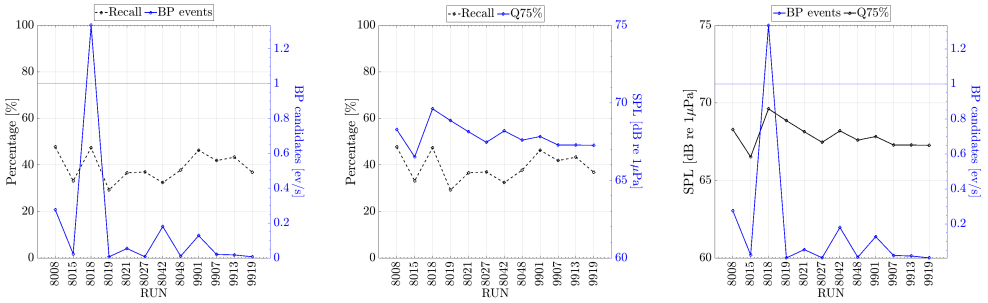

Figure 5.10: **(a)** Efficiency vs Background. **(b)** Efficiency vs Noise. **(c)** Background vs Noise.

In an attempt to study the trend of detection parameters according to whether they are TP or FP, the *Figure 5.11* is presented.

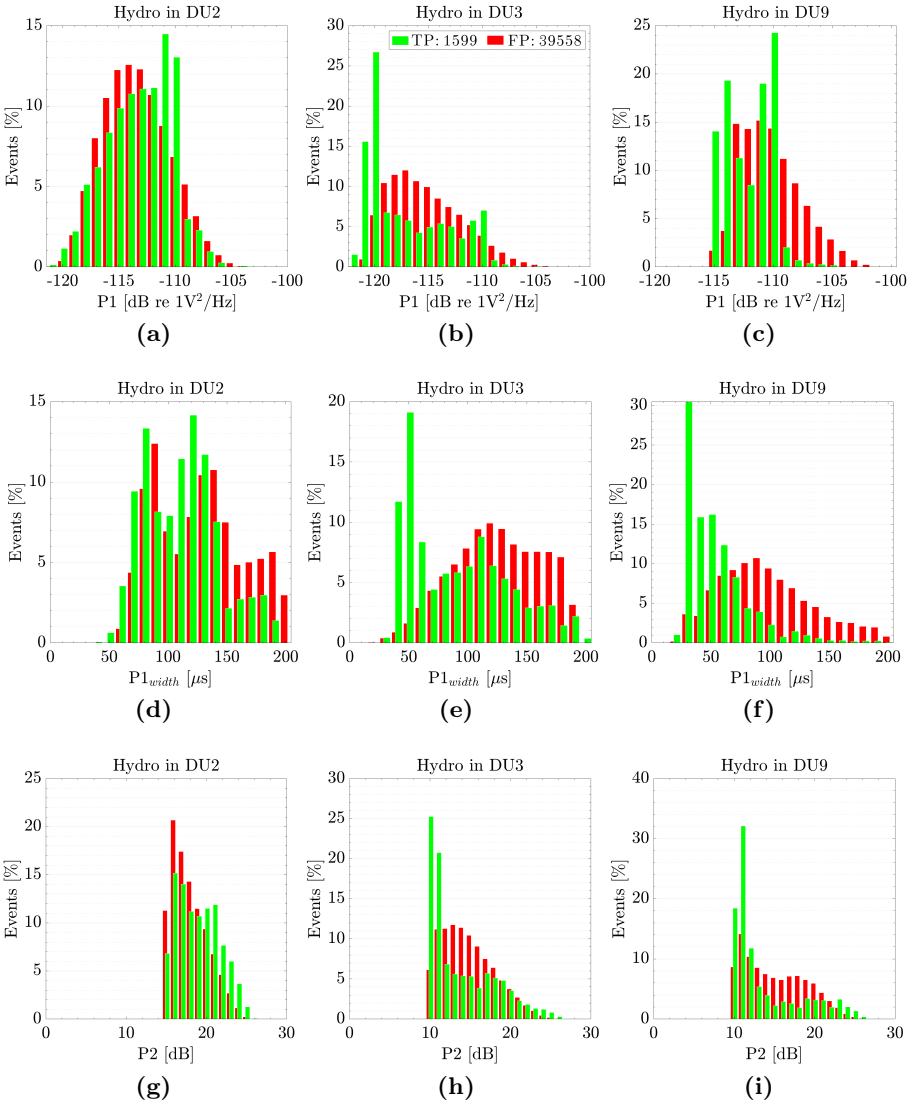

Figure 5.11: BP events trend of detection parameters (marked in green to TP and marked in red to FP): **(a)** $P1$ in hydrophone of DU2. **(b)** $P1$ in hydrophone of DU3. **(c)** $P1$ in hydrophone of DU9. **(d)** $P1w$ in hydrophone of DU2. **(e)** $P1w$ in hydrophone of DU3. **(f)** $P1w$ in hydrophone of DU9. **(g)** $P2$ in hydrophone of DU2. **(h)** $P2$ in hydrophone of DU3. **(i)** $P2$ in hydrophone of DU9.

Finally, *Figure 5.12* aims to demonstrate some correlation between the *Precision* and background value versus the semi-interquartile range of noise. As expected there is a correlation between SPL and the background events. Also the variability of the SPL in the frequency band of interest plays an important role on this.

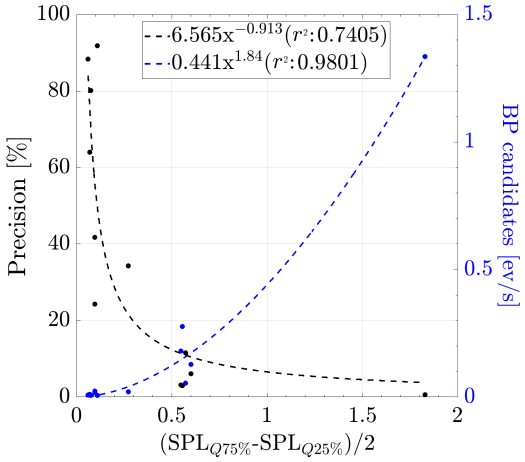

Figure 5.12: Correlation between the *precision* and background value (ev/s) in the three hydrophones versus the semi-interquartile range of noise, $(SPL_{Q75\%} - SPL_{Q25\%})/2$, recorded by the hydrophone in DU3 with an exponential fit.

5.5.2 TP and FP example detections

An example of TP and an example of FP from the BP candidates detected are presented in this subsection. The spectrogram of the BP event, its detection parameters ($P1$, $P1w$, and $P2$), and the directly recorded signal will be displayed.

TP event

Figure 5.13 shows the spectrogram of the TP event. Here it can be seen how the hydrophone in DU9 is more sensitive to the DPs (horizontal lines), and how other signals not corresponding to the BP can be discerned in the spectrogram. Furthermore, it can be noticed how the spectrogram is "smeared" below the f_{valid}. In any case, the artificial BP is appreciable between the white vertical lines.

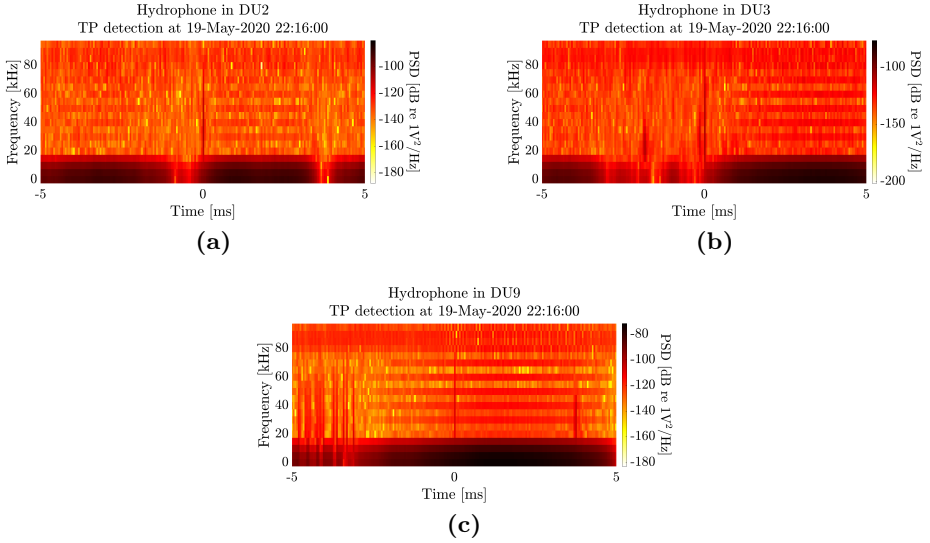

Figure 5.13: Spectrogram of a detected TP candidate in **(a)** the hydrophone in DU2, **(b)** the hydrophone in DU3, and **(c)** the hydrophone in DU9.

From the PSD between 20 and 60 kHz of the spectrogram, $P1$ is estimated and the threshold level for the first cut is calculated. In addition, $P1w$ and $P2$ are calculated for those samples that exceed them. *Figure 5.14* shows the result of these calculations for the presented TP event.

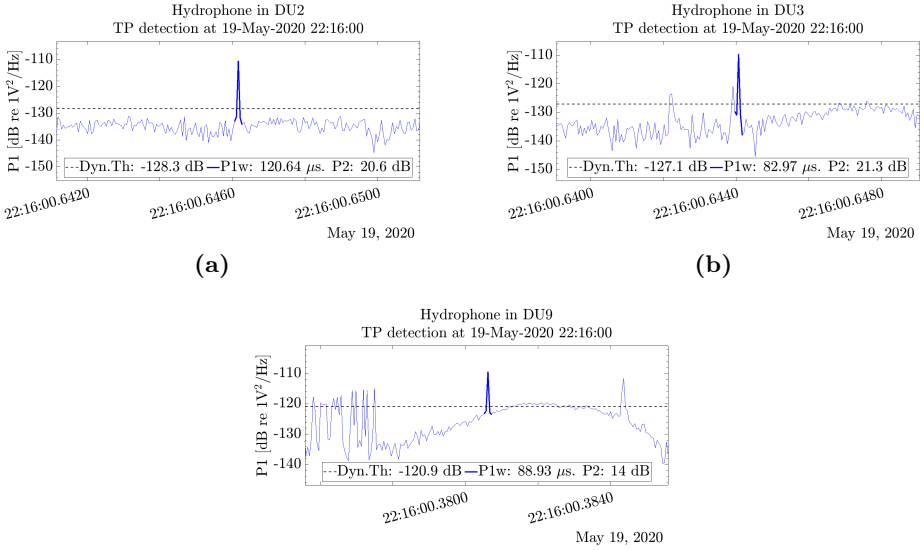

Figure 5.14: Detection params of a detected TP candidate in **(a)** the hydrophone in DU2, **(b)** the hydrophone in DU3, and **(c)** the hydrophone in DU9.

Finally, the recorded signal that was able to trigger the BP alert is represented. In this case, *Figure 5.15* shows an artificial BP (TP candidate).

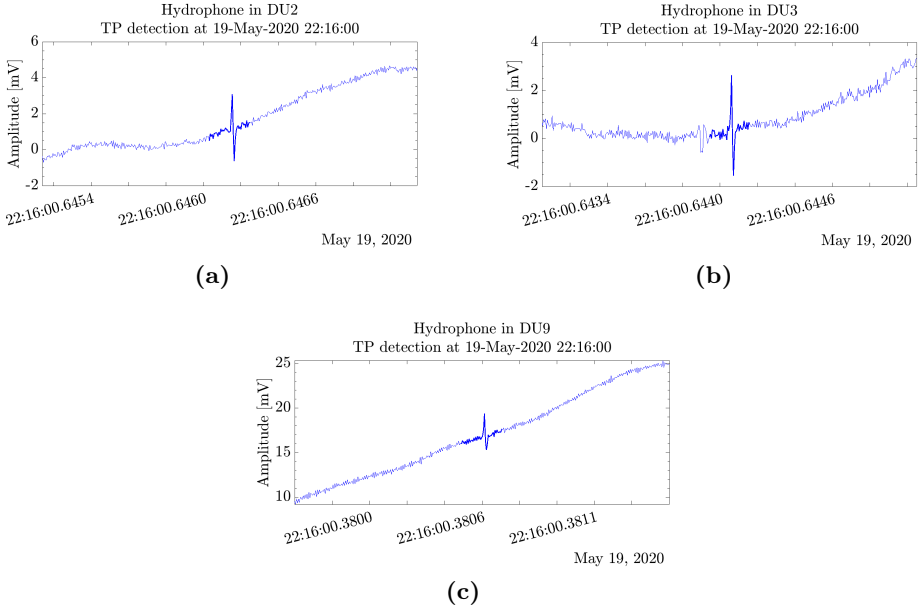

Figure 5.15: Signal part with a detected TP candidate by **(a)** the hydrophone in DU2, **(b)** the hydrophone in DU3, and **(c)** the hydrophone in DU9.

FP event

Figure 5.16 shows the spectrogram of the FP event. Here it is demonstrated how other signals are able to overcome the cuts and trigger the alert.

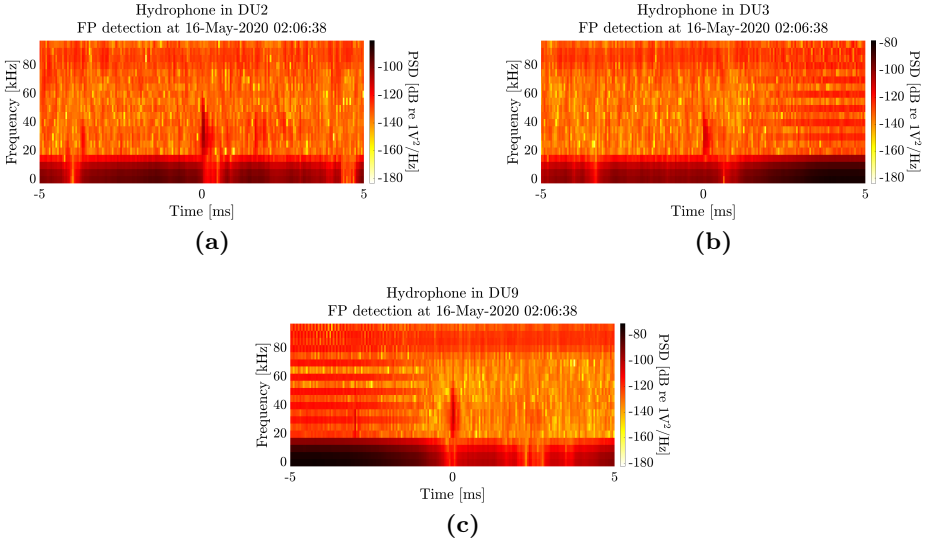

Figure 5.16: Spectrogram of a detected FP candidate in **(a)** the hydrophone in DU2, **(b)** the hydrophone in DU3, and **(c)** the hydrophone in DU9.

In this case, the detection (see *Figure 5.17*) appears to be wider than in the presented TP. Nonetheless, a TP may be mixed with other signals and it may broaden the $P1$ peak. For this reason, two cuts have been created to evaluate the duration of the event, and although they are not perfect, they are needed to eliminate many other residual events (see *Figure 5.9*).

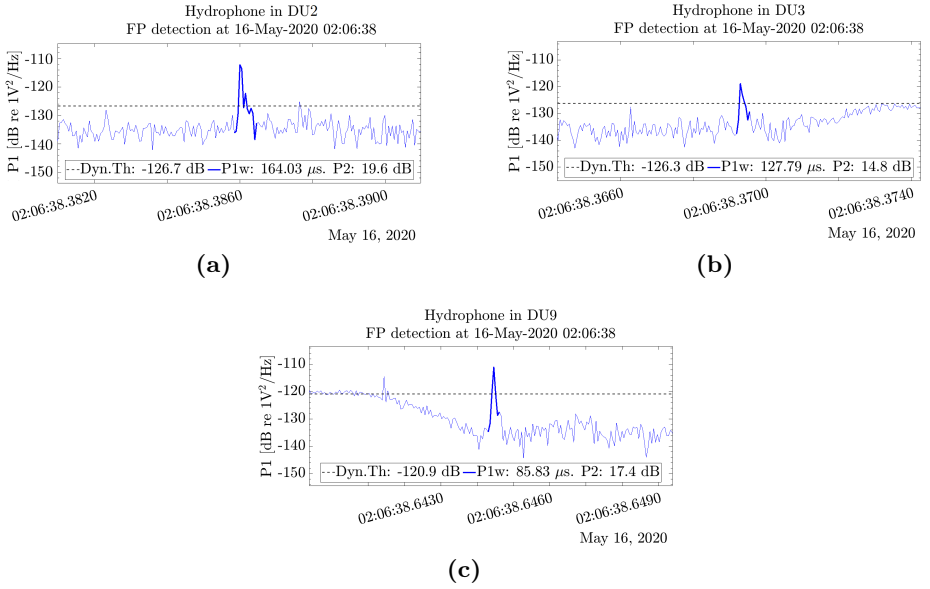

Figure 5.17: Detection params of a detected *FP* candidate in **(a)** the hydrophone in DU2, **(b)** the hydrophone in DU3, and **(c)** the hydrophone in DU9.

Figure 5.18 shows that other signals that are not exactly BP can trigger the alert. This is because the detector only takes into account the energy from the spectrogram, not fixing completely the waveform. This feature should be understood as an advantage, since the BP produced by the neutrino interaction will not always be detected at the same incident angle or conditions, and this will change the pattern of the signal, distorting the shape of the artificial BP that has been simulated. Naturally, post-processing will be needed to analyze all the candidate events and classify the events with higher-level cuts and determine the parameters of the detection, source location, directivity of the source, energy, etc. Naturally, this will be done more easily and better with a larger acoustic array, as it will be happening as detectors ORCA and ARCA become larger.

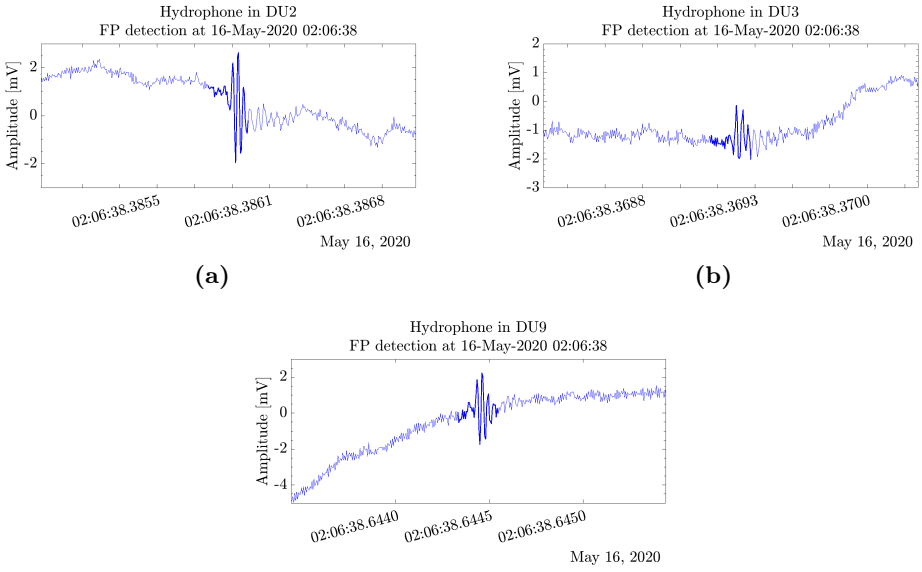

Figure 5.18: Signal part with a detected FP candidate by **(a)** the hydrophone in DU2, **(b)** the hydrophone in DU3, and **(c)** the hydrophone in DU9.

5.6 Conclusions and future steps

Conclusions

A method has been proposed to have a trigger in KM3NeT that allows detecting of the reference signal (an artificial BP) with good efficiency, around 50%, having an acceptable background detection rate, below one event per second, which is assumable and convenient from the point of view of data storage and for further post-processing.

The idea is to implement the trigger on the ADF to study the data in each DAR, but recommended using quiet data (see *Figure 5.12*). If a BP event appears in a lot of DARs, it is possible to estimate if its directivity is narrow or not. In case of ample directivity, the candidate should be discarded.

Future steps

There is still a lot of ORCA006 data to be examined since only 6% of the data between the two periods of the consecutive years presented has been analyzed. The idea would be to continue applying the trigger to the rest of the data, obtain enlarged results with more statistics, and get a more accurate concept of the real applicability of the proposed trigger, as well as to keep adjusting it with the value of cuts.

In addition, as the detector grows, there will be more hydrophones and it would be convenient to design a cut about the directivity studying the coincidences between receivers, as well as to better define the process of "configurating" every hydrophone for trigger application.

The effectiveness of applying the trigger on piezoceramic sensors could also be studied, which is expected to have worse results in terms of efficiency, given its low sensitivity compared to that of hydrophones, but can help in the directivity parameter to be developed.

Chapter 6

Conclusions

The work of this thesis is realized during the commissioning phase of KM3NeT. During these years, as far as positioning and acoustic calibration were concerned, there was an idea about the main objectives to be achieved, but the way to attain them remained to be defined.

For example, the installation of three autonomous ABs was approved, but their location was unknown. As a result of the work discussed in *subsection 2.3.1*, the position of the first three ABs in ORCA was defined to allow the development of tools to position the piezoceramic sensor of each DOM (XYZ_{piezo}) and to better define the operation of the APS, which is discussed in *section 2.5*. Currently, the location of the ABs fired at the bases of the DUs is under discussion for both ARCA and ORCA. *Subsection 2.3.2* shows what was our first proposal. On the other hand, ABs were already produced by the UPV, but now we have a robust measurement process and an analysis of these automatic measurements, explained in *section 2.2*. In addition, we have presented how to check the sensitivity of the transmitter-receiver system (AB–DAR) in *section 2.4*, a process that could be implemented routinely in the ADF and automatically control failures in any sensor involved in the system or notice the low battery of the autonomous ABs.

Given that the position of the piezoceramic sensor does not provide the center of the DOM and the DOM may be tilted by sea currents, an AHRS system

is installed to report the Yaw, Pitch, and Roll (YPR) of each DOM. It has been shown in *subsection 3.1.1* that these values require correction: making an adjustment in the case of Yaw and applying an offset in the case of Pitch and Roll. In *subsection 3.1.2*, a rotation matrix was developed to translate the YPR of every DOM to a common reference system between DOMs. In addition, in *subsection 3.1.3* a method has been developed to position each DOM in the DU only using the YPR data. This option is not better than the one provided by the APS, but it allows positioning without the use of ABs, which would be useful at times when a minimum of three ABs are not operating. On the other hand, in *section 3.2* a Mechanical Model (MM) that is able to reconstruct the position of the DOMs given a current effective velocity and direction, and vice-versa, has been developed. Furthermore, *section 3.3* presents the DU Line Fit, which combines data from the APS and AHRS, with the application of the MM, for a more reliable position each DOM. The DU Line Fit application was tested for ORCA006.

To test whether it is possible to perform an assumed acoustic detection of neutrinos in KM3NeT, a very comprehensive calibration process has been developed in *section 4.2*. The calibration is designed for using an array especially developed to be able to generate a Bipolar Pulse (BP) as would be generated by a neutrino interaction in water. The emitter array will be installed on a ship. Since the neutrino BP contains frequencies between 10 and 70 kHz and a narrow directivity more characteristic of much higher frequencies, we make use of the Parametric Effect to obtain a similar BP. Given the difficulty of signal generation and detection, we propose a calibration divided into steps, from less to more difficult. The first step consists of a simple emission in order to assess the frequency response of the entire detector. The second step would emit a parametric tone or sweep to achieve a directive low-frequency emission (directing the beam to a certain region of the detector). An experimental case that validates the process of emitting-receiving a parametric sweep is demonstrated. The last step would consist of emitting a parametric BP and demonstrating whether one is able to both record and detect the peculiar signal. This whole process can help in the development of new detection tools.

Thanks to the experience in the acoustic signals acquired up to this point of the thesis, it was possible to perform an experiment looking for a way to extend the coverage of KM3NeT by taking advantage of the APS in order to develop a trigger algorithm, which will help decide if you have a BP event candidate (see *chapter 5*). A BP is artificially added to every minute of data with the amplitude of the interaction of an Ultra-High-Energy (UHE) neutrino in water. This will allow evaluating the behavior and efficiency of the proposed trigger.

Finally, it has been possible to analyze up to 2.9 days of raw acoustic data from the hydrophones in ORCA006.

Acknowledgements

No puc acabar aquesta tesi sense agrair als meus directors tot el seu suport durant aquests anys, us admire. Hem passat per moltes experiències enriquidores, heu sabut fer de mi una persona entusiasta al món de la investigació. Tants viatges, congressos, intercanvi d'idees, i sobretot hores de laboratori i discussions, i mai m'heu deixat de costat. Miquel i Joan han tingut la paciència necessària perquè als pitjors moments sempre tirarem endavant el treball amb la millor qualitat. Soc afortunat d'haver-me creuat en persones tan professionals, dedicades i apassionades de l'acústica i la ciència, i mai oblidaré com al Perú es va plantar aquella llavoreta en mi. Tinc a la ment a cadascuna de les persones que han fet de mi el que soc avui, i la idea és no parar. Ara soc un apassionat de la raó i el ben fer, perquè m'han ensenyat que aquest és el bon camí a seguir. I no cal mencionar família, parella, amistats i companys que m'han sabut aguantar tants anys, i els que els queden... **gràcies**.

i Jo crec que ja ho he tingut bé d'escriure.

"Finalitzar una tesi t'acredita com investigadora, ara cal voler (i poder) continuar."

References

[1] S. Adrián-Martínez et al. «Letter of intent for KM3NeT 2.0». In: *J. Phys. G: Nucl. Part. Phys.* 43.8 (June 2016), p. 084001. DOI: 10.1088/0954-3899/43/8/084001.

[2] S. Aiello et al. «The KM3NeT multi-PMT optical module». In: *Journal of Instrumentation* 17.07 (July 2022), P07038. DOI: 10.1088/1748-0221/17/07/p07038. arXiv: 2203.10048 [astro-ph.IM].

[3] S. Aiello et al. «Deep-sea deployment of the KM3NeT neutrino telescope detection units by self-unrolling». In: *Journal of Instrumentation* 15.11 (Nov. 2020), P11027–P11027. DOI: 10.1088/1748-0221/15/11/p11027.

[4] Sebastiano Aiello et al. «KM3NeT front-end and readout electronics system: hardware, firmware, and software». In: *J. Astron. Telesc. Instrum. Syst.* 5.04 (Dec. 2019), p. 1. DOI: 10.1117/1.jatis.5.4.046001.

[5] S. Aiello et al. «Sensitivity of the KM3NeT/ARCA neutrino telescope to point-like neutrino sources». In: *Astroparticle Physics* 111 (Sept. 2019), pp. 100–110. ISSN: 0927-6505. DOI: 10.1016/j.astropartphys.2019.04.002.

[6] S. Aiello et al. «Event reconstruction for KM3NeT/ORCA using convolutional neural networks». In: *Journal of Instrumentation* 15.10 (Oct. 2020), P10005–P10005. DOI: 10.1088/1748-0221/15/10/p10005.

[7] Jonathan David Perkin. «The Acoustic Detection of Ultra High Energy Neutrinos». Ph.D. thesis. Department of Physics and Astronomy, Apr. 2007. arXiv: 0801.0991 [astro-ph].

[8] I. A. Belolaptikov et al. «The Baikal underwater neutrino telescope: design, performance, and first results». In: *Astropart. Phys.* 7.3 (1997), pp. 263–282. ISSN: 0927-6505. DOI: 10.1016/S0927-6505(97)00022-4.

[9] V.A. Balkanov et al. «The lake baikal neutrino telescope NT-200: status, results, future». In: *Nuclear Physics B - Proceedings Supplements* 75.1-2 (Mar. 1999), pp. 409–411. DOI: 10.1016/s0920-5632(99)00308-4.

[10] E. Andres et al. «The AMANDA neutrino telescope: principle of operation and first results». In: *Astropart. Phys.* 13.1 (2000), pp. 1–20. ISSN: 0927-6505. DOI: 10.1016/S0927-6505(99)00092-4.

[11] G. Riccobene. «NEMO: NEutrino Mediterranean Observatory». In: *Astrophysical Sources of High Energy Particles and Radiation*. Springer Netherlands, 2001, pp. 355–361. DOI: 10.1007/978-94-010-0560-9_32.

[12] Petros A. Rapidis and for the NESTOR Collaboration. «The NESTOR underwater neutrino telescope project». In: *Nucl. Instrum. Methods Phys. Res., Sect. A* 602.1 (2009). Proceedings of the 3rd International Workshop on a Very Large Volume Neutrino Telescope for the Mediterranean Sea, pp. 54–57. ISSN: 0168-9002. DOI: 10.1016/j.nima.2008.12.216.

[13] A. D. Avrorin et al. «Status and recent results of the BAIKAL-GVD project». In: *Physics of Particles and Nuclei* 46.2 (Mar. 2015), pp. 211–221. DOI: 10.1134/s1063779615020033.

[14] R. Abbasi et al. «Background studies for acoustic neutrino detection at the South Pole». In: *Astropart. Phys.* 35.6 (Jan. 2012), pp. 312–324. DOI: 10.1016/j.astropartphys.2011.09.004.

[15] Michel Ageron et al. «ANTARES: the first undersea neutrino telescope». In: *Nucl. Instrum. Methods Phys. Res., Sect. A* 656.1 (2011), pp. 11–38. DOI: 10.1016/j.nima.2011.06.103.

[16] Elisa Resconi and P-ONE Collaboration. «The Pacific Ocean Neutrino Experiment». In: *Proceeding of Science* (Nov. 2021). arXiv: 2111.13133 [astro-ph.IM].

[17] Edward Berbee. *KM3NeT DU: Description of components*. Technical Report v2. KM3NeT, Oct. 2018.

[18] Dominique Lefevre et al. *EMSO-Ligure Ouest observatory data (MII) from 2019-08*. 2021. DOI: 10.17882/75839.

[19] D. Real, e.a and on behalf of the KM3NeT collaboration. «KM3NeT acquisition: the new version of the Central Logic Board and its related power board, with highlights and evolution of the Control Unit». In: *J. Instrum.* 15.03 (Mar. 2020). 15th Topical Seminar on Innovative Particle and Radiation Detectors. 14–17 October 2019. Siena, Italy, pp. C03024–C03024. DOI: 10.1088/1748-0221/15/03/c03024.

[20] Christian Spiering. «Towards High-Energy Neutrino Astronomy. A Historical Review». In: *Eur. Phys. J. H* 37.3 (July 2012), pp. 515–565. ISSN: 2102-6467. DOI: 10.1140/epjh/e2012-30014-2. arXiv: 1207.4952 [astro-ph.IM].

[21] G. A. Askariyan et al. «Acoustic detection of high energy particle showers in water». In: *Nuclear Instruments and Methods* 164.2 (1979), pp. 267–278. ISSN: 0029-554X. DOI: 10.1016/0029-554X(79)90244-1.

[22] Clara Gatius Oliver. «Acoustic signals from ultra high energy cosmic neutrinos». Master Thesis. Universiteit van Amsterdam. Vrije Universiteit Amsterdam, Sept. 2020.

[23] Manuel Bou-Cabo and Miguel Ardid. «Calibración de sensores acústicos, y simulación del pulso acústico del neutrino mediante hidrófono». In: *37° Congreso Español de Acústica –Tecniacústica 06-*. Gandia: La Sociedad Española de Acústica (SEA), Oct. 2006.

[24] Pablo Gómez Magenti. «Estudio de la calibración de sensores acústicos por el método de reciprocidad para diferentes geometrías. Aplicación a la evolución temporal de la sensibilidad de los hidrófonos en instalaciones in situ». *hdl.handle.net/10251/74662*. Bachelor's Thesis. Escola Politècncia Superior de Gandia, Sept. 2016.

[25] L. Kopp et al. «Potential performance of parametric communications». In: *IEEE Journal of Oceanic Engineering* 25.3 (July 2000), pp. 282–295. DOI: 10.1109/48.855259.

[26] Riku Fukuda et al. «Digital acoustic communication in air using parametric loudspeaker». In: *IEICE Communications Express* advpub (2020). DOI: 10.1587/comex.2020XBL0007.

[27] A. Tobias. «Acoustic-emission source location in two dimensions by an array of three sensors». In: *Non-Destr. Test.* 9.1 (1976), pp. 9–12. ISSN: 0029-1021. DOI: https://doi.org/10.1016/0029-1021(76)90027-X.

[28] Peter Henry Milne. *Underwater acoustic positioning systems*. OSTI Identifier: 6035874. Gulf Publishing Co., Houston, TX, 1983.

[29] Dídac D.Tortosa, Iván Herrero-Durá, and Jorge E. Otero. «Acoustic Positioning System for 3D Localization of Sound Sources Based on the Time of Arrival of a Signal for a Low-Cost System». In: *Engineering Proceedings* 10.15 (Nov. 2021). ISSN: 2673-4591. DOI: 10.3390/ecsa-8-11307.

[30] CO.L.MAR. *Web page*. https://colmaritalia.it/. Accessed: 2020-09-30. 1982.

[31] Salvatore Viola et al. «Acoustic positioning system for KM3NeT». In: *Proceeding of Science* ICRC2015 (Aug. 13, 2015). ICRC2015, p. 1169. DOI: 10.22323/1.236.1169.

[32] Muller, Rasa et al. «Hydrophone characterization for the KM3NeT experiment». In: *EPJ Web of Conferences* 216 (Sept. 2019), p. 02007. DOI: 10.1051/epjconf/201921602007.

[33] Carlos David Llorens Alvarez. «Diseño y desarrollo de la electrónica de los emisores acústicos para los sistemas de posicionamiento y calibración de telescopios submarinos de neutrinos». Ph.D. thesis. Escola Politècnica Superior de Gandia, July 2017. DOI: 10.4995/Thesis/10251/88401.

[34] C. D. Llorens et al. «The sound emission board of the KM3NeT acoustic positioning system». In: *J. Instrum.* 7.01 (Jan. 2012), pp. C01001–C01001. DOI: 10.1088/1748-0221/7/01/c01001.

[35] Miguel Ardid et al. «Acoustic transmitters for underwater neutrino telescopes». In: *Sensors* 12.4 (Mar. 2012), pp. 4113–4132. DOI: 10.3390/s120404113.

[36] *Sensor Technology Ltd, FFR Transducers. Technical specs.* https://sensortechcanada.com/products/. Accessed: 2022-06-21.

[37] Carlos Alberto Quiroz Rangel. «Caracterización y evaluación de un emisor acústico para el detector submarino de neutrinos KM3NeT». ID: *hdl.handle.net/10251/186498*. Bachelor's Thesis. Universitat Politècnica de València, July 2022.

[38] Lawrence E Kinsler et al. *Fundamentals of acoustics*. John Wiley & sons, 2000. ISBN: 9780471847892.

[39] John G. Proakis and Dimitris G. Manolakis. *Digital signal processing: principles, algorithms, and applications*. 3rd. ed. Upper Saddle River: Prentice Hall, 1996. ISBN: 0133737624.

[40] S. Adrián-Martínez et al. «Acoustic signal detection through the cross-correlation method in experiments with different signal to noise ratio and reverberation conditions». In: *Ad-hoc Networks and Wireless*. Berlin, Heidelberg: Springer Berlin Heidelberg, 2015, pp. 66–79. ISBN: 978-3-662-46338-3. DOI: 10.1007/978-3-662-46338-3_7.

[41] R.E. François and G.R. Garrison. «Sound absorption based on ocean measurements. Part II: Boric acid contribution and equation for total absorption». In: *The Journal of the Acoustical Society of America* 72.6 (1982), pp. 1879–1890. DOI: 10.1121/1.388673.

[42] Dídac Diego-Tortosa, Miguel Ardid, and Juan Antonio Martínez-Mora. *Acoustic Beacon localization in ORCA Phase-2*. Technical Report v2. KM3NeT, June 2019.

[43] Herman Medwin. «Speed of sound in water: A simple equation for realistic parameters». In: *The Journal of the Acoustical Society of America* 58.6 (Dec. 1975), pp. 1318–1319. DOI: 10.1121/1.380790.

[44] Salvatore Viola and on behalf of the KM3NeT collaboration. «KM3NeT acoustic positioning and detection system». In: *EPJ Web of Conferences* 216 (2019), p. 02006. DOI: 10.1051/epjconf/201921602006.

[45] Giorgio Riccobene and for the KM3NeT Collaboration. «The positioning system for KM3NeT». In: *EPJ Web of Conferences* 207 (May 2019). Ed. by C. Spiering. Very Large Volume Neutrino Telescopes, p. 07005. DOI: 10.1051/epjconf/201920707005.

[46] S. Adrián-Martínez et al. «The positioning system of the ANTARES neutrino telescope». In: *J. Instrum.* 7.08 (Aug. 2012), T08002–T08002. DOI: 10.1088/1748-0221/7/08/t08002.

[47] Dídac D.Tortosa and on behalf of the KM3NeT collaboration. «Mechanical Line Fit Model to Monitor the Position of KM3NeT Optical Modules from the Acoustic and Compass/Accelerometer Sensor System Data». In: *Proceedings* 42.1 (Nov. 2019), p. 33. ISSN: 2504-3900. DOI: 10.3390/ecsa-6-06583.

[48] José Vicente González Calatayud. «Simulación CFD del comportamiento mecánico de las Unidades de Detección del telescopio submarino de neutrinos KM3NeT». ID: *hdl.handle.net/10251/173704*. Bachelor's Thesis. Universitat Politècnica de València, Sept. 2021.

[49] Dídac D.Tortosa et al. «Underwater acoustic positioning system for the monitoring of KM3NeT optical modules». In: *Revista de Acústica* 50.3-4 (2019), pp. 24–33. ISSN: 0195-175x.

[50] Askold Sergeevich Belyakov. «Doppler Effect and Acoustic Trails of Neutrinos». In: *Journal La Multiapp* 3.1 (Mar. 2022), pp. 1–7. DOI: 10.37899/journallamultiapp.v3i1.552.

[51] S. Bevan et al. «Study of the acoustic signature of UHE neutrino interactions in water and ice». In: *Nucl. Instrum. Methods Phys. Res., Sect. A* 607.2 (May 2009), pp. 398–411. ISSN: 0168-9002. DOI: 10.1016/j.nima.2009.05.009.

[52] Mark B. Moffett and Robert H. Mellen. «Model for parametric acoustic sources». In: *The Journal of the Acoustical Society of America* 61.2 (Feb. 1977), pp. 325–337. DOI: 10.1121/1.381310.

[53] Mark B. Moffett and Peter Mello. «Parametric acoustic sources of transient signals». In: *The Journal of the Acoustical Society of America* 66.4 (1979), pp. 1182–1187.

[54] María Campo-Valera et al. «Acoustic Parametric Signal Generation for Underwater Communication». In: *Sensors* 18.7 (2018). ISSN: 1424-8220. DOI: 10.3390/s18072149.

[55] María Campo-Valera and Ivan Felis. «Underwater Acoustic Communication for The Marine Environment's Monitoring». In: *Proceedings* 42.1 (2020). ECSA6. ISSN: 2504-3900. DOI: 10.3390/ecsa-6-06642.

[56] Apurba Das. «Amplitude Modulation». In: *Signal Conditioning*. Berlin, Heidelberg: Springer Berlin Heidelberg, 2012, pp. 77–114. ISBN: 978-3-642-28818-0. DOI: 10.1007/978-3-642-28818-0_4.

[57] Miguel Ardid. «Calibration in acoustic detection of neutrinos». In: *Nucl. Instrum. Methods Phys. Res., Sect. A* 604.1, Supplement (June 2009). 2nd International workshop on Acoustic and Radio EeV Neutrino detection Activities, S203–S207. ISSN: 0168-9002. DOI: 10.1016/j.nima.2009.03.071.

[58] M. Ardid et al. «A compact array calibrator to study the feasibility of acoustic neutrino detection». In: *EPJ Web Conf.* 116 (2016), p. 03001. DOI: 10.1051/epjconf/201611603001.

[59] Dídac D.Tortosa et al. «A Compact Transmitter Array to Reproduce the Acoustic Signature of Neutrino in Water». In: *Proceedings* 4.1 (Nov. 2018), p. 4. DOI: 10.3390/ecsa-5-05748.

[60] W. Ooppakaew, S. Danaher, and M. Saldaña. «Acoustic array calibration and signal processing for UHE neutrinos generation». In: *2011 IEEE Eighth International Conference on Mobile Ad-Hoc and Sensor Systems*. IEEE, Oct. 2011, pp. 910–915. DOI: 10.1109/mass.2011.109.

[61] Wichian Ooppakaew. «Advanced signal processing techniques for underwater acoustic transmission using steerable transducer arrays». Ph.D. thesis. UK: School of Computing, Engineering, Information Sciences, and in collaboration with the ACoRNE, Oct. 2012.

[62] M. Ardid et al. «R&D studies for the development of a compact transmitter able to mimic the acoustic signature of a UHE neutrino interaction». In: *Nucl. Instrum. Methods Phys. Res., Sect. A* 662 (Jan. 2012). 4th International workshop on Acoustic and Radio EeV Neutrino detection Activities, S206–S209. ISSN: 0168-9002. DOI: 10.1016/j.nima.2010.11.139.

[63] Silvia Adrián-Martínez et al. «A compact acoustic calibrator for ultra-high energy neutrino detection». In: *Nucl. Instrum. Methods Phys. Res., Sect. A* 725 (Dec. 2012). NOauthor, pp. 219–222. ISSN: 0168-9002. DOI: 10.1016/j.nima.2012.11.142.

[64] Silvia Adrián Martínez. «Design and Development of an Acoustic Calibrator for Deep-Sea Neutrino Telescopes and First Search for Secluded Dark Matter with ANTARES». Ph.D. thesis. Gandia: Escola Politècnica Superior de Gandia, Mar. 2015. DOI: 10.4995/Thesis/10251/48877.

[65] María Saldaña et al. «Transducer development and characterization for underwater acoustic neutrino detection calibration». In: *Sensors* 16.8 (Aug. 2016), p. 1210. ISSN: 1424-8220. DOI: 10.3390/s16081210.

[66] María Saldaña-Coscollar. «Acoustic System Development for Neutrino Underwater Detectors». Ph.D. thesis. Escola Politècnica Superior de Gandia, June 2017. DOI: 10.4995/thesis/10251/85981.

[67] Dídac D.Tortosa, Miguel Ardid, and Juan A. Martínez-Mora. «A compact array transducer for full calibration of underwater acoustic detection neutrino telescopes». In: *Sixth International Conference on Internet of Things: Systems, Management and Security (IOTSMS)*. International Workshop on Marine Sensors and Systems (MARSS 2019). Granada: IEEE, Oct. 2019, pp. 591–595. DOI: 10.1109/IOTSMS48152.2019.8939244.

[68] Dídac D.Tortosa et al. «Acoustic parametric techniques for neutrino telescopes». In: *EPJ Web of Conferences* 216 (Sept. 2019), p. 04001. DOI: 10.1051/epjconf/201921604001.

[69] Dídac Diego Tortosa. «Caracterización de un transductor paramétrico para emular el patrón acústico de neutrinos de energía ultra alta como calibrador del telescopio de neutrinos KM3NeT». ID: *hdl.handle.net/10251/89407*. Master's Thesis. Universitat Politècnica de València, Sept. 2017.

[70] Guillermo Fernán Lara Martínez. «Caracterización y modelado de la producción de sonidos de las ballenas beluga (Delphinapterus Leucas) basado en modelos de análisis / síntesis de voz». Ph.D. thesis. Universitat Politècnica de València, Oct. 2016. DOI: 10.4995/Thesis/10251/74645.

[71] Ramón Miralles et al. «Improved visualization of large temporal series for the evaluation of good environmental status». In: *Applied Acoustics* 148 (May 2019), pp. 55–61. ISSN: 0003-682X. DOI: 10.1016/j.apacoust.2018.12.009.

The grammar of this thesis document was reviewed by Lara Tortosa–Signes